Cyclopentadienyl-Based Lanthanoid Complexes Exhibiting Magnetic and Luminescence Properties

Master's thesis
University of Jyväskylä
Department of Chemistry
02.09.2021
Essi Barkas

ABSTRACT

This thesis familiarizes with compounds exhibiting magnetic and optical properties, and discusses the structural correlations with both single-molecule magnetic (SMM) and luminescence properties. The thesis consists of two parts: the literature part and the experimental part. The literature part familiarizes with the concepts of single-molecule magnetism and luminescence, and concentrates on lanthanocene complexes exhibiting either magnetic or optical properties. The synthetic, structural and physical properties of the forementioned compounds are discussed, after which the focus is shifted towards combining these magnetic and optical properties. Because the existing optomagnetic compounds do not include lanthanocene-based compounds, the optomagnetic compounds that are reviewed are lanthanoid-based complexes bearing ligands that include donor-atoms. These complexes, however, do not possess optimal ligand fields, which leads to poor SMM properties compared to the lanthanocene structures.

Although the design of single-molecule magnets has developed greatly during the recent years, only one lanthanocene SMM that can function above liquid nitrogen boiling point (77 K) exists. This is due to the strong structural dependence of the magnetic properties and the difficulty of controlling the ligand field in high coordination number lanthanoid complexes. In addition, trivalent lanthanoid complexes exhibit stronger magnetic properties, but divalent lanthanoid complexes show more efficient luminescence properties. Synthesizing trivalent optomagnetic complexes would require ligands that can enhance the SMM properties, as well as function as antenna-ligands that sensitize the emission of the Ln^{3+} ions. Thus, it is believed that aryl-substituted cyclopentadienyl ligands could be a promising component in the design of optomagnetic compounds.

The experimental part will discuss the possibilities of using aryl-substituted cyclopentadienyl (Cp) ligands in trivalent lanthanoid-based complexes, as their structural properties could allow both single-molecule magnetic and luminescence properties. The synthesized ligands 1,2,4-triphenylcyclopenta-1,3-diene and 2-(2,3,4,5-tetraphenylcyclopenta-2,4-dienyl)-1--(*p*-tolyl)hydrazone were characterized successfully by conducting single-crystal X-ray crystallographic measurements. These ligands were then deprotonated, and their alkali salts with potassium and lithium were obtained. The lithium salts were particularly sensitive and decomposed in an inert atmosphere over time.

The deprotonated ligands were further used in multiple syntheses to create yttrim-based homoleptic complexes with polyphenyl-substituted Cp ligands. In addition, two examples of heteroleptic derivatives bearing one polyphenyl-substituted and one alkyl-substituted cyclopentadienyl ligand were synthesized. None of the syntheses yielded crystalline products, which is the reason why no structural data were obtained. However, several syntheses yielded pure powdery solids which could be attempted to crystallize. Once the targeted compounds are characterized, magnetic and optical measurements can be conducted.

Ultimately, the SMM compounds could be applied in the study of information stor-

ages, spintronics and quantum computing. Particularly, the miniaturizing of modern day devices would benefit from SMMs that function above the liquid nitrogen boiling point, because the SMM properties reside at a molecular level. In addition, the optomagnetic compounds could be applied in the study of optical thermometers, which could be used to design SMM-based devices that have built-in optical thermometers. This way, the SMM properties and the optical thermometer properties could both originate from a molecular level and allow for miniaturized everyday appliances.

TIIVISTELMÄ

Tässä tutkielmassa tutustutaan yhdisteisiin, joilla on sekä mielenkiintoisia magneettisia että optisia ominaisuuksia. Lisäksi perehdytään yhdisteiden rakenteen, magneettisten ja optisten ominaisuuksien väliseen suhteeseen. Tutkielman koostuu sekä kirjallisesta että kokeellisesta osasta. Kirjallisessa osassa perehdytään yksittäismolekyylimagneetteihin ja luminesenssiin sekä lantanoseeni-komplekseihin, joilla on edellä mainittuja ominaisuuksia. Kompleksien synteettiset, rakenteelliset ja fysikaalisten ominaisuuksien yksityiskohdat käydään läpi, jonka jälkeen perehdytään yhdisteisiin, joissa magneettiset ja optiset ominaisuudet ovat yhdistetty. Tällaiset optomagneettiset yhdisteet eivät kuitenkaan pohjaudu lantanoseeneihin, joten tutkielmassa esitellään muita lantanoideihin pohjautuvia komplekseja, joissaa hyödynnetään donori-atomeja sisältäviä ligandeja. Nämä kompleksit eivät kuitenkaan luo optimaalista ligandikenttää, minkä takia näiden kompleksien magneettiset ominaisuudet ovat huonompia kuin lantanoseeneilla.

Vaikka yksittäismolekyylimagneettien suunnittelu on kehittynyt paljon viime vuosina, vain yksi lantanoseeni yksittäismolekyylimagneetti, joka säilyttää ominaisuutensa nestemäisen typen kiehumispisteen (77 K) yläpuolella, on olemassa. Tämä johtuu siitä, että sellaisten lantanoidi-kompleksien syntetisointi, joilla on optimaalinen ligandikenttä, on haastavaa, koska lantanoidit suosivat korkeita koordinaatiolukuja. Yleensä trivalenttiset lantanoidien kompleksit omaavat paremmat magneettiset ominaisuudet kuin divalenttiset, mutta tämä trendi on päinvastainen luminesenssin osalta. Tästä syystä optomagneettisten kompleksien synteesi vaatii hyviä antenni-ligandeja, jotka siirtävät energiaa lantanoidille vahvistaen sen luminesenssia. Tästä syystä aryyli-substituoidut syklopentadieeniligandit voisivat olla erittäin lupaavia lähtöaineita optomagneettisten yhdisteiden valmistuksessa.

Kokeellinen osa keskittyy aryyli-substituoitujen syklopentadieenien yttrium-kompleksseihin, sillä näiden ligandien rakenteelliset ominaisuudet voisivat vahvistaa sekä magneettisia että luminesenssi ominaisuuksia. Kokeellisessa osassa syntetisoitiin kaksi ligandia, jotka olivat 1,2,4-trifenyylisyklopenta-1,3-dieeni sekä 2-(2,3,4,5-tetrafenyylisyklopenta-2-4-dienyyli)-1-(*p*-tolyyli)hydratsoni. Molemmista rakenteista mitattiin yksittäiskide-röntgendiffraktion avulla kiderakenteet. Ligandit deprotonoitiin, jolloin niistä saatiin alkalisuoloja sekä kaliumin, että litiumin kanssa. Ligandien alkalisuolat etenkin litiumin tapauksessa olivat todella herkkiä, ja ne hajosivat hanskakaapissa.

Yllä mainittuja deprotonoituja ligandeja käytettiin homoleptisten yttium-kompleksien synteeseissä. Myös sellaisia heteroleptisiä rakenteita pyrittiin syntetisoimaan, joissa toinen ligandi on aryyli-substituoitu ja toinen on alkyyli-substituoitu. Yhdestäkään kompleksista ei kuitenkaan saatu kiteistä tuotetta, minkä takia kiderakennetta ei voitu mitata. Jos halutut yhdisteet olisi saatu karakterisoitua täysin, niiden magneettisia ja luminesenssi ominaisuuksia olisi voitu mitata.

Yksittäismolekyylimagneetteja voitaisiin tulevaisuudessa soveltaa esimerkiksi korkean tallennuskapasiteetin muisteissa, spintroniikassa sekä kvanttilaskennassa. Etenkin muistin tal-

lennuksessa näistä molekulaarisista magneeteista voitaisiin hyötyä, sillä ne mahdollistavat erittäin pienien tallennuslevyjen valmistuksen. Lisäksi optimagneettisia yhdisteitä voitaisiin soveltaa optisten molekulaaristen termometrien suunnittelussa.

PREFACE

The experimental part of the thesis was carried out between the fall 2020 and the summer 2021 in the Main Group Chemistry research group in the University of Jyväskylä. The supervisor of the project was Academy Research Fellow Jani Moilanen. The references were sought from Reaxys, Google Scholar, Scifinder and the ConQuest program of the Cambridge Crystallographic Data Centre using either keywords or structure searches. The subject area was limited to lanthanocene complexes that exhibit either single-molecule magnetic or luminescence properties, and lanthanoid-based complexes that exhibit optomagnetic and optical thermometer properties. The experimental part was limited to combining magnetic and optical properties in polyphenyl-substituted lanthanocene complexes.

I would like to thank my supervisor Academy Research Fellow Jani Moilanen for offering me a great opportunity to work in the Main Group Chemistry research group and familiarize with this interesting research topic. I also want to express my gratitude to Jani Moilanen for all the support I have received, as well as the numerous new laboratory techniques I have learnt during the project. In addition, I would like to thank Senior Lecturer Manu Lahtinen for the excellent support in familiarizing with the X-ray crystallographic measurements and analysing the data. My gratitude also goes to Academy Research Fellow Aaron Mailman, Dr. Chris Gendy, Dr. Petra Vasko and Dr. Mikko Rautiainen for all the help I have received while working in the laboratory. The whole Main Group Chemistry research group has offered me new insight on my research topic and a lot of support.

Jyväskylä, 31.8.2021

Essi Barkas

TABLE OF CONTENTS

ABBREVIATIONS

AC Alternating current

CF Crystal field

Cp Cyclopentadiene

Cp* Pentamethylcyclopentadiene

Cp$^{i\mathbf{Pr}_4}$ tetraisopropylcyclopentadienyl

Cp$^{i\mathbf{Pr}_5}$ Pentaisopropylcyclopentadienyl

CpLn Cyclopentadienyllanthanoid

CpPh$_3$ Triphenylcyclopentadiene

CpPh$_5$ Pentaphenylcyclopentadiene

Cp$^{\mathbf{ttt}}$ 1,2,4-Tri(*tert*-butyl)-cyclopentadienyl

DC Direct current

DCM Dichloromethane

DME 1,2-Dimethoxyethane

Et$_2$O Diethyl ether

EtOH Ethanol

FC Field cooled

Ln Lanthanoid

Ln-SMM Lanthanoid-based single-molecule magnet

MeCN Acetonitrile

MeOH Methanol

NMR Nuclear magnetic resonance

QTM Quantum tunneling of magnetization

RT Room temperature

RTP Redox transmetallation/protolysis

SMM Single-molecule magnet

SOC Spin-orbit coupling

SQUID Superconducting quantum interference device

^{t}Bu *tert*-Butyl

THF Tetrahydrofuran

XRD X-ray diffraction

ZFC Zero-field cooled

ZFS Zero-field splitting

LITERATURE PART

1 INTRODUCTION

Magnets are seen in many everyday applications, and they are used for countless different purposes in several different fields like research, medicine and electronics. One of the most relevant applications for magnets is information storage, as the capacities of hard drives are being increased gradually. Developing molecular-scale magnets would allow for even greater storage sizes in smaller devices. The magnetic properties of a particle tend to scale with the particle size, and one of the most important scaling features of a compound is the operating temperature. Molecule-scale magnets often require extremely low working temperatures, which makes them less applicable in everyday appliances.[1]

In 1993, a manganese cluster $[Mn_{12}O_{12}(O_2CCH_3)_{16}(H_2O)_4]\cdot 4H_2O\cdot 2CH_3CO_2H$, nowadays often referred to as Mn_{12}, was synthesized and its physical properties were investigated. It was found that the cluster could retain a magnetic moment for several months after removing an applied magnetic field. The research indicated that this slow relaxation of a magnetic moment was purely of molecular origin, and it did not arise from the intermolecular interactions.[2] Later in 1996, the compounds with this kind of magnetic memory gained the name single-molecule magnets (SMM).[3] SMMs have gotten increasing attention during the recent years, and the use of lanthanoids has become more popular due to the interesting physical properties of the f-block metals.[4] In addition to the information storage applications, these lanthanoid-based single-molecule magnets (Ln-SMM) are promising components for quantum computing and spintronics, both of which rely heavily on magnetism.[5,6]

Furthermore, lanthanoids also exhibit luminescent character due to their unique electronic configurations, and Ln^{3+} ion series have been reported to cover the whole emission spectrum from UV range (Gd^{3+}) up to near-infrared range (e.g. Nd^{3+} and Er^{3+}).[7] The large variety in the emission wavelengths makes lanthanoids suitable for many applications, such as molecular bio-imaging and sensing,[8] optical waveguide amplifiers,[9] and economical light-emittion diodes (LED), that are used in numerous modern-day devices.[7]

These interesting finds lead us to the challenge of finding lanthanoid-based compounds that exhibit both SMM and luminescence properties in temperatures applicable in electronics, quantum computing and so on. The choice of ligands plays a significant role in the investigation of both magnetic and optical properties, and one highly promising candidate is a cyclopentadienyl ligand. Cyclopentadienyls can be substituted with countless different groups and they offer a broad selection of derivatives for tailoring the properties of the targeted compound. For instance, aryl-substituted cyclopentadienyl ligands have shown great promise in the synthesis of luminescent lanthanoid-based compounds, and alkyl-substituted derivatives in the development of lanthanoid-based single-molecule magnets.[10,11]

The main focus of this thesis is to familiarize with both magnetic and luminescent materials and examine the possibility of combining these properties on a molecular scale in lanthanocene compounds. The literature part will first consider the theoretical background of

the physical phenomena, as well as the basics of lanthanoids and cyclopentadienes, after which a review of existing lanthanocene SMMs and luminescent cyclopentadienyl-based lanthanoid complexes is covered. Moreover, some existing optimagnetic lanthanoid-complexes will be introduced as well. The experimental part will consider a synthetic series of yttrium-based complexes utilizing three different cyclopentadienyl ligands. The main goal was to synthesize and characterize multifunctional SMM complexes, as well as examine their magnetic and luminescence properties.

2 THEORETICAL BACKGROUND

2.1 SINGLE-MOLECULE MAGNETS

Single-molecule magnets (SMM) are molecular compounds that exhibit magnetic anisotropy and slow relaxation of magnetization below a certain blocking temperature T_B. If these properties are purely of molecular origin, the term SMM can be used.[12] When a SMM is magnetized in an external magnetic field, its spins align with the field, orienting the magnetic moments of a compound in single direction. After removing the external magnetic field the spins remain in the same orientation, retaining the magnetic moment for a certain period of time before the magnetization relaxes. This so called magnetically blocked state occurs below the T_B of a compound, above which the relaxation time becomes significantly shorter and the spins are free to flip more frequently.[13,14]

The parameter T_B has three different definitions, all of which are quite widely used. The textbook definition for T_B is the temperature at which the zero-field cooled (ZFC) susceptibility reaches the maximum value. The second definition for T_B is the temperature at which the relaxation time is 100 s, and the third definition is the temperature at which the hysteresis loop remains open at zero field. Nonetheless, the second and the third definition are widely accepted, but they do not regard all the factors affecting the T_B, such as the sweep rate which affects the hysteresis loop properties.[15]

If the ZFC susceptibility is plotted alongside the field cooled (FC) susceptibility as a function of temperature, another important temperature T_{IRREV} is observed at the point where the susceptibilities diverge. T_{IRREV} is the maximum temperature at which the magnetism is not in an equilibrium state and shows history-dependent character, which gives rise to a magnetic memory.[15]

Magnetic hysteresis occurs when the compound is first magnetized using an external field, followed by the slow relaxation in the absence of the field. The hysteresis loop is observed when the magnetization is measured and plotted as a function of the magnetic field. The hysteresis loop should remain open in order for the SMM to function as an information storage, in other words, the magnetization should possess a non-zero value at zero field.[16,17]

One of the key factors in SMMs is magnetic anisotropy, which means that the mag-

netic properties of a compound depend on the magnetization direction. When a magnetic material is anisotropic, its magnetization lies parallel to the crystallographic z-axis that is chosen for each compound.[18,19] A system of this type is called an easy-axis system, where the term easy axis indicates the axis of the spontaneous magnetization in the structure. There are also easy-plane systems, where the magnetization lies on a crystallographic plane. In terms of the axial systems, when an external magnetic field is applied, the spins tend to reorient, or "flip", parallel to the applied field. If the applied field lies along the easy axis of the system, no work is needed to flip the spins. Therefore the magnetic properties are direction dependent.[18]

The magnetic anisotropy causes the bistability of a compound, which means that there are only two stable spin orientations, "spin up" and "spin down". The anisotropy originates from an interaction called spin-orbit coupling (SOC), which is namely the interaction between the spin (quantum number S) and the orbital momentum (quantum number L) of an electron.[20] However, the SOC is not the only factor that affects the anisotropy and magnetic properties of a material. An interaction called crystal field (CF) effect, which considers the interactions between a metal and coordinated ligands, plays an important role in terms of magnetism.[21]

In case of most 3d-systems the orbital angular momentum L is quenched and therefore the CF effects are much more significant than the SOC. For this reason the total spin quantum number S, and the quantized spin quantum number m_S obtained from the projection of S on a field dependent axis, are good quantum numbers in the determination of the orbital energy levels.[21] It should be noted that the theory in this thesis is covered using the 3d-systems, as they are known as the pioneers in the field of SMMs.[1] The current trend in the field is highly fixated on the development of the 4f-systems using lanthanoids. However, it is emphasized that the 4f-systems differ highly from the 3d-systems in terms of the electronic structures. Thus, the quantum numbers S and m_S are not used for the 4f-systems, and instead the total angular momentum quantum number J and the quantized state quantum number m_J are used. These quantum number and the properties of lanthanoids will be covered in more detail in Section 2.2.[21]

The CF effects are highly linked to the zero-field splitting (ZFS) of the degenerate spin states labeled with the quantum number m_S, in the absence of an external magnetic field. ZFS is a magneto-structural property usually seen in molecules that exhibit axial symmetry, and can thus be modified by the choice of the metal center and the ligand field. Stronger axial ligation and shorter axial bond lengths have been reported to strengthen the ZFS effects, giving rise to larger magnetic anisotropy.[22] The magneto-structural properties are often characterized with the spin Hamiltonian shown in Equation (1)

$$\hat{H} = D(\hat{S}_z^2 - \frac{1}{3}\hat{S}^2) + E(\hat{S}_x^2 - \hat{S}_y^2), \tag{1}$$

where D and E are the axial and rhombic ZFS parameters, respectively, $\hat{S}$ is the total spin moment and $\hat{S}_{x,y,z}$ are the components of $\hat{S}$ along x, y and z-axes. Relating to anisotropy, the D value is positive in case of an easy-plane system and negative in case of an easy-axis

system.[23,24] Altogether, in the presence of axial ZFS in an easy-axis system ($D < 0$) the degenerate spin states m_S are split into $2S+1$ different states, where S is the total spin of the ground state. For example in case of a $S = 7$ system, there are 15 different m_S states, as presented in Figure 1.

The splitting of the states leads to a formation of an energy barrier, often referred to as a magnetic blocking barrier, that separates the $m_S > 0$ (spin-down) and $m_S < 0$ (spin-up) states. The height of the energy barrier (U_{eff}) is the energy required to overcome magnetic blocking barrier and return to the equilibrium state. U_{eff} correlates with the total spin of the system and it is obtained from $|D| \cdot S^2$ and $|D| \cdot (S^2 - 1/4)$ for integer and half-integer spins, respectively. This implies that a larger ground state spin gives rise to higher energy barriers. It is worth noting that often only ground state systems are considered, as the excited states contribute less to the D value.[23]

When a system constains an odd number of electrons, and consequently a half-integer total spin, it is called a Kramer's ion. In case of Kramer's ions each $\pm m_S$ state is degenerate and these states are called Kramer's doublets (KD). Because the bistability of the KDs is independent of the CF effects, Kramer's systems do not require an axial CF to possess bistable ground states, unlike non-Kramer's systems (integer total spin).[25]

However, when a strong magnetic field is applied, it interacts with the magnetic moments of a molecule. This phenomenon is called the Zeeman effect and it results in the lifting of degeneracy of the KD $\pm m_S$ states that would be degenerate in the absence of a magnetic field. The effect changes the shape of the double quantum well by lowering the negative m_S states, as seen in Figure 1. The negative m_S state is then favored due to the lower energy, which is called the "blocked" state.[26] It it emphasized that this theory is not sufficient in case of lanthanoids, because their SOC is much more important than the CF effects, unlike in 3d-systems.[21]

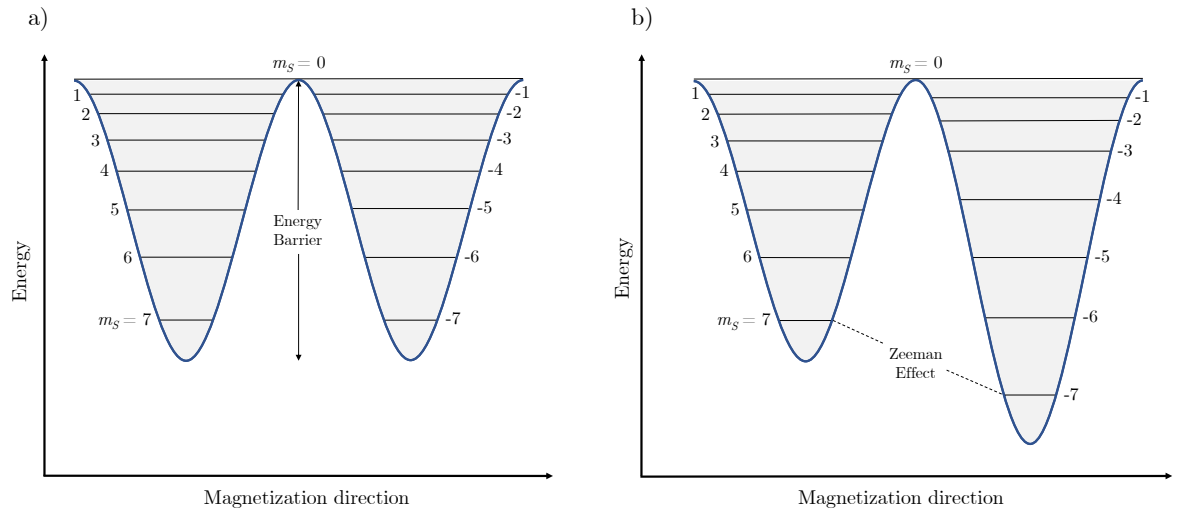

Figure 1. (a) Doubly degenerate m_S states divided by ZFS energy barrier. (b) Degeneracy lifted by Zeeman effect and the $m_S = -7$ state becomes populated.

When the applied magnetic field is removed, the magnetization persists and relaxes

extremely slowly due to the energy barrier and magnetic anisotropy. The relaxation time depends on the states between which the relaxation occurs. Different relaxation paths from one quantized state to another are called relaxation processes and they will now be covered in more detail.[1]

2.1.1 Slow Relaxation Processes

The theoretical background of the SMMs was covered using 3d-systems, as they are the first SMMs developed. However, the relaxation processes will be covered using 4f-systems, as the current trend in the development of SMMs is concentrated of these systems. The slow relaxation of the magnetization in SMMs can occur via several different processes: Direct, Orbach, Raman and Quantum tunneling of magnetization (QTM), all of which are shown in Figure 2. In the direct process the excitation or the relaxation occurs via absorption or emission of one phonon. The energy of the phonon is equivalent to the energy between the adjacent m_J states in the process.[27]

In the Orbach process, a phonon is absorbed, which leads to the excitation to a higher energy $\pm m_J$ state. The required excitation energy has to be at least the size of the energy difference between the ground and the excited m_J states. The excitation is followed by the phonon emission, i.e. the relaxation to a lower energy $\pm m_J$ state. If the excitation from the negative ground state proceeds to a negative excited state, the relaxation to a positive state can proceed either via Orbach mechanism or quantum tunneling of magnetization (QTM), or more precisely, thermally assisted QTM (TA-QTM).[28]

In the QTM process the relaxation proceeds from the lowest energy state to it's corresponding doublet state by tunneling through the energy barrier. In a TA-QTM process the relaxation proceeds from a higher energy excited state to its corresponding degenerate state. When focusing on maximizing the U_{eff} energy barrier height, the QTM processes are unfavorable due to their fast relaxation time, and hence their propability is often attempted to minimize.[28,29] The Raman process is similar to the Orbach process, but instead of proceeding via m_J state, the excitation takes place on a temporary virtual state from which the relaxation can occur.[28]

2.1.2 Measurement Of Magnetic Properties

As it has been discussed, the magnetic properties of a compound depend on several different factors. Therefore, a comprehensive selection of measurements and calculations is usually conducted to characterize the properties. It is widely understood that the study of Ln-SMMs is a challenging field that requires a deep knowledge of the quantum level phenomena. The characterization of the magnetic properties in 4f-complexes is often difficult, specially in case of the computational studies where several factors should be taken into account, such as the probability of each relaxation process.[30]

Typically the SMMs are characterized with a SQUID (superconducting quantum in-

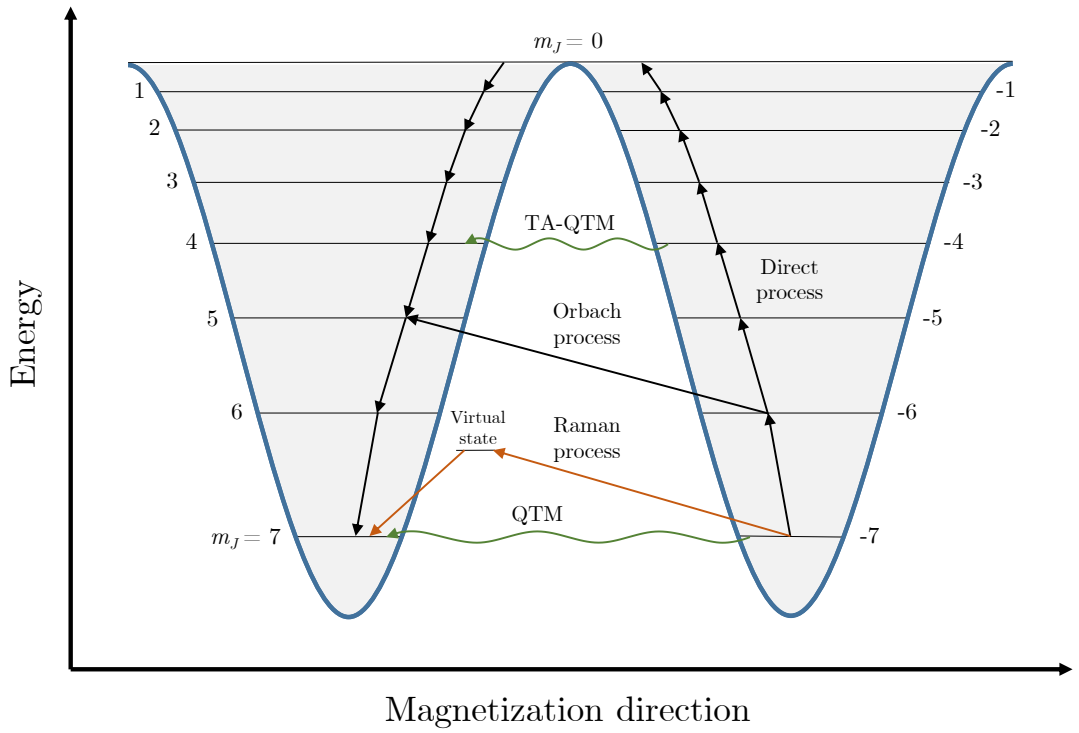

Figure 2. Generalized Direct, Orbach, Raman, and quantum tunneling pathways for magnetic relaxation.

terference device) magnetometer using either alternating current (AC) or a direct current (DC) in zero field. The SQUID is utilized to measure the magnetic susceptibility, which plays a crucial role in the characterization.[31] The in-phase (χ') and the out-of-phase (χ'') susceptibilities are obtained with the AC measurements using variable temperatures and frequencies. The susceptibility data is then processed to yield information about the frequency- and temperature-dependence, predominant relaxation processes, the presence of the slow magnetic relaxation and the temperature dependent relaxation rates. The information can be fitted in Equation (2) to determine the U_{eff} energy barrier. However, this Arrhenius-equation does not consider all the possible relaxation processes and often has to be modified, for example by adding the Raman and QTM terms.[31,32]

$$\tau = \tau_0 \exp(U_{\text{eff}}/k_{\text{B}}T) \tag{2}$$

The determination of the energy diagrams of the m_J multiplet states in Ln-SMMs has proven to be challenging. One strategy is to exploit paramagnetic NMR (nuclear magnetic resonance) shifts in variable temperatures. Using the ^{2}H NMR spectra allows the determination of the axial magnetic susceptilibity anisotropy χ_{AX}, as well as it's temperature dependence in different Ln^{3+} ions. Ultimately, the obtained values can be utilized in the determination of the CF splitting parameters. This method is relatively quick and has given reliable results.[30,33]

Moreover, the determination of the electronic transitions of a compound can help determine the m_J state energies and explain the magnetic relaxation paths of a compound. One

approach is to exploit the photoluminescence and emission spectra of a complex to obtain information about the ground and multiplet states (or Kramer's doublets), as well as the transitions between the states. An example of both spectra is presented in Figure 3, where the photoluminescence spectrum shows three different transitions from the ground term $^6H_{15/2}$, and the emission spectrum shows eight multiplet states characteristic to a Dy^{3+} compound. These eight multiplets can be assigned to the Kramer's doublets of the ground term.[34]

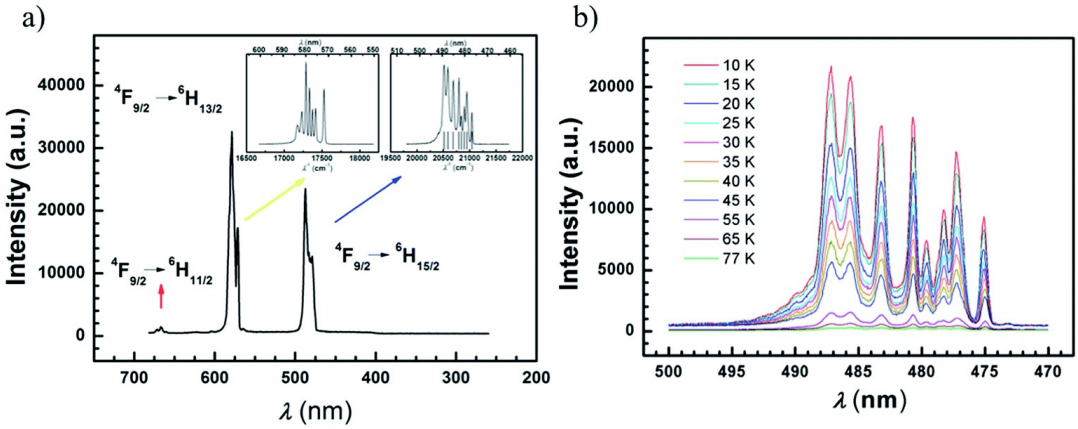

Figure 3. (a) A photoluminescence spectrum of $DyCs[\mu_2\text{-}C_8H_3N_2I(CN)Me]_4$. (b) Emission spectra of the same compound in different temperatures. Reproduced from Ref. Chem. Sci., 2016,7, 5020-5031 with permission from the Royal Society of Chemistry.[34]

In addition to the experimental approaches, computational methods are also widely used in the characterization. *Ab initio* calculations are the main approach used to predict the magneto-structural correlations and the magnetic performance in the SMMs. For the most accurate results both experimental and computational methods should be combined and compared with each other.[35] Density Functional Theory (DFT) and Complete Active Space Self Consistent Field (CASSCF) calculations are often established to yield information about the magnetic properties, structural properties, anisotropy and electronic structures.[36]

2.2 LANTHANOIDS AND THEIR PROPERTIES

Lanthanoids (Ln) are metallic f-block elements ranging from La to Lu, and their valence orbitals are 4f-orbitals. The f-block consists of two groups, lanthanoids and actinoids, that are often called lanthanides and actinides. Nevertheless, the IUPAC preferred terms are lanthanoids and actinoids, as the -ide suffix usually indicates a negative ion, which is contraty to these two groups. In their zero valent metallic form the lanthanoids possess an electron configuration of $[Xe]4f^n6s^2$, with the exeptions of Cerium, Gadolinium and Lutetium that possess an electron configuration of $[Xe]4f^n5d^16s^2$.[37]

The 4f orbitals are unique when compared to other orbitals. Their radial extension is small, which causes the 4f orbitals to extend approximately as far as filled 5s and 5p orbitals. Consequently the valence orbitals of the lanthanoids do not significantly participate in

the bonding with ligands, and the metal-ligand interaction is more electrostatic compared to the transition metals.[37]

Lanthanoids mainly appear in their most stable oxidation state +3, although some lanthanoids also appear in oxidation states +2 and +4, for example Eu^{2+}, Sm^{2+}, Yb^{2+} and Ce^{4+}. Stable divalent and tetravalent species form when the ionization energy required to reach empty, half-filled or full 4f-shell is low.[27,38] Most trivalent Ln^{3+} ions have an electron configuration [Xe]$4f^n$ and several unpaired 4f-electrons, giving these ions a very paramagnetic nature and for some ions, such as Dy^{3+} and Er^{3+}, a large ground state total spin S. La^{3+} and Lu^{3+} however are exceptions, given that the former has no f-electrons and the latter has a completely filled 4f-shell, constituting a lack of unpaired electrons.[27,39] The unpaired 4f-electrons and the properties of the 4f-shells are the main reasons why lanthanoids are so widely studied in the field of molecular magnetism.[21]

Lanthanoids in SMMs are also known for their strong intrinsic magnetic anisotropy resulting from the spin-orbit coupling. Due to the shielded 4f-orbitals the SOC effects are much stronger than the ligand-field effects, unlike in most 3d-systems. In Ln^{3+} ions the SOC effect splits the ^{2S+1}L states generated by the Coulomb repulsion, giving rise to $^{2S+1}L_J$ states. When a ligand is coordinated with an Ln^{3+} ion and the ligand-field effects are taken into account, the low lying $^{2S+1}L_J$ states split into quantized m_J states similar to the m_S states in 3d-systems.[21]

Owing to the orbital differences between lanthanoids and transition metals, the total spin S is not a good quantum number when considering the Ln ion energy levels. Therefore the total angular momentum quantum number J, where $|L-S| \leq J \leq L+S$, must be used instead. Similarly to the m_S states acquired from S, J can also be projected on an axis to provide $2J+1$ different quantized states m_J.[21] When the electron configuration is an odd-number type, the m_J states are degenerate Kramers doublets, similar to the m_S Kramers doublets observed in Figure 1. A more clear view on the discussed effects is shown in Figure 4.[27]

As it has been stated earlier, the symmetry plays a vital role in maximizing the magnetic anisotropy and hence must not be overlooked even in case of weaker CF effects. The choice of the Ln^{3+} ion should be considered with regard to the shape of the electron density in the 4f-shells. For instance Tb^{3+} and Dy^{3+} have been discovered to possess oblate shaped electron density, whereas Er^{3+} and Yb^{3+} possess prolate shaped electron density (Figure 5).[40]

The former type is often more favorable due to it's stabilization in an axial crystal field, while the latter type should be stabilized in an equatorial field. Therefore the anisotropy of Dy^{3+} ion for instance is increased when the ion is introduced to a strong axial and a weak equatorial crystal field.[28] Although this model can be exploited to predict the anisotropy and the CF effects in a complex, it should be used critically as the model is hypothetical.[40]

With regard to the multifunctional SMMs that exhibit both magnetic and optical properties, lanthanoids are certainly prominent candidates, as they not only exhibit magnetic properties, but also display a luminescent character. The trivalent Ln cations are unique in terms of luminescence because they show characteristic emission and absorption bands arising from

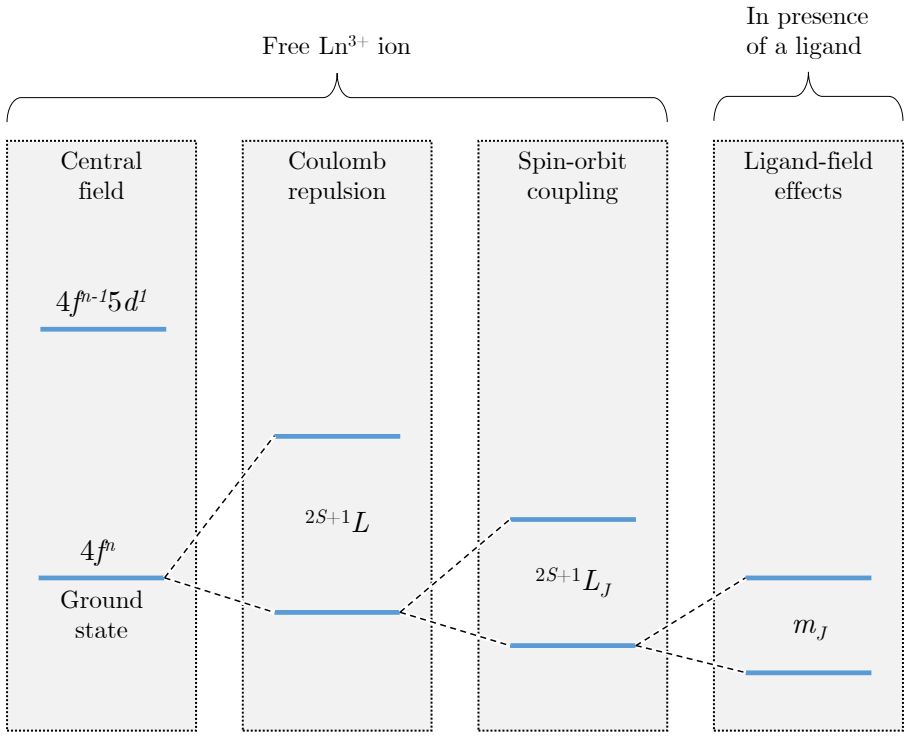

Figure 4. The ground state splittings for both a free Ln3+ ion and an Ln3+ ion in presence of a ligand.

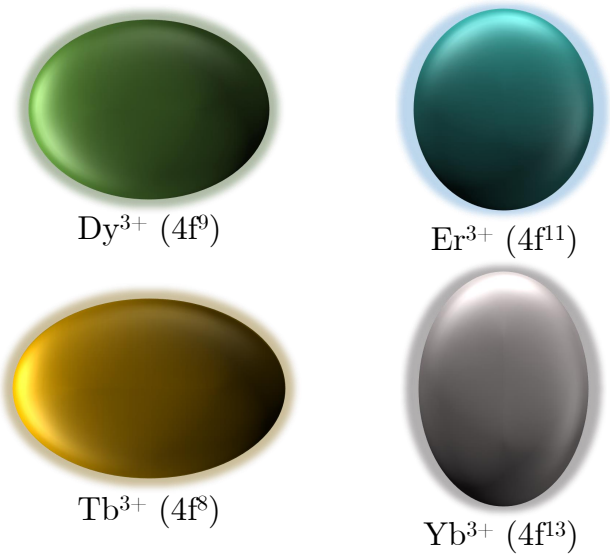

Figure 5. The shapes of the electron densities of Dy^{3+}, Tb^{3+}, Er^{3+} and Yb^{3+} ions.

the f-f transitions.[39] Due to the weak CF effects caused by the nearly inert 4f-orbitals, the f-f transitions are Laporte forbidden. Consequently, an efficient direct excitation of the lanthanoid becomes very unlikely, making the indirect excitation with a ligand that absorbs energy and transfers it to the lanthanoid (antenna-ligand) more convenient.[4]

The energy gaps between the adjacent states as well as the spin multiplicities affect

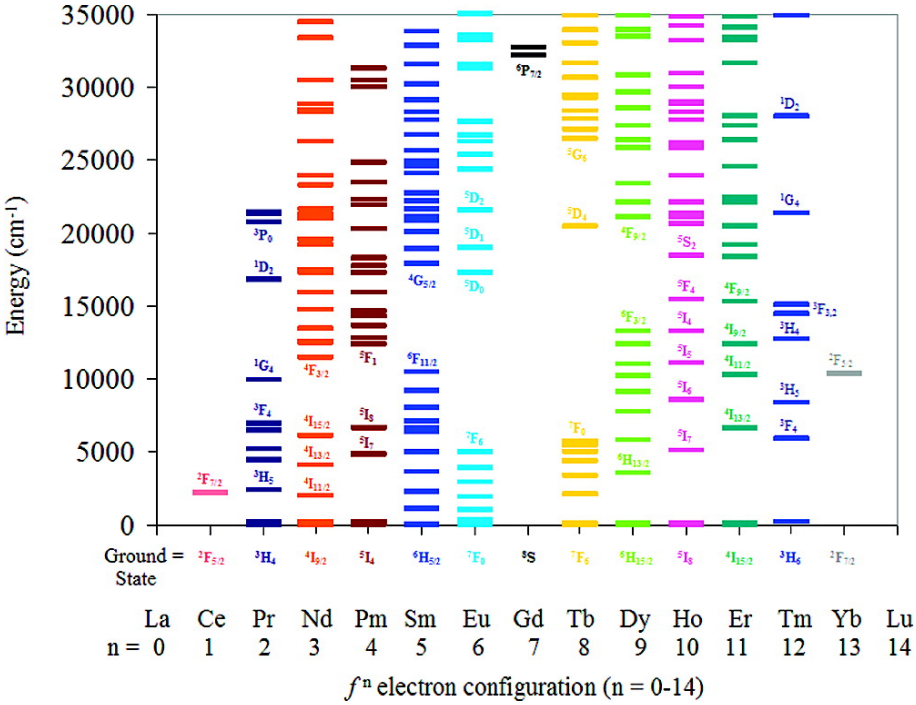

Figure 6. The energy levels, electron configurations and terms symbols of the Ln series. Reprinted with permission from Acc. Chem. Res. 2009, 42, 4, 542-552. Copyright 2021 American Chemical Society.[39]

the luminescence of the lanthanoid. For elements with larger energy gaps and spin multiplicities between the states the luminescent emissions increase in time. For instance Eu^{3+} luminescence is more long-lived than that of Sm^{3+}. The energy levels of the ground and excited states as well as the electron configurations and term symbols of the lanthanoid series can be seen in Figure 6.[39]

2.3 CYCLOPENTADIENYL LIGANDS

Cyclopentadienyl (Cp) ligands play an essential role in organolanthanoid chemistry, as they are the most common ligands used in the synthesis of Ln-SMMs. Cyclopentadiene (**1**) in it's neutral form typically exists as a dimer, dicyclopentadiene (**2**). The monomer and the more stable dimer are both shown in Figure 7. Although **1** dimerizes spontaneously, it can be dissociated back to it's monomeric form at high temperatures.[41]

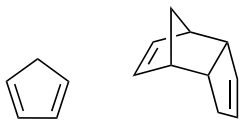

1 **2**

Figure 7. Cyclopentadiene and dicyclopentadiene.

As discussed earlier, lanthanoids are predominantly used as cations and therefore anionic ligands are required. Cp ligands can be deprotonated with several different methods using

alkali metals to obtain dehydrogenated $Cp^{-}M^{+}$ salts (M = Na, K, Li). For example, the dimer **2** can be reacted with a pure alkali metal at a high temperature to receive NaCp or KCp.[42] Other Cp reduction reaction can be done with e.g. sodium amide,[43] benzyl potassium[44] or *n*-butyl lithium.[45] In an anionic Cp ligand the free electron pair and the conjugated π-bonds are delocalized in the five-membered ring, allowing the aromatic ring to coordinate to an Ln ion with η^5 hapticity.

Cyclopentadienyls are also excellent ligands because of their formability. With the choice of substituents in the Cp ring the steric hindrance, reactivity and crystal field effects in SMMs can be manipulated without necessarily altering the pentahapto coordination. One prominent group of Cp derivatives is alkyl substituted cyclopentadienyls. Adding a different number of different size alkyl groups into the Cp rings gives the possibility to tailor the targeted properties. Adding methyl groups can change the Cp anion basicity and affect the electron-donating properties towards the metal ion. For example in case of pentamethylcyclopentadienyl (**3**), often abbreviated as Cp*, the electron-donating effect is stronger than in **1** and the steric bulk is noticeably larger.[46]

The steric bulk is essential in terms of crystal field effects, since it can significantly change the axial and equatorial crystal field strengths. Steric crowding can be increased further by for example replacing the methyl groups in **3** with *tert*-butyl (^{t}Bu) groups. Penta or tetra alkylated Cp rings with *tert*-butyl groups have not been synthesized, but 1,2,4-tri(*tert*-butyl)-cyclopentadienyl (**4**), abbreviated Cp^{ttt}, is large enough to eliminate the equatorial field of a complex completely. For instance in a Cp^{ttt} sandwich complex of Dy (complex **7**, reviewed in Section 3.1) the steric bulk allows the crystal field to become crowded and prevents other ligands from coordinating.[47] The chemical structures of Cp* and Cp^{ttt} are presented in Figure 8.

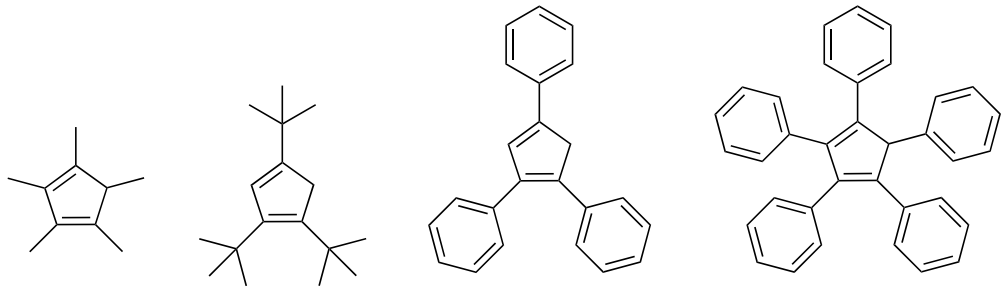

Figure 8. The chemical structures of Cp* (**3**), Cp^{ttt} (**4**), $CpPh_3$ (**5**) and $CpPh_5$ (**6**).

In order to increase the steric bulk, the cyclopentadienes can also be substituted with aryl groups. For instance, phenyl groups have gained attention for their usage in tailoring symmetric and geometric properties. A very bulky pentaphenylcyclopentadienyl (**6**), abbreviated $CpPh_5$, is known to coordinate to several rare-earth metals, such as Y, Yb and Sm, and give rise to several interesting structures.[48] A less bulky tri-substituted version, triphenylcyclopentadienyl (**5**), has also shown promise in complexes with rare-earths.[10] The chemical structures of

both $CpPh_3$ and $CpPh_5$ are presented in Figure 8.

3 TRIVALENT LANTHANOCENE SINGLE-MOLECULE MAGNETS

This section introduces trivalent lanthanocene complexes that can function as single-molecule magnets. Trivalent Ln-based complexes are excellent candidates for SMMs due to their electronic structure, and their study is still progressing with novel excellent Ln-SMMs being developed. This survey will cover the synthesis, structures and principal properties of the lanthanocene compounds.[49]

Lanthanocenes are homoleptic or heteroleptic sandwich-type complexes that consist of a lanthanoid (or a rare-earth metal) ion and two cyclopentadienyl ligands, as presented in Figure 9. These bis(cyclopentadienyl) lanthanoid complexes offer great capability of tailoring the steric and structural properties due to the variety in different substituents of the Cp ligands. In addition, the Cp ligands are good π-donating ligands, which can stabilize the lanthanocene complexes.[49]

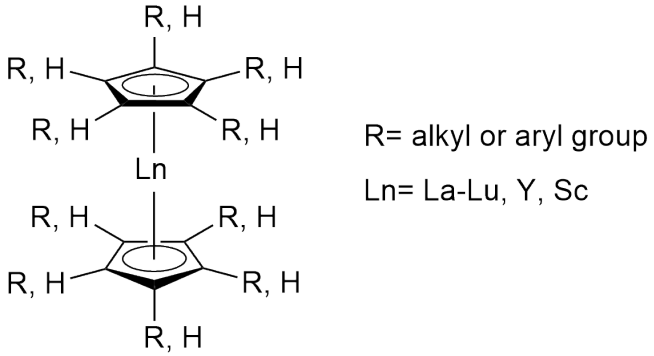

Figure 9. Lanthanocene sandwich complex comprises of a rare-earth metal center and two alkyl, aryl or non-substituted cyclopentadienyl ligands.

As it has been discussed, enhancement of the axial CF is often required to observe SMM properties and magnetic blocking in a compound. This can be achieved by, for instance, shortening the M–L bonds as well as increasing the L–M–L bond angle via correct ligand modifications. Hence, lanthanocenes are excellent SMM candidates and can be modified in countless ways.

3.1 $[Dy(Cp^{ttt})_2]^+$ CATION

3.1.1 Synthetic and structural details

A lanthanocene SMM functioning at 60 K was synthesized successfully by two research groups in 2017.[47,50] The complex consists of a $[Dy(Cp^{ttt})_2]^+$ (**7**) cation and a non-coordinating counter

anion $[B(C_6F_5)_4]^-$. Initially a precursor $[Dy(Cp^{ttt})_2Cl]$ was prepared by refluxing KCp^{ttt} and $[DyCl_3(THF)_3 \cdot 5]$ in toluene. The precursor was then reacted with $[H(SiEt_3)_2][B(C_6F_5)_4]$ in benzene[50] or in hexane to obtain **7**, as seen in Scheme 1.[47]

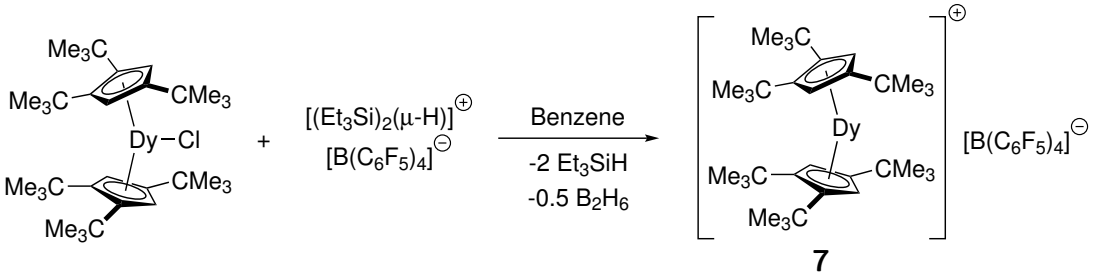

Scheme 1. The synthesis route of **7**.

Complex **7** crystallizes in a triclinic crystal system in the space group $P-1$, and the cation possesses the bent metallocene structure. The asymmetric unit of **7** is shown in Figure 10, where the hydrogen atoms and the disorder are omitted for clarity. The bond lengths between

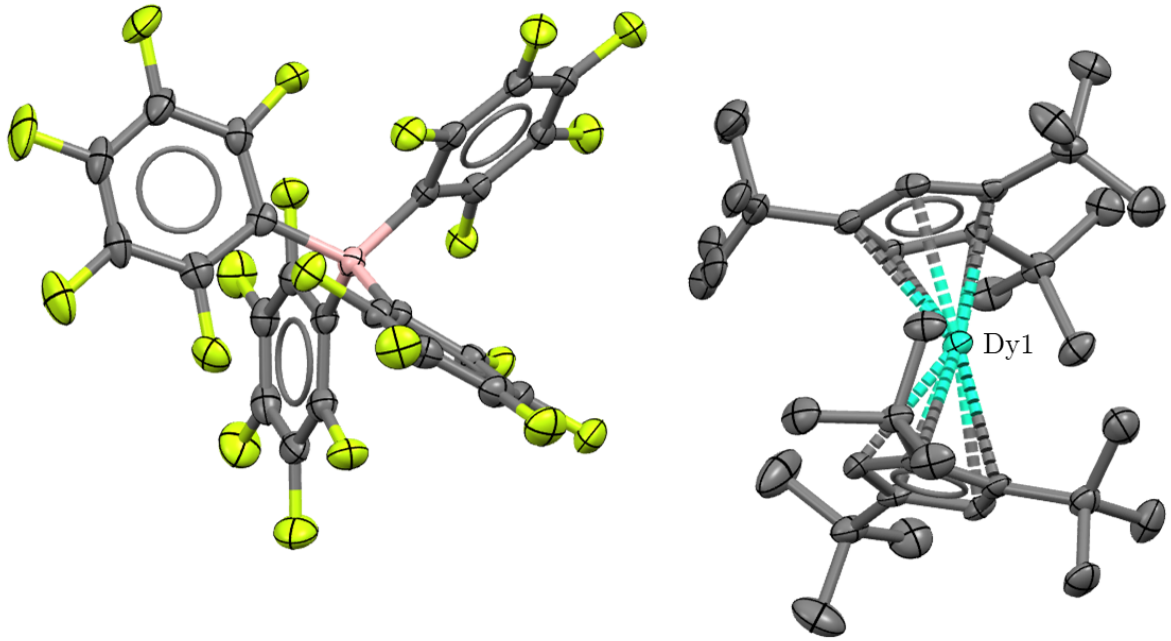

Figure 10. The asymmetric unit of **7**, with the Dy lanthanocene cation on the right and the $[B(C_6F_5)_4]^-$ anion on the left. Hydrogens are omitted for clarity and thermal ellipsoids are drawn at the probability level of 50%. CSD: MEKDOY.[50]

the centroids of the Cp rings and the metal are 2.324(1) Å and 2.309(1) Å. These bond lengths are 0.089-0.104 Å shorter than those of the precursor, making the axial CF of **7** stronger. The Cp^{ttt}–Dy–Cp^{ttt} bond angles between the Cp ring centroids and the metal are 152.845(2)° and 147.59(7) for **7** and the precursor, respectively, which confirms that the CF is less axial in the precursor. This is due to the equatorial ligand Cl in the precursor, which is lacked in **7**.[47]

3.1.2 Magnetic properties

The AC susceptibility studies were utilized to determine the frequency dependent out-of-phase susceptibility $\chi''(\nu)$ in zero applied field using temperatures from 72 to 110 K. χ'' was plotted as a function of the in-phase susceptibility χ', and the obtained data was used to determine the blocking barrier height $U_{eff} = 1277(14)$ cm^{-1}. DC magnetic measurements were employed to determine the temperature at which the relaxation time is 100 s, and the result was 53 K. In addition, this temperature corresponded to the lowest temperature at which the dependence between τ and T showed linear growth. The point where the ZFC and FC susceptibilities diverged, in other words T_{IRREV}, was found at 60 K. The hysteresis loops were measured using an average sweep rate of 39 Oes^{-1}. The complex exhibited an open hysteresis loop up to 60 K, which was very consistent with the T_B and T_{IRREV} results.[47]

Ab initio calculations were performed to explain the relaxation processes and compare the experimental and computational values. It was found that QTM is fully suppressed in the ground m_J Kramer's doublet and only becomes significant in the fourth m_J doublet. However, QTM occurred most probably in the sixth doublet, which was the highest lying excited doublet where any kind of relaxation was presumed to occur. This assumption was made based on the large QTM in the sixth m_J. The calculated barrier height of the sixth m_J doublet state was U_{eff} = 1156 cm^{-1}, which was consistent with the experimentally determined value. The results imply that **7** is very suitable as a SMM, but due to the axial crystal field strength and the U_{eff} barrier height, the complex should be modified so it could function at liquid nitrogen temperatures.[47]

3.2 [(Cp^{iPr5})Dy(Cp*)]$^+$ CATION

3.2.1 Synthetic and structural details

In 2018 a lanthanocene SMM showing magnetic hysteresis up to 80 K was synthesized. This dysprosium based Ln-SMM is very similar to **7**, but instead of the three *tert*-butyl groups in both Cp rings, one Cp ligand is substituted by five *iso*-propyl groups and one by five methyl groups. The complex consist of [(Cp^{iPr5})Dy(Cp*)]$^+$ (**8**) cation (Cp^{iPr5}= pentaisopropylcyclopentadienyl) and a non-coordinating counter anion [B(C$_6$F$_5$)$_4$]$^-$, and it is the first lanthanocene SMM to function above the boiling point of liquid nitrogen (77 K). The synthesis was carried out by first preparing a precursor complex [(η^5-Cp^{iPr5})Dy(η^5-Cp*)(BH$_4$)] by reacting KCp* with [Dy(η^5-Cp^{iPr5})], as seen in Scheme 2. The precursor was then treated with [(Et$_3$Si)$_2$(μ-H)][B(C$_6$F$_5$)$_4$] to obtain **8** in 60% yield.[51]

Complex **8** crystallizes in a monoclinic crystal system in the space group $P2_1/c$ and the asymmetric unit is shown in Figure 11. The hydrogen atoms and the disorder are omitted for clarity. The bond lengths between the metal and the centroids of the Cp rings are 2.284(1) Å and 2.296(1) Å for Cp^{iPr5} and Cp*, respectively, both of which are shorter than the Dy–Cp lengths in **7**. The bond angle between the Cp ring centroids and the metal (Cp^{iPr5}–Dy–Cp*)

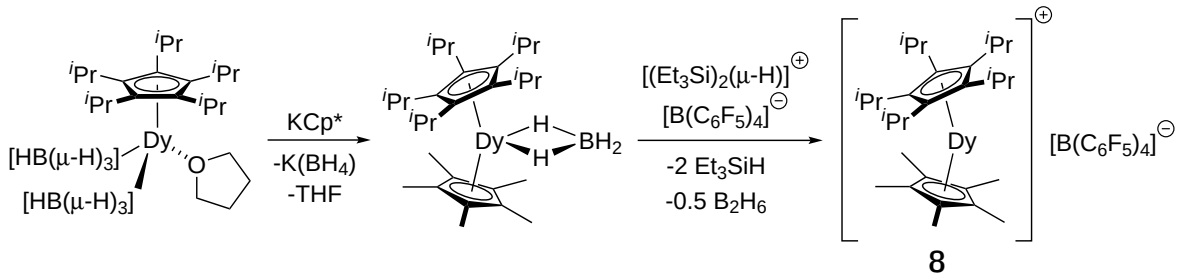

Scheme 2. The two-step synthesis route of **8**.

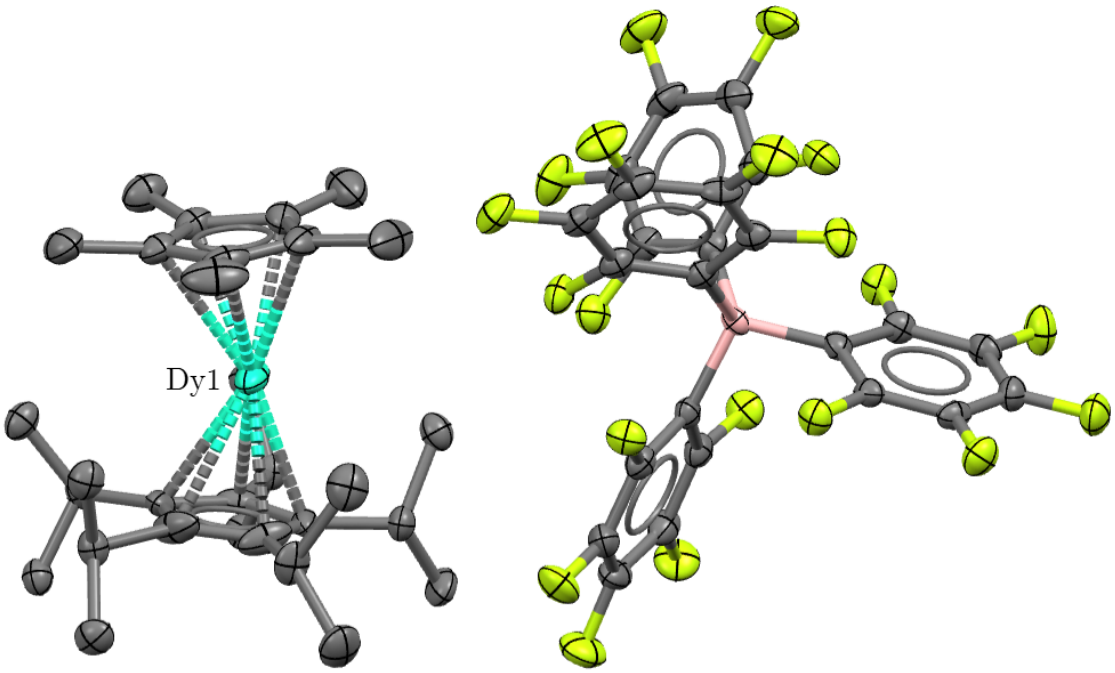

Figure 11. The asymmetric unit of **8**, with the Dy lanthanocene cation on the left and the $[B(C_6F_5)_4]^-$ anion on the right. Hydrogens and disorder are omitted for clarity and thermal ellipsoids are drawn at the probability level of 50%. CSD: LIRQUB.[51]

is 162.507(1)°, implying that the CF is more axial than in **7**. The differences in the structural parameters between **8** and **7** are 9.662 ° and 0.013 - 0.040 Å, which could be one of the reasons why the blocking temperature of **7** is 20 K smaller than that of **8**.[51]

3.2.2 Magnetic properties

The SMM properties were characterized by measuring the χ' and χ'' susceptibilities in AC field, with zero DC field, as a function of temperature and frequency. The susceptibility data was used to determine the temperature dependent relaxation rates, giving τ = 50 s in 77 K and τ = 500 min at 15 K. Relaxation time of 100 s was found at the temperature of 65 K. The relaxation rate showed strong linear temperature-dependence above 55 K and temperature-independence below 10 K. The experimentally determined U_{eff} energy barrier reached the value of 1541(11) cm^{-1}. Compared to **7**, the blocking barrier of **8** is noticeably higher, which could also explain the difference in the blocking tempeartures.[51]

The hysteresis loops were measured using sweep rates from 25 Oe s^{-1} to 700 Oe s^{-1} at different temperatures. With a sweep rate of 200 Oe s^{-1} the hysteresis loop remained open up to 85 K, and with the slowest sweep rate of 25 Oe s^{-1} the loop closed after surpassing 80 K. The ZFC and FC susceptibility measurements at variable temperatures gave T_{IRREV} = 78 K.[51]

Ab initio calculations were performed to explain the relaxation processes and compare the experimental and computational values. According to the results, the relaxation proceeds from the fourth excited m_J doublet state correspondent to U_{eff} = 1524 cm^{-1} via Orbach process. The U_{eff} value correlates remarkably well with the experimentally determined value, with the difference of only 17 cm^{-1}. Conclusively, **8** is more linear and has shorter axial bonds and higher U_{eff} barrier than **7**, making the axial CF and the magnetic properties of **8** stronger. The complex is also undoubtedly suitable for SMM applications at liquid nitrogen temperatures.[51]

3.3 $[Tb(Cp^{ttt})_2]^+$ CATION

3.3.1 Synthetic and structural details

In 2018, a terbium based lanthanocene complex consisting of a $[Tb(Cp^{ttt})_2]^+$ cation and a $[B(C_6F_5)_4]$ anion was synthesized. The magnetic properties of this complex were of great interest after the discovery of **7**, which showed excellent SMM properties. The synthesis was initiated by preparing $[Tb(BH_4)_3(THF)_3]$ from TbI_3 and an excess of KBH_4 (Scheme 3). The product was then treated with KCp^{ttt} to yield a precursor complex $[Tb(Cp^{ttt})_2(BH_4)]$ (**9**) via a salt metathesis reaction. Finally, the precursor was treated with $[Ph_3C][B(C_6F_5)_4]$ in benzene to yield the targeted product $[Tb(Cp^{ttt})_2][B(C_6F_5)_4]$ (**10**).[52]

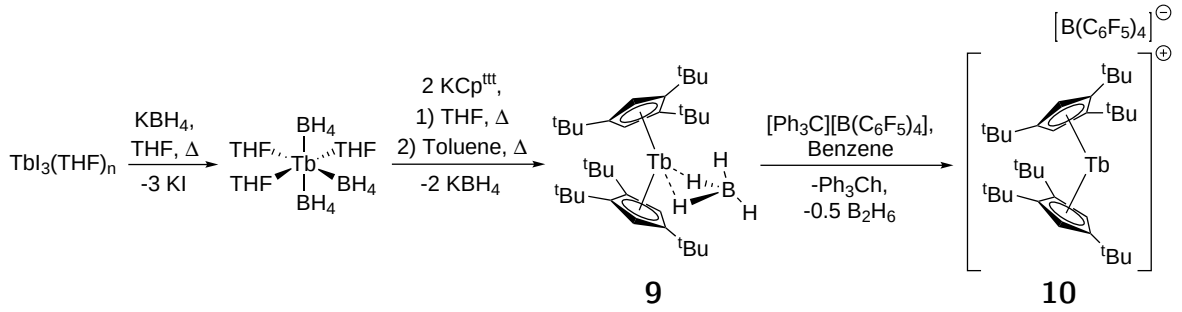

Scheme 3. The two-step synthesis route of **10**.

Complex **10** was crystallized from a dichloromethane (DCM) solution layered with hexane to obtain single crystal for X-ray measurements. The XRD data indicated that **10** crystallizes in the triclinic crystal system in the space group *P-1*. The asymmetric unit consists of the anion-cation pair and is presented in Figure 12, where the disorder and hydrogens are omitted for clarity.[52]

The Tb–Cp (centroid) bond lengths for **10** are 2.325 Å and 2.339 Å, which are 0.001-0.03 Å longer than those of the analoguous Dy complex **7**. The Cp–Tb–Cp (centroid) bond angle is 152.23 °, and it is 0.615 ° smaller than that of **7**. The bond parameters of the complexes

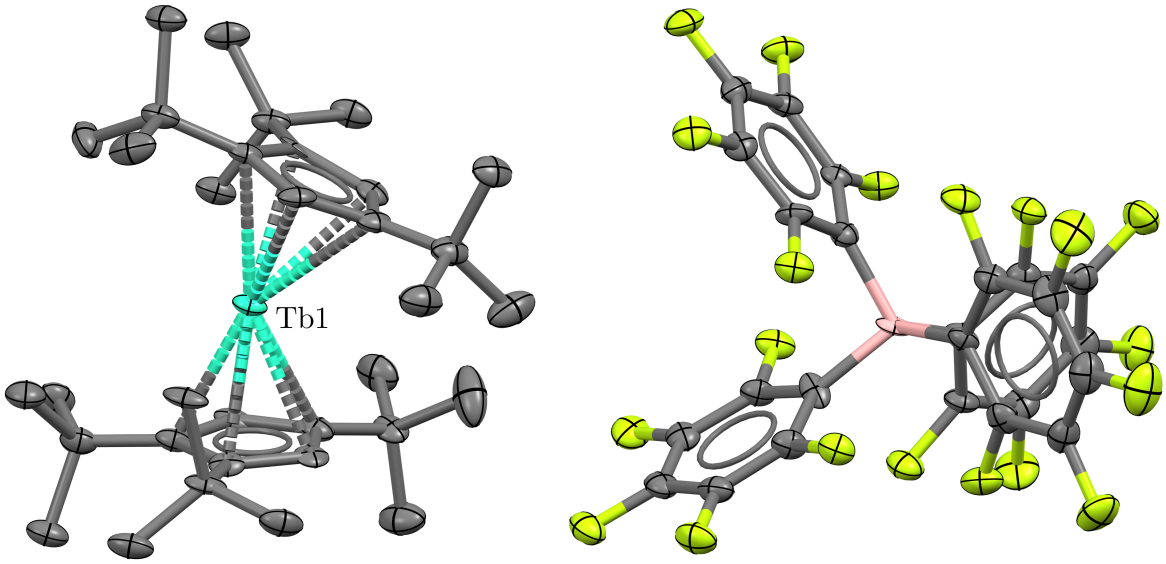

Figure 12. The asymmetric unit of **10**, with the Tb lanthanocene cation on the left and the $[B(C_6F_5)_4]^-$ anion on the right. Hydrogens and disorder are omitted for clarity, and thermal ellipsoids are drawn at the probability level of 30%. CSD: UFASUS.[52]

are very similar to each other and neither of them exhibit interactions between the Ln^{3+} center and the $[B(C_6F_5)_4]^-$ anion, but the axial CF of **7** is slightly stronger.[52]

Furthermore, single crystal XRD measurements were done for the precursor **9**, and the data revealed the Tb–Cp (centroid) bond lengths to be 0.076-0.095 Å longer compared to **10**. The Cp–Tb–Cp (centroid) bond angle was 4.1 ° smaller in **9** and it is apparent that the differences between **9** and **10** are even greater than between **7** and **10**.[52]

3.3.2 Magnetic properties

The magnetic properties of **9** and **10** were measured with a SQUID magnetometer from polycrystalline samples. The AC susceptibility studies were done for **9**, which gave no out-of-phase χ'' signal in zero field. The precursor showed signs of slow magnetic relaxation under 0.1 T applied field, however, tha data indicated temperature-dependent relaxation above 6 K, and the relaxation was suggested to proceed via QTM. The data that was obtained above 6 K was used to determine the U_{eff} barrier height, which was only 29 cm^{-1}.[52]

The AC susceptibility measurements for **10** showed that the complex exhibits slow magnetic relaxation in zero field. However, the hysteresis loop measurements using mean field sweep rate of 21(8) Oe s^{-1} at variable temperatures did not show open hysteresis even at 2 K. In addition, the blocking barrier height was only $U_{eff} = 6.8$ cm^{-1} and the FC and ZFC measurements showed no clear maximum above 2 K.[52]

The complete active space self-consistent field spin-orbit (CASSCF-SO) calculations were established for the precursor and the complex, both of which showed near-degenerate pseudo-doublets in their ground states. In case of **9**, the most excited states resembled pseudo-doublets with the m_J value of ±6, which was also calculated to be the m_J value of the ground

state doublet. However, the first excited state was dominated by the $m_J = \pm 5$ state. Furthermore, all the m_J states were suggested to be quantised along an axial vector (Cp–Tb–Cp direction) in the ground state, and an equatorial vector in the most excited states. As for **10**, the ground state $m_J = \pm 6$, as well as the four lowest lying excited states were all quantised along an axial vector. For both **9** and **10** the ground state was mixed between the positive and negative ground states in zero field, which occurs due to the non-Kramers nature of Tb^{3+}.[52]

The results suggest that no magnetic blocking occurs for either **9** or **10**. The non-Kramers nature of Tb3+ is supposedly the reason for this unexpectedly large difference between the magnetic properties of **10** and **7**. Non-Kramers ions require very high symmetry and axiality of the CF, and the degeneration of the states is not quaranteed. Thus, the ground state can be mixed between the two states, which enhances QTM and weakens the slow magnetic relaxation. This does not occur in the Dy analogue due to the Kramers nature of Dy^{3+} ion. In conclusion, neither **9** nor **10** are good SMMs due to the lack of magnetic blocking, which results in an open hysteresis loop.[52]

3.4 $[Dy(Cp^{iPr_4R})_2]^+$ CATIONS

3.4.1 Synthetic and structural details

A series of Cp^{iPr_4} (tetraisopropylcyclopentadiene) based dysprosocenium salts was synthesized in 2018 to shed more light on the Cp substituent effects on the magnetic properties. It was hypothesized that adding more rigid substituents to the Cp–H positions could prevent equatorial ligands from coordinating and improve magnetic relaxation and T_B. The synthesized complexes $[Dy(Cp^{iPr_4R})_2][B(C_6F_5)_4]$ (R = H (**11**), Me (**12**), Et (**13**), *i*Pr (**14**)) were all synthesized via similar route, which is presented in Scheme 4. First, a precursor $[Dy(Cp^{iPr_4R})_2I]$ was synthesized

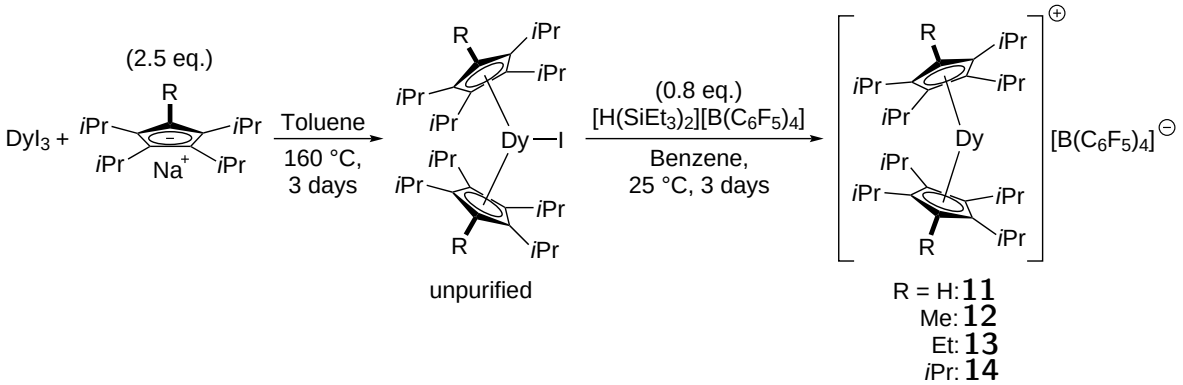

Scheme 4. The synthesis route of **15**.

by refluxing a mixture of DyI_3 and $NaCp^{iPr_4R}$ in toluene for three days. The precursor was then reacted with $[H(SiEt_3)_2][B(C_6F_5)_4]$ in benzene, and the mixture was stirred at 25 °C for three days to obtain products **11**-**14** via halide abstraction. The products were recrystallized from a DCM solution that was layered with pentane, and good quality single-crystals were obtained.[53]

The crystal structures for complexes **11**-**14** were obtained by single-crystal X-ray diffraction analysis, and the crystal structure of **13** is presented in Figure 13. Hydrogens and disorder are omitted for clarity, and only one of the four structures is presented, as all the complexes have very similar structures. Complexes **11** and **12** crystallize in the monoclinic crystal system in the space groups $P2_1$ and $P2_1/c$, respectively, and their asymmetric units consist of two anion-cation pairs. The asymmetric units of **13** and **14** consist of only one anion-cation pair and they both crystallize in the monoclinic crystal system in the space group $P2_1/n$.[53]

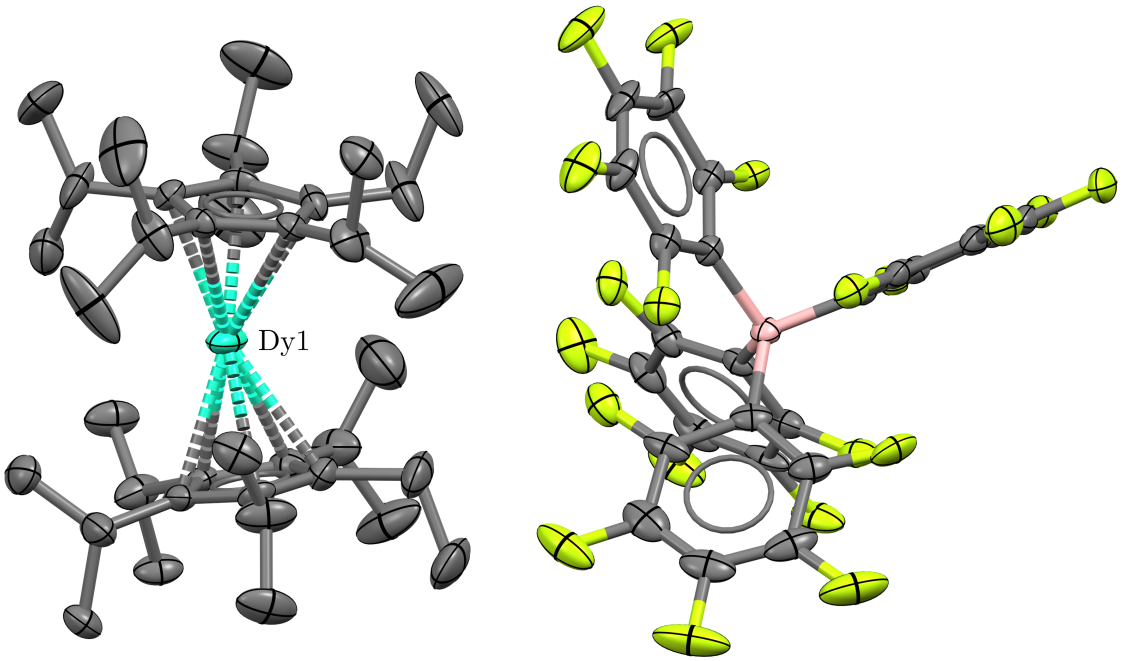

Figure 13. The asymmetric unit of **13**, with the Dy lanthanocene cation on the leftt and the $[B(C_6F_5)_4]$ anion on the right. ydrogens and disorder are omitted for clarity, and thermal ellipsoids are drawn at the probability level of 30%. CSD: WIRHEN.[53]

The Dy–Cp (centroid) distances vary from 2.27(1)–2.30(1) Å, 2.273(3)–2.382(3) Å, 2.297(4)–2.306(4) Å and 2.245(15)–2.392(16) Å for **11**-**14**, respectively. The scale of distances in **14** is quite large, but it is in agreement with the Dy–Cp$^{i\mathrm{Pr}_5}$ (centroid) distances in **8**. When comparing the mean values of the aforementioned distances in **11**-**14**, a very small increase in the bond lengths can be observed when adding more bulky R-group substituents, except for **12**, the mean value of which exceeds the others. However, when measuring the Dy–Cp (centroid) bond lengths for only the major (highest occupancy) components of the structures, the mean values are 2.29(1) Å, 2.298(5) Å, 2.302(6) Å and 2.340(7) Å for **11**-**14**, respectively, and a more clear trend of bond elongation can be observed. Moreover, the mean values for the Cp–Dy–Cp (centroid) bond angles are 147.2(8) °, 156.6(3) °, 161.1(2) ° and 162.1(7) for **11**-**14**, respectively, and a clear trend of bond angle opening when increasing steric bulk is observed. The difference between the bond angles in the complexes is further highlighter in Figure 14, where the Cp substituents are omitted for clarity and the centroids of the Cp rings are presented as orange opaque balls.[53]

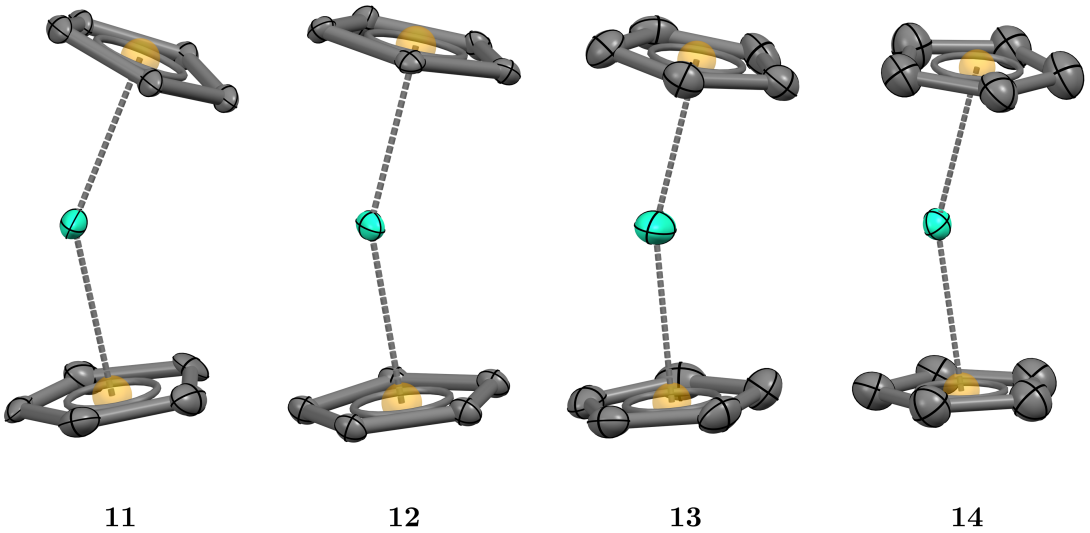

Figure 14. Comparison of the Cp–Dy–Cp (centroid) bond angles in complexes **11** (Cp^{iPr_4H}), **12** (Cp^{iPr_4Me}), **13** (Cp^{iPr_4Et}) and **14** (Cp^{iPr_5}).

3.4.2 Magnetic properties

The SMM properties were determined experimentally, and a SQUID magnetometer was used for the measurements. The DC susceptibility studies were established in an external magnetic field of 1000 Oe using temperatures from 2 to 300 K. The $\chi_M T$ values that were obtained showed nearly linear decrease when lowering the temperature, and a steep drop was observed at very low temperatures, which indicates that magnetic blocking is occuring in all complexes from **11** to **14**. Low temperatire DC susceptibility data was exploited to obtain the temperatures at which the relaxation time is 100 s, which yielded T_B values of 17, 62, 59, 56 K for **11**-**14**, respectively. The AC susceptibility studies were done in zero applied field using temperatures from 70 to 114 K, and the χ' and χ'' data were received. The blocking barrier heights for **11**-**14** were derived from the fitted AC susceptibility data, giving the U_{eff} values 1285, 1468, 1380 and 1334 cm^{-1}, respectively. None of the values surpasses that of **8**, but all of them have higher barrier heights than **7**.[53]

The FC and ZFC susbeptibilities were measured using an applied field of 1000 Oe, and the results suggested that all four complexes have magnetic memory. The temperatures at which the FC and ZFC susceptibilities diverge were found at $T_{IRREV} = 28$, 65, 60 and 60 K for **11**-**14**. The differences across the series indicate that changing the substituents of the Cp ring can drastically alter the magnetic properties of a complex. The T_{IRREV} values across the series were very similar to that of **7** (60 K), except the value of **11**, which was found to be much smaller. In addition, none of the $TIRREV$ values exceeded that of **8**, which has the highest $TIRREV$ and T_B values so far.[53]

The magnetic hysteresis data was recorded using temperatures from 2 to 72 K and a field sweep rates of 31 and 132 Oes^{-1} at different applied fields. The temperatures at which the

hysteresis loop stayed open for **11**-**14** were 32, 72, 66 and 66 K, respectively, and the results are consistent with the T_{IRREV} and hundred-second T_B values. The hysteresis studies suggest that complexes **12**-**14** can function at even higher temperatures than **7**, but not quite at the liquid nitrogen boiling point, which is 77 K.[53]

In conclusion, changing the R-group substituent in the Cp ring does not affect the Dy–Cp distances very significantly, but it has a great impact on the Cp–Dy–Cp bond angles. Morevoer, these structural parametes have a notable effect on the magnetic properties, which arise from the interplay of both bond distances and angles. Complex **11**, for instance, has the shortest Dy–Cp (centroid) bond distances due to least steric crowding. On the other hand, it has the largest Cp–Dy–Cp (centroid) bond angle, which seems to affect the T_B values of the complex significantly. The most well-performing complex across the series was **12**, which did not have the shortest bond lengths or the largest bond angle. These results suggest that the substituents should be carefully chosen, as the increse in steric bulk yields in more linear molecules but simultaneously longer bond lengths.[53]

3.5 $[Dy(Dtp)_2]^+$ CATION

3.5.1 Synthetic and structural details

A dysprosium based SMM was synthesized in 2019 using Cp derivatives, phospholyls, as the pentahapto coordinated ligands. The complex **15** consists of a $[Dy(Dtp)_2]^+$ cation (Dtp = $P(C^tBuCMe)_2$)and a non-coordinating counter anion $[AlOC(CF3)3_4]^-$. A phospholyl is similar to the Cp ring with one carbon atom replaced by a phosphorus atom. In **15** the phospholyl is substituted with two ^{t}Bu groups and two methyl groups.[54] Phospholyls have been used to obtain Ln sandwich complexes, because they are known to maintain the η^5-coordination well with lanthanoids due to the soft nature of the free electron pairs of phosphorus.[55,56]

The synthesis route of **15** is presented in Scheme 5, where $[Dy(Dtp)_2I]$ was first treated with C_3H_5MgCl in toluene by a salt metathesis reaction. The $[Dy(Dtp)_2(C_3H_5)]$ obtained from the metathesis reaction was used *in situ* and reacted with $[NEt_3H][Al\{OC(CF_3)_3\}_4]$ in benzene to obtain **15**.[54]

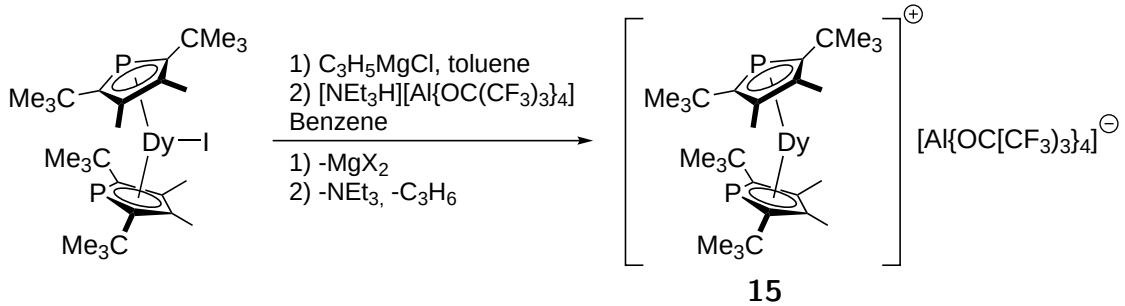

Scheme 5. The synthesis route of **15**.

Complex **15** crystallizes in a monoclinic crystal system in the space group $P2_1/c$ and

the asymmetric unit is shown in Figure 15. Hydrogens and disorder are omitted from the figure for clarity. The mean bond length between the centroids of the Dpt ligands and the metal is 2.353

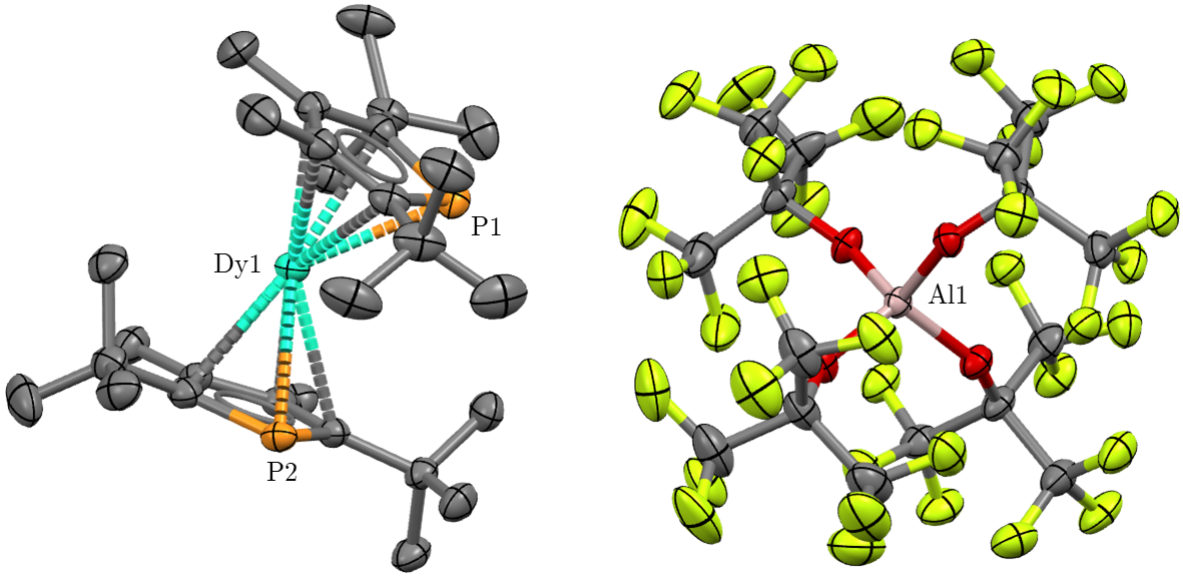

Figure 15. The asymmetric unit of **15**, with the $[Dy(Dtp)_2]^+$ cation on the leftt and the $[AlOC(CF3)3_4]^-$ anion on the right. Hydrogens and disorder are omitted for clarity, and thermal ellipsoids are drawn at the probability level of 50%. CSD: DUBKET.[54]

Å. The Dpt–Dy–Dpt bond angle measured from the centroids of the Dpt rings is 157.94(4)°. Adding the phosphorus atom into the Cp ring affects the bond parameters, comparing to **7**, which also possesses ^{t}Bu groups. The L–M–L bond angle is increased in **15**, which strengthens the axial field. In contrast, the L–M bond lengths are also increased, which weakens the axial field. The difference between the bond lengths in **7** and **15** falls between 0.030 Å and 0.045 Å, which are larger values than between **8** and **7**.[54]

3.5.2 Magnetic properties

The SMM properties were determined both experimentally and computationally. A SQUID magnetometer was employed to determine the temperature-dependent molar magnetic susceptibility $\chi_M T$ at 300 K, which was then plotted as a function of temperature. The curve showed near linear decrease down to 25 K, below which the decrease was drastic. This indicates the magnetic blocking below 25 K and the result is consistent with the ZFC susceptibility peak at 25 K. Furthermore, these results coincide with the temperature at which the relaxation time is 100 s, which was directly measured at 23 K. The temperature at which magnetic memory can still be observed, in other words the point where the FC and ZFC susceptibilities diverge, was found at $T_{IRREV} = 54$ K.[54]

The AC susceptibility studies in zero applied field were utilized to determine the χ' and $\chi''(\nu)$ susceptibilities using temperatures from 60 to 80 K. The data from these measurements was then exploited to determine the blocking barrier height, which was $U_{eff} = 1220(50)$

cm^{-1}. The value was very similar to that of **7** with the difference of only 57 cm^{-1}. The hysteresis loops were measured using an average sweep rate of *ca.* 39 Oes^{-1}. The complex exhibited an open hysteresis loop up to 48 K, which agreed with the and T_{IRREV}, but not with the T_B results. The blocking temperature is 12 K lower than that of **7** despite the fact that the U_{eff} values are very similar.[54]

Ab initio calculations were performed to explain the relaxation processes and compare the experimental and computational values. The relaxation by Orbach process was found to proceed via the seventh m_J Kramer's doublet which has the U_{eff} value of approximately 1190 cm^{-1}. The value is greater than that of **7**, which is due to the excitation from a higher m_J doublet state in **15**. Nonetheless, more detailed calculations of the energy gaps between adjacent m_J doublet states in both complexes revealed the relaxation in **7** to be more efficient.[54]

In conclusion, even though **15** has parameters very similar to **7**, the small differences between the axial crystal field strengths, the U_{eff} values, and the energy gaps between the adjacent m_J doublets are most likely one cause for the larger difference between the hysteresis loops and T_Bs.[54]

4 DIVALENT LANTHANOCENE SINGLE-MOLECULE MAGNETS

The divalent lanthanocene SMMs are not yet very prominent, as the trivalent species is much more dominant in the Ln series and the divalent species is very well known as highly reducing compounds that are profoundly reactive. Thus, their physical properties, such as magnetism, were unexplored for a long time. However, a few recent studies of divalent Ln complexes have shown that they can possess an electron configuration $4f^n5d^1$. This observation can show promise in the synthesis of highly symmetric complexes, as the 5d electrons can bond covalently while the 4f electrons retain the anisotropy. This allows very symmetric, linear molecules, which are required specially for non-Kramer's ions that do not necessarily have degenerate m_J doublets. The design and synthesis of divalent Ln sandwich complexes with magnetic properties has been provoked by these findings.[57,58]

4.1 $Tb(Cp^{iPr_5})_2$ AND $Dy(Cp^{iPr_5})_2$

A divalent lanthanocene SMM with Tb^{2+} was synthesized in 2019, and it possessed a strikingly high blocking barrier and a blocking temperature of 52 K(τ = 100 s). This discovery had a great impact on the potential uses of Ln^{2+} metals, as there are not many divalent lanthanocene SMMs and the T_B value was the highest value so far for any non-dysprosium SMM. The compound consists of a central Tb^{2+} ion sandwiched between two Cp^{iPr_5-} ions, resulting in the neutral $Tb(Cp^{iPr_5})_2$ (**17**) lanthanocene. In addition, a dysprosium version $Dy(Cp^{iPr_5})_2$ (**18**) and a trivalent $[Tb(Cp^{iPr_5})_2][B(C_6F_5)_4]$ (**16**) complex were synthesized for comparison. All three

compounds were synthesized using the same precursor $Ln(Cp^{iPr_5})_2(I)$ (Ln = Tb, Dy), which was obtained by reacting trivalent LnI_3 with sodiated Cp^{iPr_5}. The precursor was reduced with potassium graphite (KC_8) in benzene to obtain the divalent species, and with $[H(Et_3Si)_2][B(C_6F_5)_4]$ in benzene to obtain the trivalent species. All synthesis routes can be seen in Scheme 6.[57]

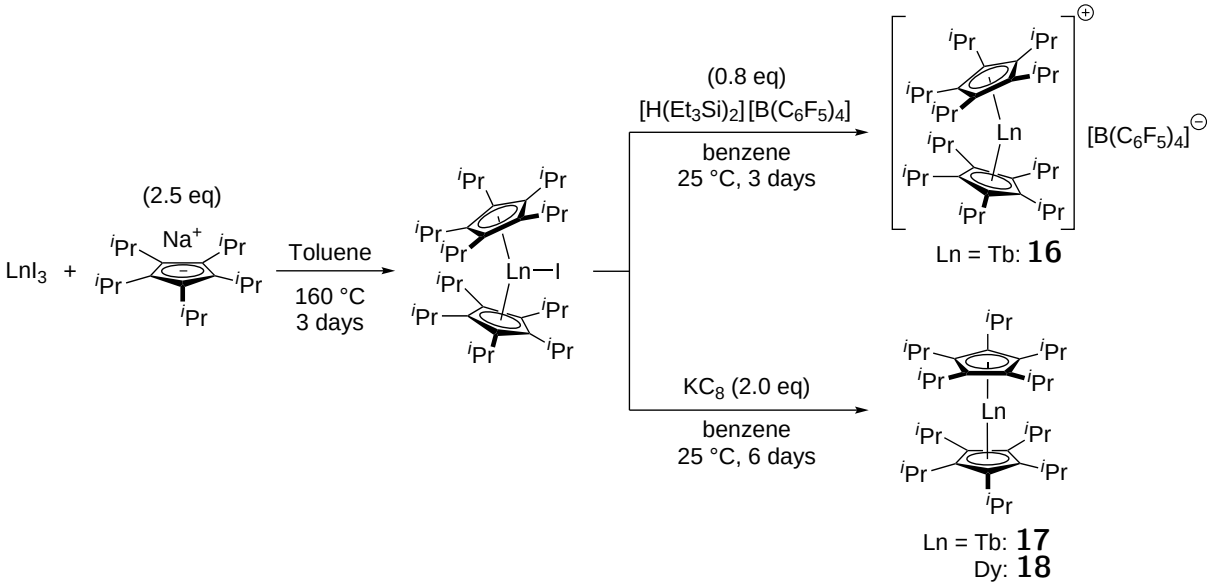

Scheme 6. The synthesis routes of **16**, **17** and **18**.

Complex **17** crystallizes in a monoclinic crystal system in the space group $P2_1/c$. The asymmetric unit of consists of the Tb metal and one ligand, and it is shown in Figure 16 beside the whole sandwich structure. Hydrogens are omitted from the figure for clarity, and as can be seen, the sandwich complex has linear symmetry, which indicates a very strong axiality. In fact, the Cp–Ln–Cp bond angles for both **17** and **18** are 180 °, as the metal atoms reside on an inversion center. The Ln–Cp bond lengths (centroid) were 2.416(1) Å and 2.385(1) Å for **17** and **18**, respectively.[57]

Comparison between the structures of **16** and **17** can be seen in Figure 16. For **16** the Cp–Tb–Cp bond angle measured from the centroids of the ligands is 159.8(4) °, which clearly makes the complex much less linear compared to **17**. The Tb–Cp bond length (centroid) is 2.356(6) Å, which indicates the lengthening of the bonds after reduction.[57] Comparing the bond lengths (centroid) in **18** and its trivalent analogue $[Dy(Cp^{iPr_5})_2]^+$ $[B(C_6F_5)_4]^-$ (lengths on a scale of 2.245(15) – 2.392(16) Å), it is most probable that bond lengthening occurs after the reduction of Dy^{3+}. However, giving that the maximum length of the trivalent analogue is 2.392 Å, shortening of the bond could also occur.[53]

DFT calculations were performed for **17** and **18** to determine the electron configuration, which was $4f^n5d^1$. The calculations also revealed slight 6s orbital character due to mixing of s and d orbitals. The calculations support the lenghtening of the bonds after reduction, as well as the linear structures associated with the covalent interactions of 5d orbitals.[57]

The AC susceptibility studies were conducted to determine the frequency dependent

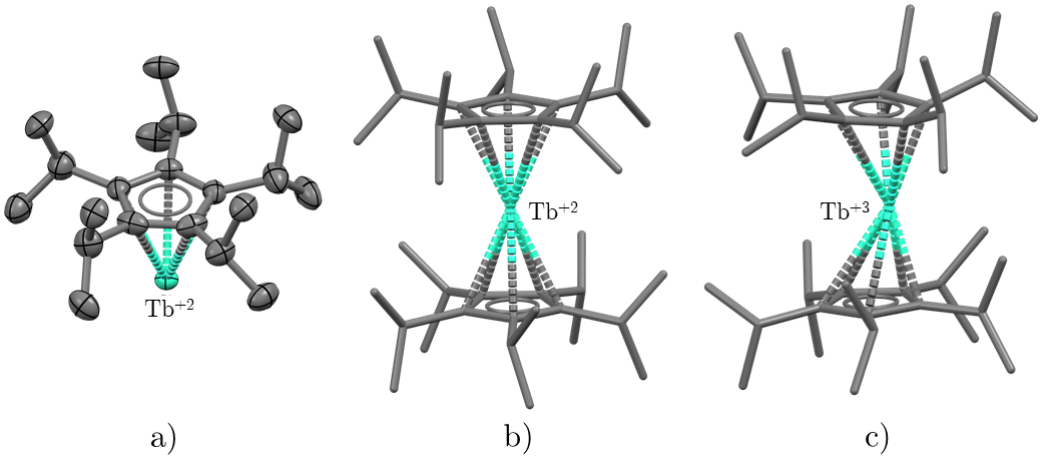

Figure 16. a) The asymmetric unit of **17**, where thermal ellipsoids are drawn at the probability level of 75% (CSD: BOLQAX). The structures of b) complex **17** and c) **16** (CSD: BOLQEB). The structure of **17** is linear, while in **16** the metal lies off-center from the nearly parallel Cp ligands.[57]

out-of-phase susceptibility χ'' in zero applied field. The χ'' data of **16** exhibited peaks from 2 to 40 K, which indicated slow relaxation of the magnetization in that T region. For **17** the region of the peaks was from 74-92 K, which is much higher than for **16**. DC magnetic measurements were employed to determine the temperature at which the relaxation time is 100 s, and the result was 52 K. The relaxation times for **17** were determined to be more than 5 orders of magnitude higher than for **16**. In addition, the susceptibility data was used to determine the U_{eff} barrier value in an Orbach process for **17**, which was 1205 cm^{-1}.[57]

The magnetic hysteresis loops were measured using a sweep rate of 103 Oes^{-1} for **16**, and 39 or 147 Oes^{-1} for **17**. The measurements showed remarkable hysteresis for **17**, which stayed open up to 55 K in zero field. In contrast, **16** did not exhibit open hysteresis loop even at 2 K.[57]

The DC magnetic measurements for **18** using an external field of 1000 Oe showed no slow magnetic relaxation past the relaxation time of 50 s. However, a blocking temperature of 5 K was extracted from the obtained data. The magnetic hysteresis loop was measured using the same sweep rates as for **17**, which resulted in an open loop up to 10 K in zero field.[57] In contrast, the hysteresis loop of the trivalent analogue of **18** stays open up to 66 K in zero field, with the similar sweep rates of 31 or 132 Oes^{-1}.[57]

In conclusion, the reduction of Tb^{3+} to Tb^{2+} greatly enhances the magnetic properties such as the T_B and the U_{eff}. This trend is reversed for the Dy derivatives, and the magnetic properties decrease after reduction. This can be explained by the electron configuration, as well as the fact that the trivalent Tb ion is not a Kramer's ion, but the divalent one is. This is also reversed for Dy, and hence this emphasizes the importance of the Kramer's nature in SMMs. Although the electron configuration in the divalent species allows a completely linear and axial crystal field, the significance is smaller than the Kramer's nature, as the T_B decreases drastically

in the linear divalent Dy complex compared to the trivalent one.[57]

5 TRIVALENT LUMINESCENT CYCLOPENTADIENYL-BASED LANTHANOID COMPLEXES

The luminescence properties of Ln^{3+} and Ln^{2+} ions differ greatly due to their electronic structures. As discussed earlier, the Ln^{3+} ions show characteristic sharp emission and excitation bands due to their parity-forbidden 4f-4f transitions, resulting in poor quantum yields. These transitions often require the utilization of electron density donating antenna ligands that sensitize the Ln luminescence.[59,60] On the other hand, Ln^{2+} ions show allowed 5d-4f transitions, which are observed as more broad bands in the emission and excitation spectra. This d-orbital character in Ln^{2+} based compounds gives rise to increasing covalency in the metal-ligand interactions, which are absent in the Ln^{3+} compounds. Weaker metal-ligand interactions yield in less intense luminescence, which means more Ln sensitization in required.[61] The Ln sensitizing can be achieved by using different antenna-ligands, which are often σ-bonded ligands such as N- or O-donors.[62] This review however will focus on σ-bonding ligands, and more precisely polyphenyl-substituted cyclopentadienyl ligands, which have been reported to be very promising antenna ligands in the Ln complexes.[10]

5.1 POLYPHENYL-SUBSTITUTED CYCLOPENTADIENYL TERBIUM AND GADOLINIUM COMPLEXES

In 2018 a very broad study on the possibilities of applying π-type ligands in luminescent organolanthanoid coordination compounds was conducted. The study concentrated on the synthesis and characterization of several different polyphenyl-substituted Cp ligands that could work as light harvesting antenna ligands to enhance the luminescence of the lanthanoids. Non-, di-, tri- and tetraphenyl-substituted cyclopentadienyls were used with Tb^{+3} and Gd^{+3} lanthanoids and their results were compared.[60]

5.1.1 Synthetic details

The non-substituted cyclopentadienyllanthanoid (CpLn) complexes of Tb and Gd were synthesized using lanthanoid trichlorides bearing THF-adducts and sodium cyclopentadienide (NaCp), as seen in Scheme 7. Products $CpTbCl_2(THF)_3$ (**19**), $Cp_2LnCl(THF)$ where Ln = Tb (**20**), Gd (**21**) and $Cp_3Ln(THF)$ where Ln = Tb(**22**), Gd (**23**) were obtained, in which THFs are coordinated to the lanthanoid centers, possibly due to the lack of steric bulk in the non-substituted Cp rings.[60]

The di-substituted CpLn complexes of Tb and Gd were synthesized in the same manner, but potassium diphenylcyclopentadienide ($KCpPh_2$) was used instead of NaCp, as

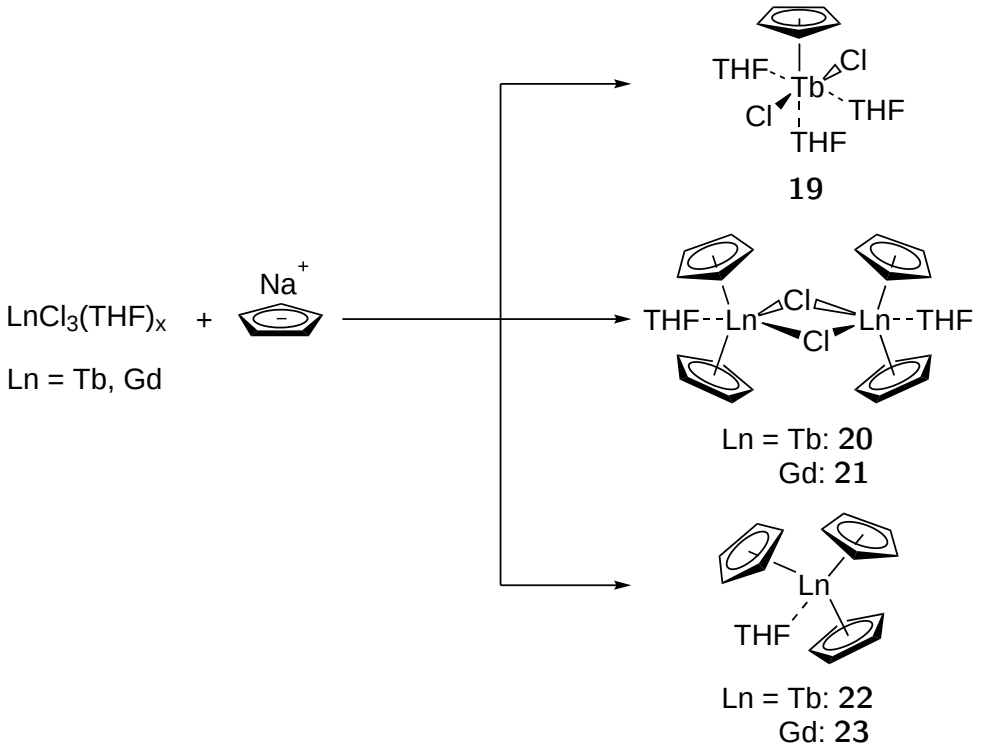

Scheme 7. The synthesis of CpLn complexes **19**, **20**, **21**, **22** and **23**.

seen in Scheme 8. The potassium salt of the $CpPh_2$ was synthesized *in situ* from the hydrogenated ligand and benzyl potassium. The potassium salts of $CpPh_3$ and $CpPh_4$ were generated in the same manner. Products $(CpPh_2)LnCl_2(THF)_3$ where Ln = Tb (**24**), Gd (**25**), $[(CpPh_2)_2LnCl_2K(THF)]_n$ where Ln = Tb (**26**), Gd (**27**), and $(CpPh_2)_3Tb$ (**28**) were obtained. Both the mono- and diligated Ln complexes contain coordinated THF molecules, but the triligated **28** does not, due to the steric bulk of the six phenyl rings around the Ln ion. In addition, **26** and **27** form coordination polymer structures, while all the other complexes are mononuclear.[60]

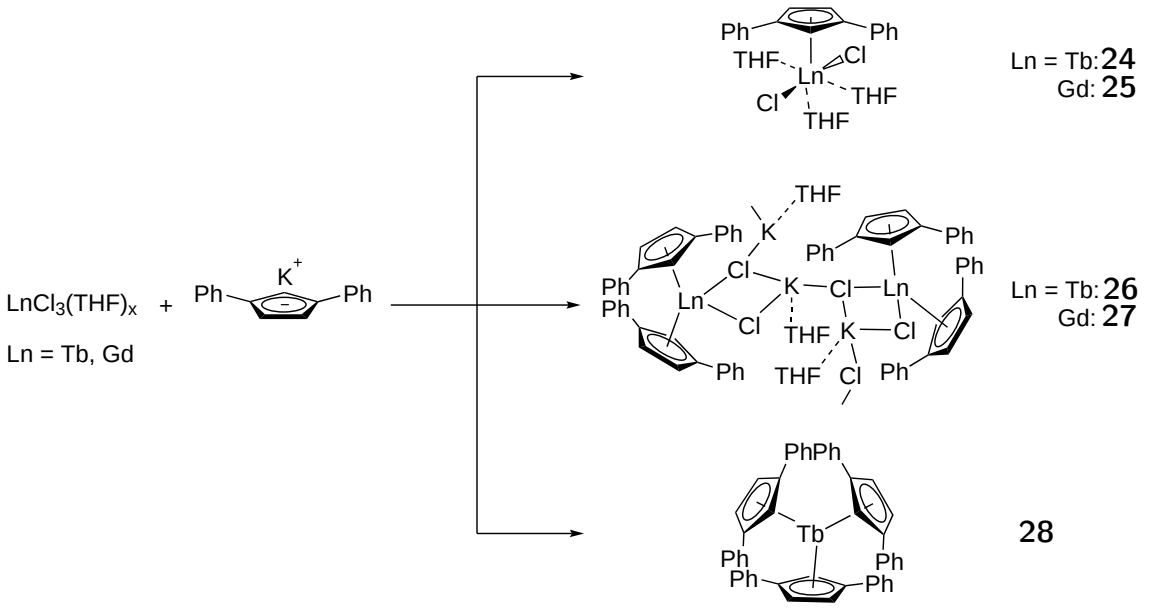

Scheme 8. The synthesis of CpLn complexes **24**, **25**, **26**, **27** and **28**.

The syntheses of the tri-substituted CpLn complexes of Tb and Gd were done similarly to the previous syntheses by reacting $LnCl_3(THF)_x$ and $KCpPh_3$, as seen in Scheme 9. Products $[\{(CpPh_3)Ln(THF)\}_2(\mu\text{-}Cl)_5K(THF)]_2$ where Ln = Tb (**29**), Gd (**30**) and $[(CpPh_3)_2Ln(\mu\text{-}Cl)_2K]_2$ where Ln = Tb (**31**), Gd (**32**) were obtained. Complexes **29** and **30** form tetranuclear ate complexes, while **31** and **32** are binuclear ate complexes. Triligated CpLn complexes with $CpPh_3$ were not obtained due to the larger steric bulk of the ligands.[60]

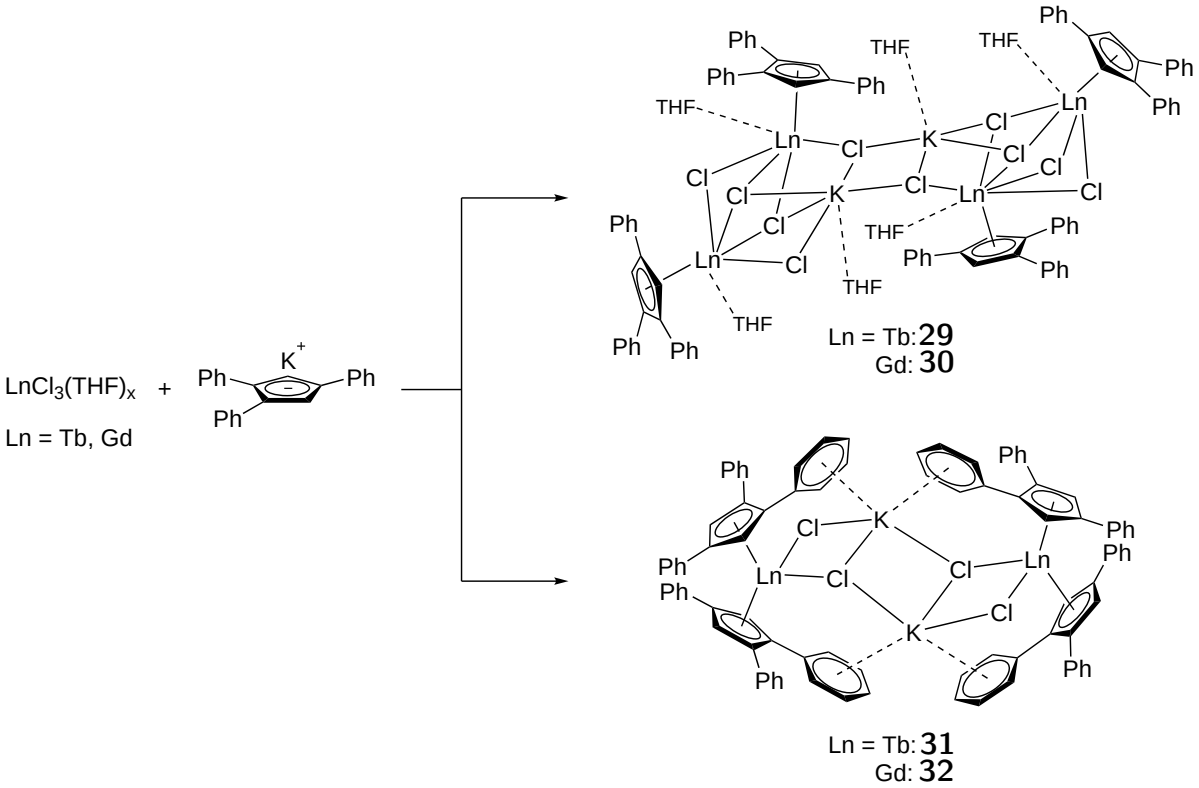

Scheme 9. The synthesis of CpLn complexes **29**, **30**, **31** and **32**.

The syntheses of the tetra-substituted CpLn complexes of Tb and Gd were done in the same manner as the previous ones by reacting $LnCl_3(THF)_x$ and $KCpPh_4$, as seen in Scheme 10. Products $[\{(CpPh_4)Ln(THF)\}_2(\mu\text{-}Cl)_5K(THF)]_2$ where Ln = Tb (**33**), Gd (**34**) and $[(CpPh_4)_2Tb(\mu\text{-}Cl)_2K(THF)_2]_2$ (**35**) were obtained. Just like the $CpPh_3$ derivatives, the CpLn complexes of $CpPh_4$ form ate complexes from which the monoligated complexes are tetranuclear and the diligated one is binuclear. Notably, increasing the steric bulk did not allow the formation of the triligated derivative.[60]

5.1.2 Structural details

X-ray crystallographic measurements were utilized to obtain information about the structural details of the synthesized CpLn complexes. Monoligated complexes **19** and **24**, both from the mononuclear species, possess similar structural character. Their Tb ions reside in a pseudooctahedral environment, and they both have chloride ions in the trans position. The Cp–Tb bond length measured from the centroid of the Cp ring is increased by 0.018 Å (from 2.413(4) Å to

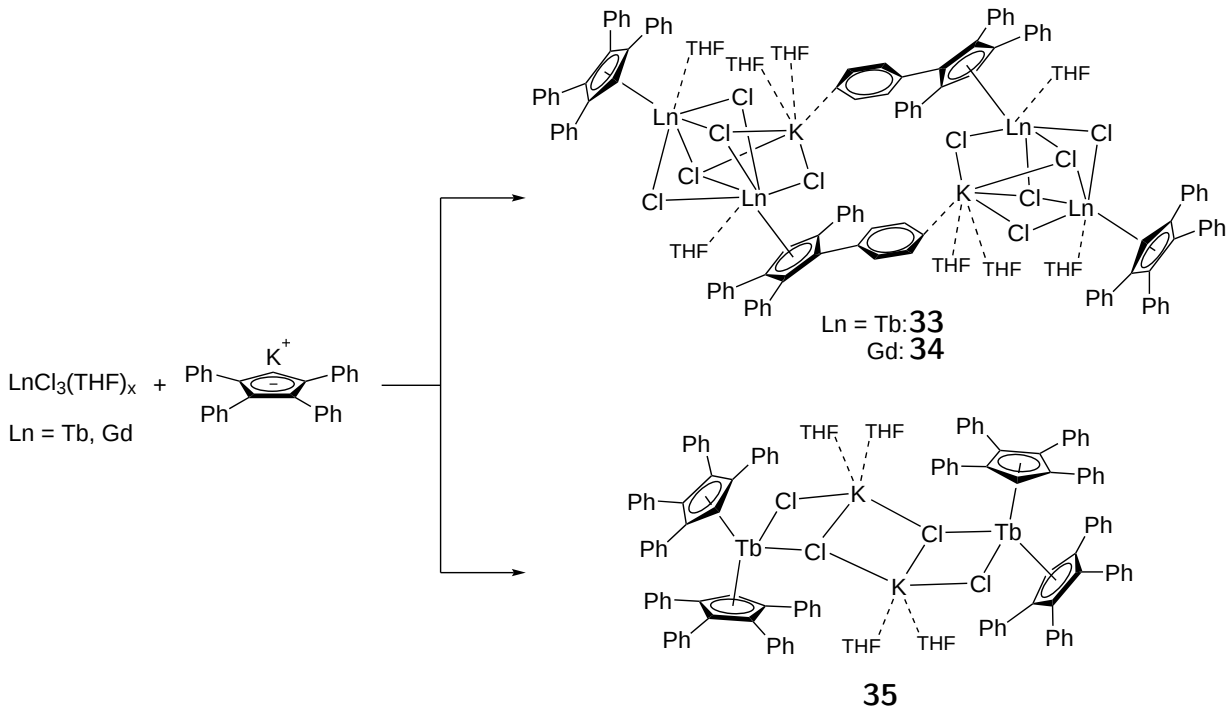

Scheme 10. The synthesis of CpLn complexes **33**, **34** and **35**.

2.431(2) Å) when the two phenyls are applied to the ring. This is caused by the increasing steric bulk.[60]

Moving to the more substituted Cp ligands generates drastic changes in the structural details of the monoligated species. All of the monoligated $CpPh_n$ (n = 3, 4) complexes form tetranuclear complexes. The most notable difference between the two families is that the $CpPh_3$ complexes **29** and **30** have two binuclear cores bonding through a K–Cl interaction, while the analogous link between the cores in **33** and **34** is a weak K···Ph interaction. Adding more phenyls to the Cp ring lengthens the Ln–Cp distances. For example, the Tb–Cp (centroid) distances increase on a scale of 0.012 - 0.040 Å in **33** compared to **29**. However, the Tb–Cp (centroid) distances in the di-substituted **24** and the tri-substituted **29** are very similar.[60]

In case of the diligated CpLn complexes, all of the Cp derivatives with both Tb and Gd yield in binuclear structures. The structures of **20** and **21** form two lanthanocene-like cores linked by two μ_2-bridging chlorides. Adding a second non-substituted Cp ligand affects the structure, but offers little steric bulk, as the Tb–Cp (centroid) bond length in **20** only increases by 0.009 Å compared to **19**.[60]

Adding two Ph substituents to the Cp rings has an impact on the diligated CpLns, because the complexes **26** and **27** form unique 1D coordination polymers, structures of which are isomorphous. The fragments of the polymer units are connected via K–Cl interactions, and each fragment has a phenyl ring that forms K···Ph interactions inside the fragment. Another unique aspect in these complexes is their Tb–Cp bond lengths (centroid) varying from 2.380(2) Å to 2.394(2) Å, which can be as much as 0.033 Å shorter than in **19**. The packing of the unique polymer structure of **26** is shown in Figure 17 along the unit cell *a*-axis.[60]

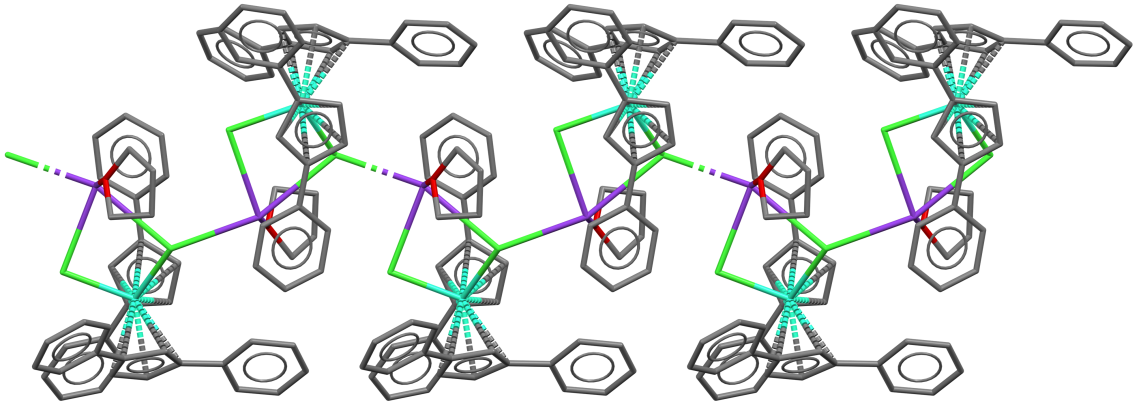

Figure 17. The crystallographic packing of the polymeric **26** along the unit cell *a*-axis. CSD: UDOCEY.[60]

The $CpPh_3$ (**31**, **32**) and the $CpPh_4$ (**35**) derivatives have similar structures. Their two cores bond via K–Cl, as well as K···Ph interactions, main difference being that in **31** and **32** the K···Ph interactions are η^6-type, while in **35** it is η^2-type coordination. Interestingly, also the Tb–Cp distance (centroid) in **31** is shortened by 0.03 Å compared to **29**. The Cp–Tb–Cp (centroid) bond angles in **31** are both 132.04 °, and the Tb–Cp (centroid) bond lengths are 2.401 Å and 2.409 Å. The two cores of the binuclear **31** are symmetrical.[60]

From the polyphenyl-substituted CpLns, only the di-substituted CpLns could form triligated complexes. The structure of **28** contains a Tb ion, which lies on a plane determined by the centroids of the Cp rings. The Cp–Tb–Cp (centroid) bond angles are 120.0(2) °.[60]

The steric properties of the ligands, as well as the K···Ph interactions of the complexes are strongly linked to the sensitization of the lanthanoid. The K···Ph π-interactions can decrease the rotation angles of the Ph substituents, allowing more planar ligand symmetry and hence shorter Ln–Cp (centroid) distances for more substituted Cp ligands with a lot of steric bulk. The shortening of the Ln–Cp (centroid) distances then allows better charge transfer to the Ln ion. Furthermore, the steric bulk can prevent solvate molecules from forming, which enhances the Ln sensitization and the luminescence efficiency. Conclusively, tailoring these antenna-ligands properly can increase the efficiency of the luminescence in the complex.[60]

5.1.3 Photophysical details

Optical spectroscopy studies were carried out to investigate the electronic transitions within the complexes. It is assumed that sensitization of an Ln ion is caused by energy transferring from an excited singlet state (S_1) to the corresponding triplet state (T_1). From this triplet state the energy is finally transferred to the excited states of the Ln ion. Hence, the S_1 and T_1 states were determined.[60]

Luminescence spectra were obtained in the range of 470-720 nm for all of the Tb complexes, and the spectra showed narrow emission bands characteristic to the 4f-4f transitions

of Tb (Figure 18). The transitions observed from the lowest to the highest wavelength were $^5D_4 \rightarrow {}^7F_6$, $^5D_4 \rightarrow {}^7F_5$, $^5D_4 \rightarrow {}^7F_4$, $^5D_4 \rightarrow {}^7F_3$, $^5D_4 \rightarrow {}^7F_2$, $^5D_4 \rightarrow {}^7F_1$ and $^5D_4 \rightarrow {}^7F_0$. The transitions found at wavelengths greater than 570 nm are much less intense than the ones below the forementioned wavelength.[60]

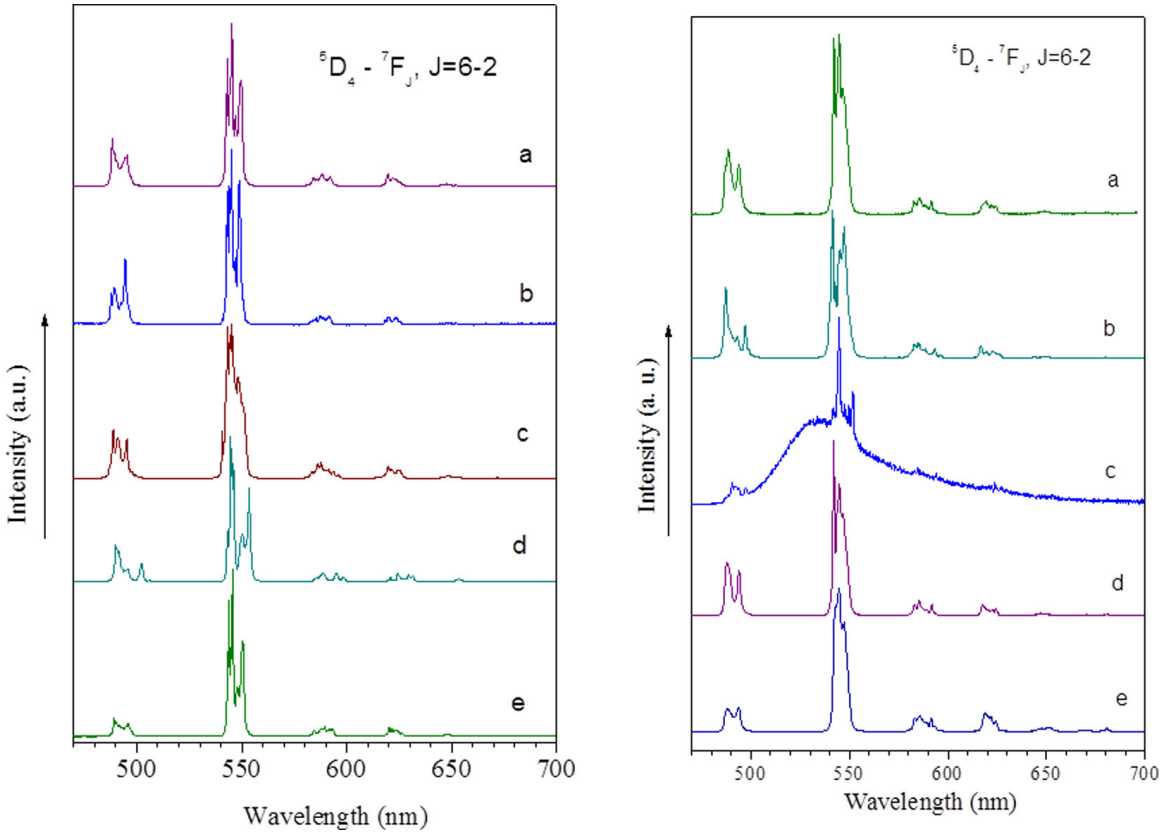

Figure 18. The luminescence spectra at 300 K for (a) **31**, (b) **35**, (c) **20**, (d) **22**, (e) **26** on the left and (a) **29**, (b) **19**, (c) **28**, (d) **24**, (e) **33** on the right. Reprinted with permission from *Inorg. Chem.*, **2018**, *57*, 16, 10199–10213. Copyright 2021 American Chemical Society.[60]

The spectra a), b), d) and e) in Figure 18 (right side), all exhibit similar splitting patterns and Stark component grouping of the $^5D_4 \rightarrow {}^7F_J$ (J = 4,5,6) transitions. The splittings are smaller than those of the spectra on the left side sceme in Figure 18. It should also be noted that the spectra of **29** and **24** look very similar. This is due to their similar charge distribution caused by the ligand positioning, and is supported by the structural experiments.[60]

As the most intense emission bands lie at 540-550 nm, the luminescence excitation spectra were recorded near aforementioned wavelengths. The spectra show very intense and broad bands that correspond to the $\pi - \pi*$ transitions that are characteristic for the Cp ligands (Figure 19). These bands extend from 250 to 320 nm, or even up to 480 nm in case of **28**. The broad band peaks are used to determine the S_1 state energies. Furthermore, the spectra exhibit weak narrow bands from 320 to 500 nm, which indicate the transitions $^7F_6 \rightarrow {}^5L_6$, $^7F_6 \rightarrow {}^5L_9$, $^7F_6 \rightarrow {}^5L_{10}$, $^7F_6 \rightarrow {}^5G_6$, $^7F_6 \rightarrow {}^5D_3$ and $^7F_6 \rightarrow {}^5D_4$, from the lowest to the highest wavelength. These results imply that the non- and polyphenyl-substituted Cps can function as antenna ligands.[60]

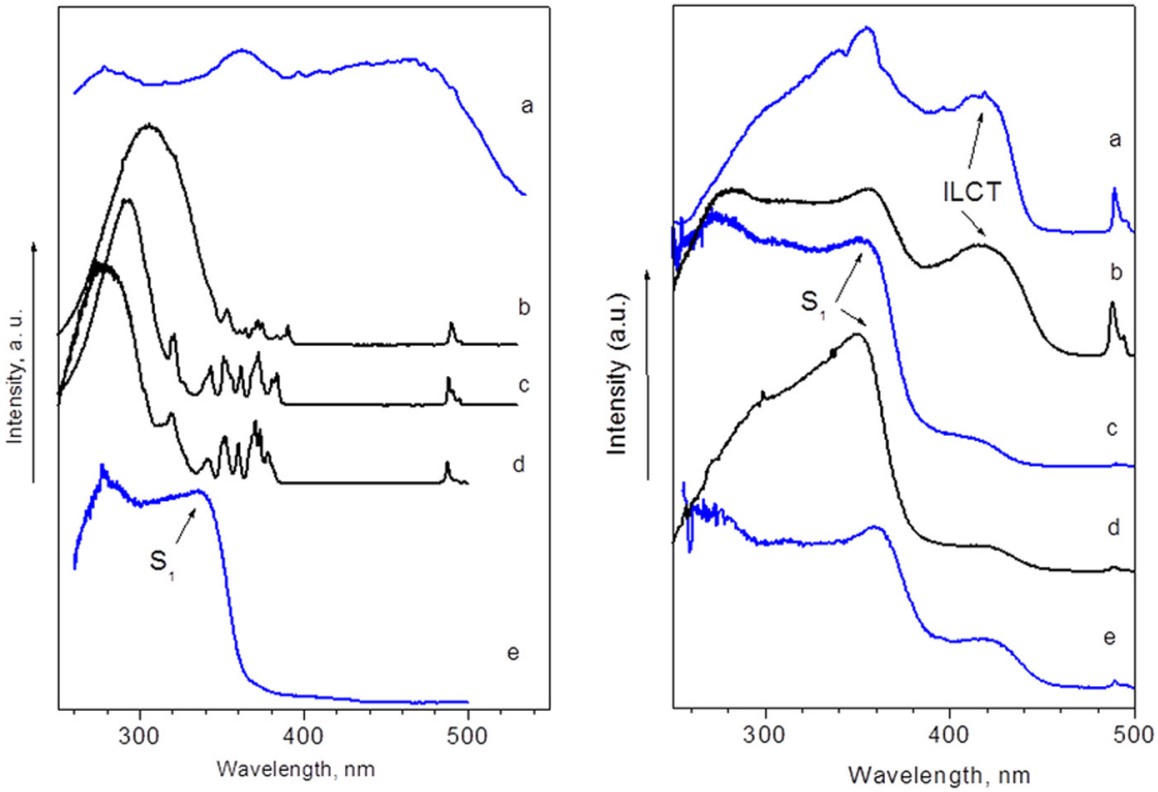

Figure 19. The excitation spectra at 300 K for (a) **28**, (b) **22**, (c) **20**, (d) **19**, (e) **24** on the left and (a) **26**, (b) **33**, (c) **35**, (d) **29**, (e) **31** on the right. Reprinted with permission from *Inorg. Chem.*, **2018**, *57*, 16, 10199–10213. Copyright 2021 American Chemical Society.[60]

The excited states T_1 of the ligands were derived from the phosphorescence data of the Gd complexes. The reason why this is done is because the Gd^{3+} f-f* transitions that have the lowest energies lie at 313 nm, and the ligand states of Ln^{3+} complexes generally lie at lower energies. The excited state energy data, as well as computational results, were then used to determine the energy gaps $S_1 \rightarrow T_1$.[60] For the non-substituted CpLns **19** and **20** the energy gaps were very large, over 10000 cm^{-1} for both complexes, when the optimal gap is considered to be 5000 cm^{-1}.[63] In **22** the energy gap is decreased by *ca.* 2800 cm^{-1} due to the C_3 symmetry of the complex. This decrease enhances the sensitization of the Ln ion. The complexes with the energy gaps closest to the optimal value were the $CpPh_n$ (n = 3, 4) Ln complexes.[60]

The luminescence decay curves were also measured to determine the lifetimes of all Tb complexes. The lifetimes values varied from 0.32 to 1.01 ms, shortest of which was found for **31** and the longest for **33**. The measured quantum yields varied greatly from 4 % to 60 %, lowest of which belonged to **19** and the highest to **33**. In case of the $S_1 \rightarrow T_1$ energy gaps, complex **26** had the energy gap closest to the optimal value from the series of the di-substituted CpLn complexes. It also had the shortest Ln–Cp (centroid) distances, as well as a quantum yield of 50 %. These properties make the luminescence of the complex very strong. However, the complex had a very short lifetime of 0.35 ms, due to the orbital mixing.[60]

In conclusion, using Ph-substituents in the CpLn complexes can be efficient in the sensitization of the Ln ion. The $CpPh_n$ (n = 2-4) substituents offer steric bulk, which prevents

the coordination of solvents and affects the bond lengths and angles between the Ln ion and the ligands. They can also make additional cation$\cdots$Ph π-interactions that can also enhance the luminescence. For example, from complex **19** to **24**, the quantum yield is multiplied by 3.5, which can be explained by the introduction of the two phenyls. Nonetheless, some complexes had unoptimal quantum yields and $S_1 \rightarrow T_1$ energy gaps. On the other hand, some complexes, such as **26** and **33** exhibited strong luminescence and high quantum yields. It is concluded that with the correct design of the ligand and the right amount of phenyl-substituents, CpPh ligands can show promise as efficient light-harvesting antenna ligands.[60]

5.2 POLYPHENYL-SUBSTITUTED CYCLOPENTADIENYL DYSPROSIUM COMPLEX

In 2020, two dysprosium based chloride bridged complexes possessing two types of polyphenyl-substituted cyclopentadienyl ligands were synthesized and characterized. These complexes were predicted to exhibit strong luminescence properties due to the sensitizing effect of the π-type ligands, as these type of ligands have been reported to function as antenna-ligands before. Furthermore, the research showed interest on the luminescence properties of the two different ligands used in the complex syntheses.[64]

5.2.1 Synthetic details

A synthesis for two different triaryl substituted Cp ligands was carried out via a three-step process, which is shown in Scheme 11. In the first step *p*-methylacetophenone and R-benzaldehyde (R = *p*-methyl, H) react via a cross-aldol condensation reaction in basic conditions to produce di-ketones. In the second step the obtained di-ketones are refluxed with an excess of Zn-dust in acidic conditions, and diols are obtained via a reductive cyclization reaction. In the last step the diols are refluxed in acidic conditions, and the products (1,2-*p*-tolyl)-4-phenylcyclopenta-1,3-diene (**36**), abbreviated $Cp(PhMe)_2Ph$, and tri(1,2,4-*p*-tolyl)cyclopenta-1,3-diene (**37**), abbreviated $Cp(PhMe)_3$, are obtained via a dehydration reaction.[64]

The potassium salts of both ligand derivatives were obtained by a reaction of the ligands with potassium metal in THF at room temperature over one day (Scheme 11). In the reaction the ligands are deprotonated and the potassium coordinates to the anionic ligands to produce potassium (1,2-*p*-tolyl)-4-phenylcyclopentadienide (**38**), abbreviated $KCp(PhMe)_2Ph$, and potassium tri(1,2,4-*p*-tolyl)cyclopentadienide (**39**), abbreviated $KCp(PhMe)_3$.[64]

The ligands **36** and **37** were then used in one pot reactions with $DyCl_3$ and potassium metal in a molar ratio of 2:1:2, respectively (Scheme 12). The reactions were done by refluxing in toluene for 2 days, and the products were crystallized from filtered and concentrated reaction solutions to obtain yellow block-like crystals of $[(CpPh(PhMe)_2)_2Ln(\mu\text{-}Cl)_2K]_2$ (**40**) and $[(Cp(PhMe)_3)_2Ln(\mu\text{-}Cl)_2K]_2$ (**41**).[64]

The binuclear complexes **40** and **41** are very similar to **31** and **32** in terms of structure

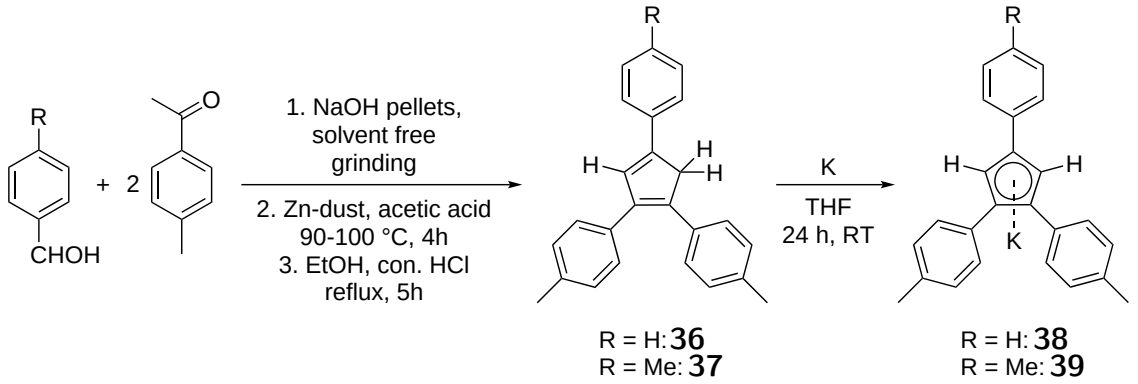

Scheme 11. The synthesis of ligands **36** and **37**, as well as their potassium salts **38** and **39**.

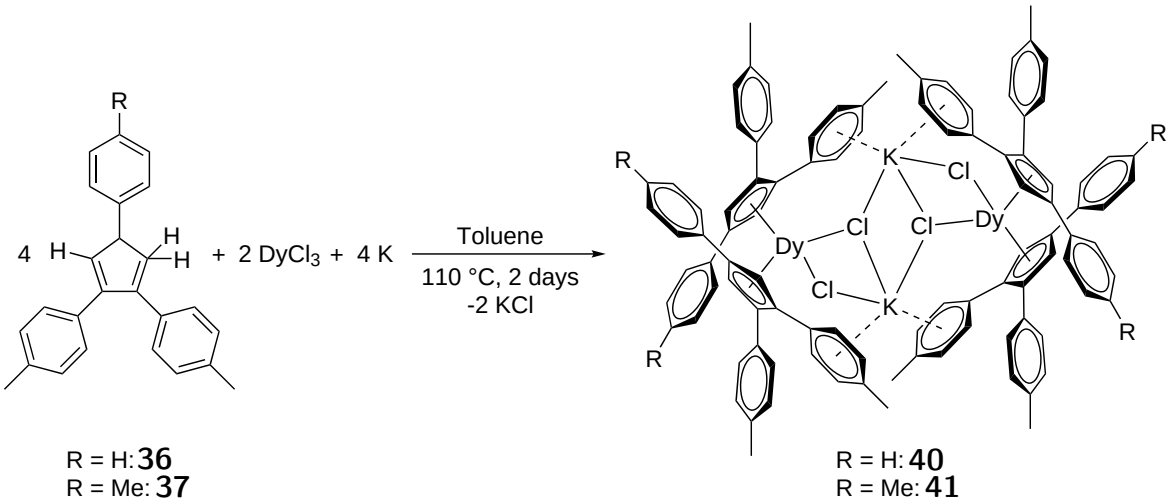

Scheme 12. The synthesis of complexes **40** and **41**.

and the intramolecular interaction. However, the synthesis routes are not similar, since the syntheses from the potassium salts of the ligands were reported uneffective in case of the Dy derivatives.[64]

5.2.2 Structural details

Ligand **36** crystallizes in the monoclinic crystal system in the space group *Cc*, while **37** crystallizes in the orthorhombic crystal system in the space group *lba2*. The asymmetric units of the ligands are similar, with both consisting of one ligand molecule, where the most notable difference is the slightly more rotated 4-Ph group in **37**. Additionally, effects caused by the one methyl group difference between **36** and **37** can also be observed in the packing structures, that are shown in Figure 20 along the unit cell *a*-axes. The molecules in the adjacent layers in **36** align quite linearly, while in **37** they make a zigzag-like pattern.[64]

Both complexes **40** and **41** crystallize in the triclinic crystal system in the space group *P-1*. The complexes are isostructural with only small differences in the unit cell parameters, and hence only one structure will be described in depth. The unit cell parameter differences are shown in Table 1 to highlight the similarity of the two Dy complexes.[64]

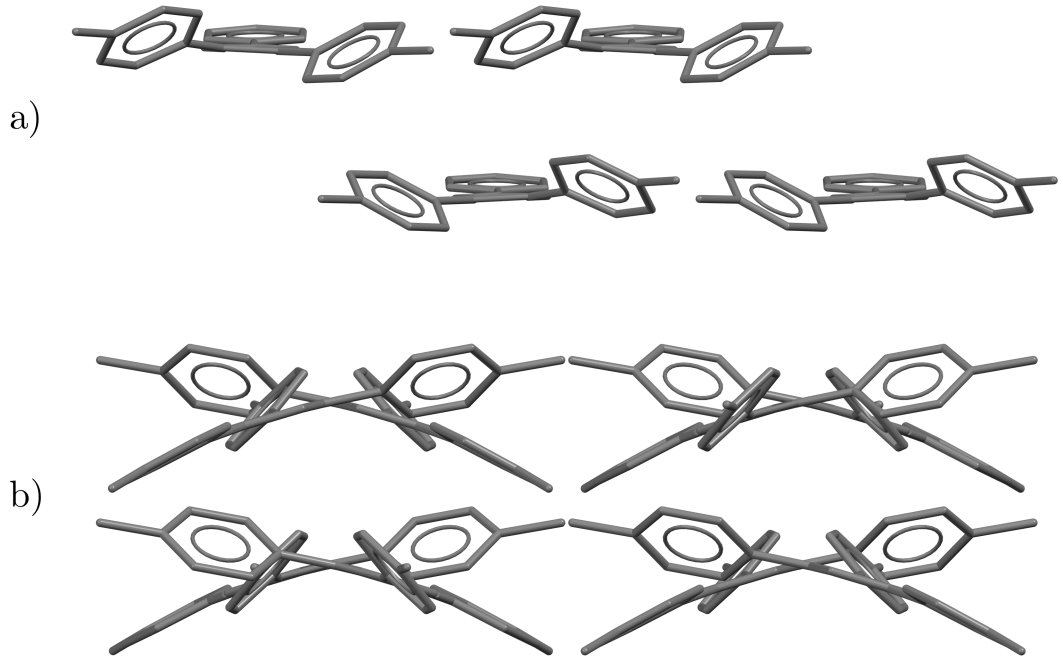

Figure 20. The packing of (a) ligand **36** (CSD: XAHFOF) and (b) ligand **37** (CSD: XAHFUL) structures along the unit cell *a*-axes.[64]

Table 1. The cell parameters of **40** and **41**

Parameter	**(40)**	**(41)**
a (Å)	15.0406(5)	17.1088(7)
b (Å)	18.9527(6)	17.7780(8)
c (Å)	21.4668(8)	20.6046(9)
α (°)	65.2020(10)	69.756(2)
β (°)	78.557(2)	79.617(2)
γ (°)	67.6990(10)	62.673(2)
V (Å^3)	5134.0(3)	5222.1(4)

The structure of **41** is shown in figure Figure 21, where the hydrogens and free solvent molecules are omitted for clarity. The core of the binuclear complex consists of a [(Cp(PhMe)$_3$)Dy(μ-Cl)K] unit and the cores are connected by the bridging chlorides. The complex also exhibits K$\cdots$Ph π-interactions between the two cores, similar to the η^6-coordination in **31** and **32**.[64]

Comparing the Cp–Ph rotation angles between the ligands and the complexes it could be suggested that the K$\cdots$Ph interactions decrease the rotation of the interacting Ph substituents. The Cp–Ph rotation angles in **37** vary from 33.16 to 36,66 °, and the corresponding rotation angles in **41** vary from 15.62 to 34.49 °. In conclusion, the intermolecular, as well as the intramolecular interactions in both the ligands and the complexes could enhance their luminescence properties.[64]

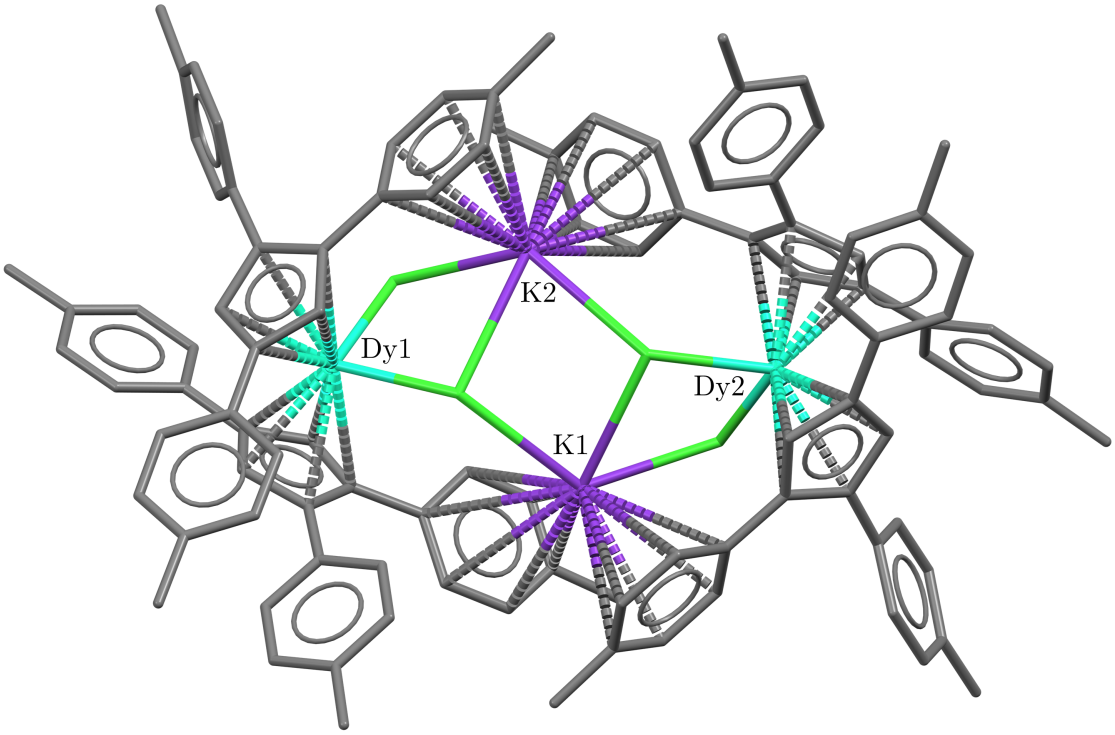

Figure 21. The asymmetric unit of complex **41**. CSD: XAHGAS.[64]

The Cp–Dy–Cp (centroid) bond angles for **37** are 129.70 ° and 130.74 °, which shows that that complex possesses the bent metallocene structure. These angles are slightly smaller than those of **31**, which are both 132.04 °. The Dy–Cp (centroid) bond lengths of **37** vary from 2.388 to 2.397 Å, which are shorter than the corresponding bond lengths of **31**, which are 2.401-2.409 Å. It should be emphasized that all bond parameters of **37** are very similar to those of **36**.[64]

5.2.3 Photophysical details

The photophysical properties of the ligands, as well as the complexes were investigated using several different methods. The UV-visible absorption and emission spectra of **36** and **37** were measured both in solid state and in solution, as seen in Figure 22. The absorption spectra showed strong absorbance at 359 nm for both ligands in DCM, resulting from the π-π* transitions of the conjugated Ph and Cp rings. The fluoresncence spectra in DCM ($\lambda_{excitation}$ = 359 nm) showed emission at 455 nm and 470 nm for **36** and **37**, respectively. The solid state UV-vis measurements for **36** and **37** showed emission at 466 nm and 480 nm, respectively, which were red-shifted by approximately 10 nm compared to the emissions in DCM, possibly due to the packing in the crystal structures.[64]

The emission lifetimes were measured in solution, as well as in solid state. The measurements in solution resulted in lifetimes of 0.3 ns for **36** and 0.2 ns for **37**, and in solid state 2.25 ns and 1.6 ns, respectively. The quantum yields measured in a toluene solution were 4.5% for **36** and 10.3% for **37**. It can thus be concluded that both ligands have very similar photo-

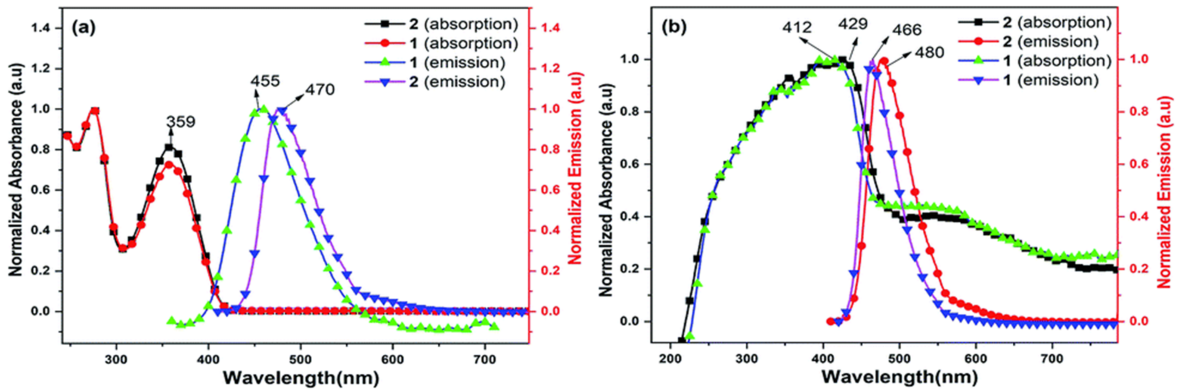

Figure 22. The absorption and emission spectra of **36** and **37** measured in (a) DCM and in (b) solid state. Reproduced from *RSC Adv.*, **2020**, *10*, 39366-39372 with permission from the Royal Society of Chemistry.[64]

physical properties, with **37** possessing a slightly better emission lifetime and quantum yield. The slight differences are suggested to arise from the different crystallographic packing of both ligands, as the packing affects the intermolecular interactions and charge transfer.[64]

The UV-visible absorption and emission spectra of **40** were measured in acetonitrile (MeCN), as seen in Figure 23. The complex showed intermediate absorbance at 232 nm, and strong absorbance at 262 nm and 354 nm. The emission spectra ($\lambda_{excitation} = 262, 320, 354$ nm) showed strong fluorescence at 426 nm with all excitations wavelengths, which was blue-shifted by approximately 30-45 nm compared to the spectra of the ligands in DCM.[64]

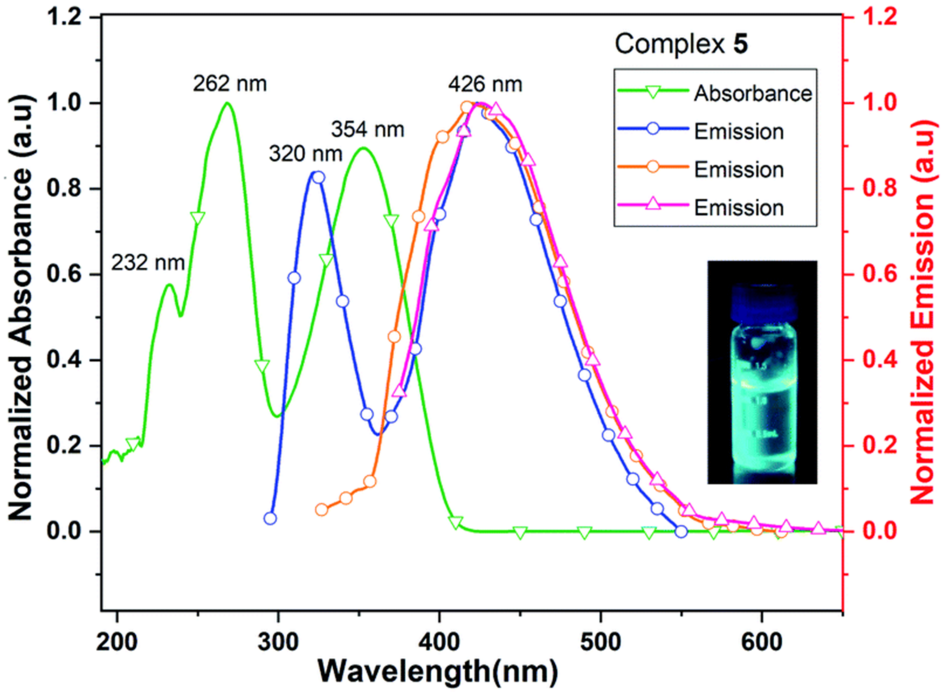

Figure 23. The absorption and emission spectra of **40** measured in MeCN. The $\lambda_{excitation}$ values for the emissions are 262 nm (blue), 320 nm (orange) and 354 nm (red). Reproduced from *RSC Adv.*, **2020**, *10*, 39366-39372 with permission from the Royal Society of Chemistry.[64]

The quantum yield of **40** in MeCN was only 0.8%, which is significantly smaller than the quantum yield measured for the ligand **36** in DCM. These results indicate the quenching of fluorescence emission in the complex **40**. As the complex **41** is structurally very similar, same kind of luminescence properties could be expected. In conclusion, there are only slight differences between the two ligands, and they both show fluorescent character in the visible light region. Their chloride bridged dysprosium complexes also show emissions in visible light region, but the quantum yields are poor. By slight modifications to the ligands or the complexes, the structural properties could be changed, which could enhance the quantum yields.[64]

6 DIVALENT LUMINESCENT CYCLOPENTADIENYL-BASED LANTHANOID COMPLEXES

As mentioned above, Ln^{3+} and Ln^{2+} ions have notable differences in their luminescence properties due to the different electronic transitions. It is typical for Ln^{2+} ions to show stronger luminescence even without sensitization, which is usually required for Ln^{3+} ions. However, using antenna ligands can further increase the luminescence and thus a review of divalent lanthanocene complexes exhibiting sensitized luminescence character will be reported here.[61]

6.1 POLYPHENYL-SUBSTITUTED CYCLOPENTADIENYL EUROPIUM COMPLEX

In 2013 an extremely bulky aryl-substituted cyclopentadienyl Eu complex was synthesized to gain more information about the relationship between structure and luminescence properties in lanthanocenes. The aryl groups were chosen as the cuclopentadienyl substituents, because the polyphenyl-substituted Cp ligands are known as efficient Ln sensitizing antennas.[59]

6.1.1 Synthetic details

A bulky europium sandwich complex [Eu(Cp^{BIG})$_2$] (**42**), where Cp^{BIG} = Cp(4-*n*Bu$-C_6H_4)_5$, was prepared by reacting [Eu(dmat)$_2$(THF)$_2$] (dmat = 2-Me_2N-α-Me_3Si-benzyl) with Cp^{BIG}H (Scheme 13). The reaction was done in benzene by heating the reaction mixture at 65 °C for three days, after which a crude product was obtained. The product was recrystallized in cold hexane, which resulted in bright orange crystals with a yield of 46%. The product was eminently soluble in hexanes, which could explain the rather low yield of the crystalline product.[59]

6.1.2 Structural details

The single crystal X-ray crystallographic measurements were carried out, and according to the data **42** crystallizes in the triclinic crystal system in the space group *P-1*. The structure is centrosymmetric and the Eu ion lies in an inversion center. The asymmetric unit consists of

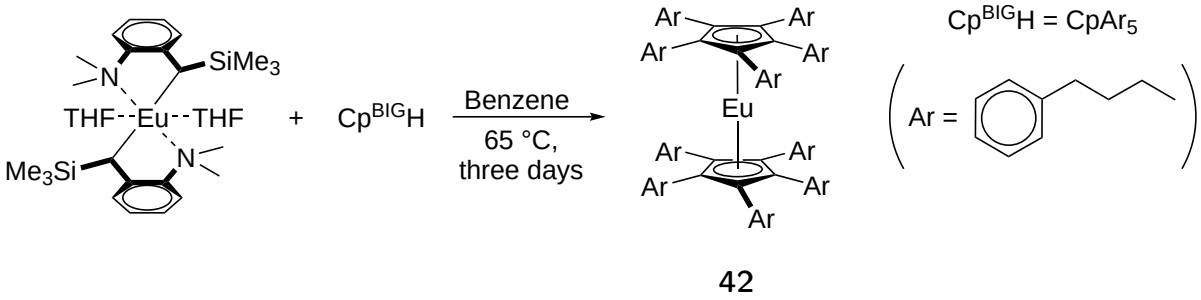

42

Scheme 13. The synthesis route of complex **42**.

the Eu ion and only one ligand, and the whole lanthanocene structure is presented in Figure 24, where the hydrogens are omitted for clarity.[59]

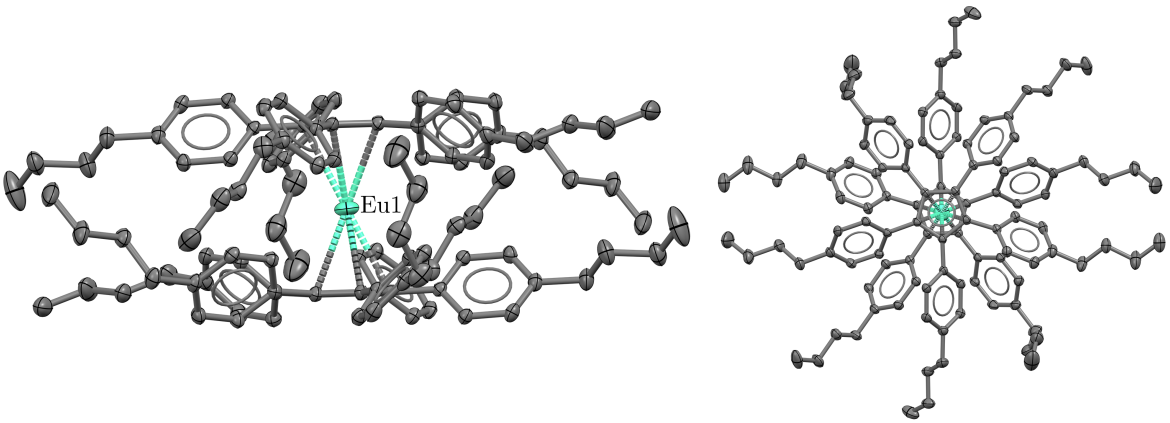

a) b)

Figure 24. The crystal structure of **42** pictured a) along the Cp–Eu–Cp plane and b) along the Cp–Eu–Cp axis. Thermal ellipsoids are drawn at the probability level of 30% CSD: LIKJAS.[59]

The Eu–Cp bond lengths measured from the centroid of the Cp ring are 2.497(2) Å, and the two facing ligands are staggered. The Ln–Cp (centroid) bond lengths are longer than those of the analoguous Yb complex, which are 2.382(1) Å. This difference can be explained by lanthanoid contraction of the ionic radii when moving to higher atomic numbers. The aryl-substituents are not in plane with the Cp rings, and their rotation angles vary from 44.40 ° to 47.33 °.[59]

The Cp–Eu–Cp bond length is 180 °, indicating a completely linear structure. However, the displacement parameters of the central Eu ion are excessively large, which indicates a large disorder of the metal ion. Thus, it is assumed that the Eu ion does not lie precisely at the center of a Cp–Cp (centroid) axis, but slightly off-center. The displacement parameters and the disorder of **42** are greater than those of the Yb analogue, which can also be explained by the Ln contraction and the disorder increasing with the ionic radii. Furthermore, complex **42** exhibits intermolecular C–H···C interactions between the butyl hydrogen atoms and the Cp and Ph carbon atoms.[59]

6.1.3 Photophysical details

The excitation and luminescence properties were measured for solid-state **42** and the spectra are presented in Figure 25. The emission spectrum of **42** ($\lambda_{excitation} = 412$ nm) showed only a single strong band with the peak maximum at 606 nm, and it was assigned to a $4f^6 5d^1 \rightarrow 4f^7$ transition of the Eu ion. The excitation spectrum showed multiple overlapping broad bands on a scale from 580 nm to less than 285 nm. The quantum yield measured for the crystalline solid was 45%, which is satisfactory.[59]

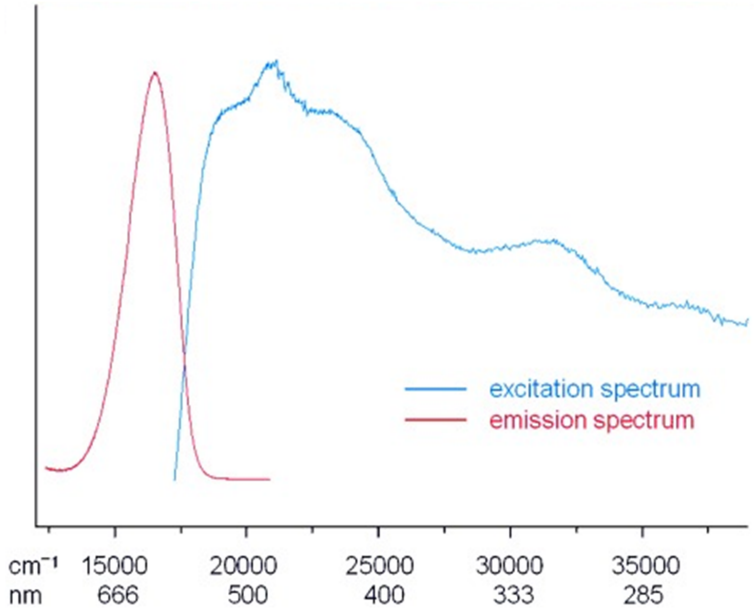

Figure 25. The normalized excitation (blue) and emission (orange) spectra for crystalline **42**. Adapted from *Chemistry – A European Journal*, **2013**, *19*, 37, 12272-12280, with permission from John Wiley and Sons.[59]

It can also be observed from the spectra that **42** does not contain Eu^{3+} impurities, as there are no characteristic bands that would indicate the 4f-4f transitions. For example, a very sharp and intense emission band at *ca.* 620 nm is distinctive to a $^5D_0 \rightarrow ^7F_2$ transition, but it is not observed in the emission spectrum of **42**. Conclusively, **42** shows very bright luminescence in the orange wavelength range and has a considerably good quantum yield. This excellent luminescence is most likely due to the rigidity of the complex which is enhanced by the intermolecular C–H$\cdots$C interactions, as well as the extremely bulky ligands.[59]

6.2 POLYPHENYL-SUBSTITUTED CYCLOPENTADIENYL EUROPIUM COMPLEXES

In 2015 two polyphenyl-substituted Cp based Eu^{2+} complexes were synthesized and characterized. The luminescence of the complexes was studied to gain more insight on the π-type ligands functioning as light harvesting antenna ligands. The study also included analoguous Sm complexes, but they are excluded from this review, as their luminescence was not explored.[65]

6.2.1 Synthetic details

A europium sandwich complex [Eu($CpPh_5$)$_2$] (**43**) was synthesized by sonicating Eu metal, $HgPh_2$ and $CpPh_5H$ at 40 °C over several days, as seen in Scheme 14. The solution was then dried and the obtained solid was washed with toluene to yield an orange powder of **43**. The product was then crystallized by slow diffusion from a THF solution layered with toluene. Additionally, **43** could also be obtained by replacing $HgPh_2$ with $Hg(C_6F_5)_2$ and stirring at room temperature.[65]

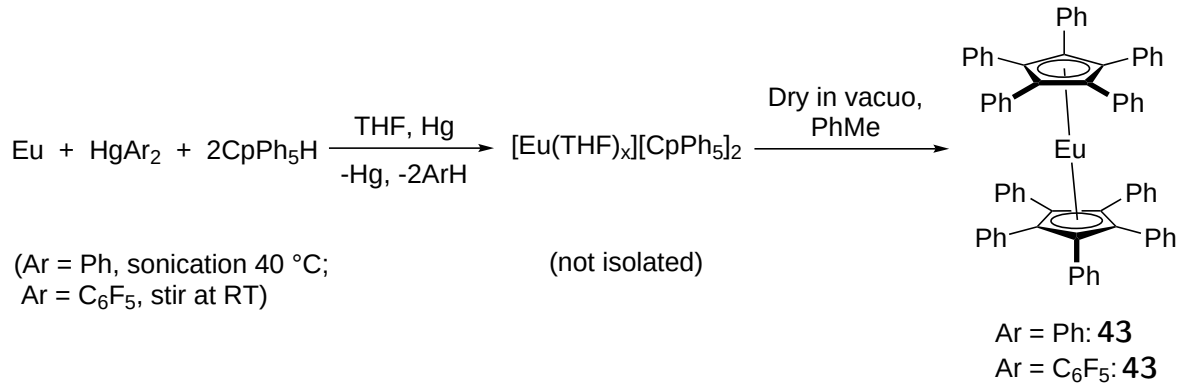

Scheme 14. The synthesis route of complex **43**.

A solvate analogue of the Eu complex was synthesized via redox transmetallation/protolysis (RTP) reaction. The reaction was done by stirring Eu metal, $HgPh_2$ and $CpPh_4H_2$ in THF for 2-3 days to obtain the crude product, which was then crystallized in 1,2-dimethoxyethane (DME) to yield [Eu($CpPh_4H$)$_2$(DME)] · 1.5 DME (**44**), as seen in Scheme 15. It should be noted

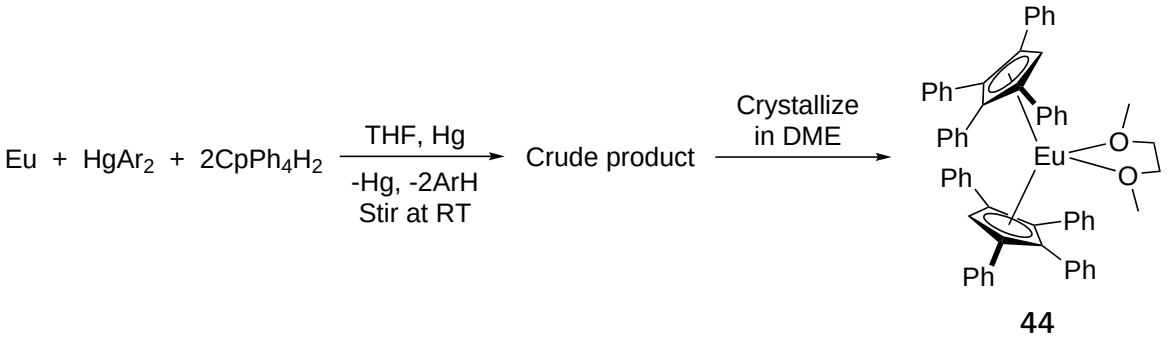

Scheme 15. The synthesis route of complex **44**.

that **43** was slightly soluble in aromatic solvents, which was unexpected due to previous reports declaring insolubility. On the other hand, **44** showed good solubility in aromatic, as well as polar solvents.[65]

6.2.2 Structural details

Single crystal X-ray measurements were done for **43** and it was assessed that the complex crystallizes in the monoclinic crystal system in the space group $P2_1/n$. The whole sandwich

structure is shown in Figure 26, however, the asymmetric unit consist of the Eu ion and only one $CpPh_5$ ligand. The Cp–Eu–Cp (centroid) bond angle is 180 °, making the complex linear. The bond lengths between the Eu ion and the Cp rings (centroid) are 2.489 Å, and the two facing ligands are staggered, congruent with the staggering ligands in **42**. The bond lengths are also very similar to those of **42** regardless of the different ligand sizes. In addition, there are also intermolecular C–H···C π-interactions between the Cp carbons and the Ph hydrogens. These interactions were analyzed to shorten the Eu–Cp (centroid) bonds from what they would typically be.[65]

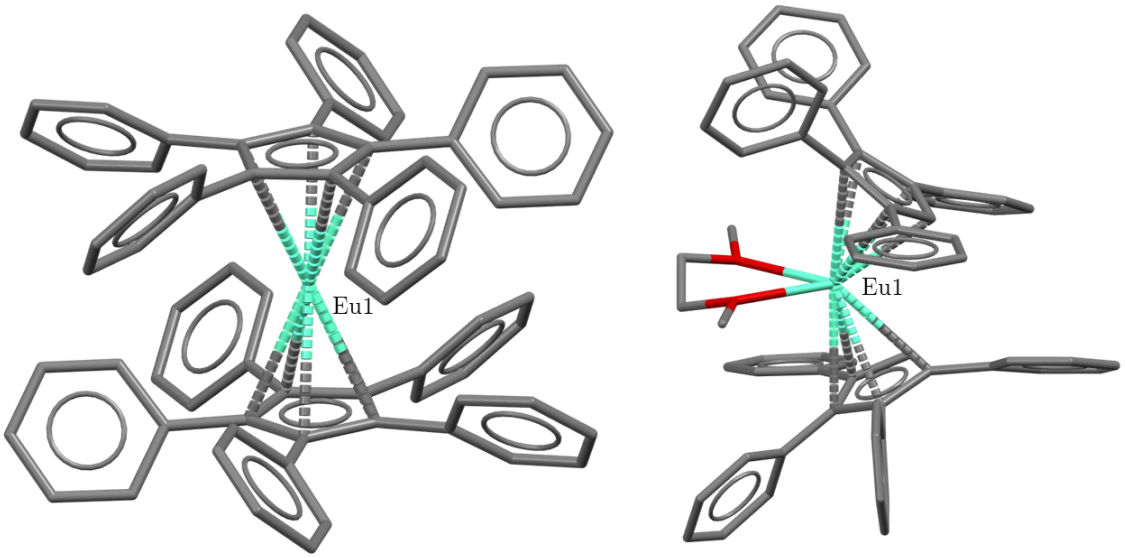

Figure 26. The structures of a) **43** (CSD: PUYKAX) and b) **44** (CSD: PUYKOL). The structure of **43** is linear, while **44** has the bent-type structure.[65]

Complex **44** crystallizes in the monoclinic crystal system in the space group $P2_1/c$, and its bent sandwich structure is shown in Figure 26. The asymmetric unit consists of three free DME molecules and two distinct **44** molecules that are very similar to each other. The Cp–Eu–Cp (centroid) bond angles for the two molecules are 128.62 ° and 129.98 ° with a difference of 1.36 °, and the bent angle is caused by the chelating DME molecule. The Eu–Cp (centroid) bond lengths are longer in **44** than in **43**, as they vary from 2.596 to 2.610 Å. Some intermolecular C–H···C π-interactions similar to **43** are present in **44**, but they are more difficult to interpret due to the lower symmetry and the bent structure.[65]

6.2.3 Photophysical details

The luminescence properties for **43** and **44** were measured in solid state and in a toluene solution. Absorbance and emission spectra for both complexes were obtained in the range of 300-800 nm and they are shown in Figure 27. The absorption band of **43** is very strong at *ca.* 300 nm, weakens exponentially up to 350 nm, and extends to 550 nm. The absorption band of

44 is very strong up to *450* nm, weakens more slowly than in **43**, and extends as far as 600 nm. The emission band of **43** ($\lambda_{excitation} = 480$ nm) ranges from 510 to 800 nm and shows peak maxima at 616 nm, while **44** ($\lambda_{excitation} = 490$ nm) ranges from 540 to over 800 nm and shows peak maxima at 645 nm. The quantum yields of **43** and **44** were 45% and 41%, respectively.[65]

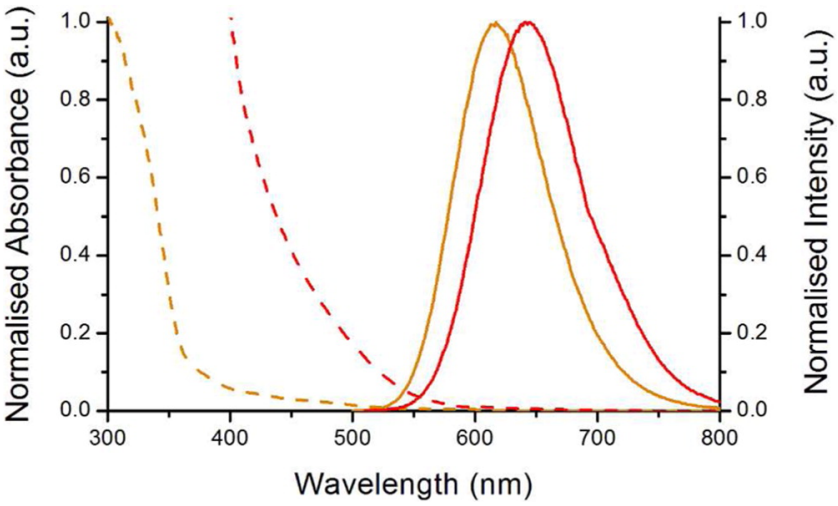

Figure 27. The normalized absorbance (dashed lines) and emission (solid lines) spectra for **43** (orange) and **44** (red) in a toluene solution. Reprinted with permission from *Organometallics*, **2015**, *34*, 23, 5624-5636. Copyright 2021 American Chemical Society.

Due to the strong emission of both complexes in a toluene solution, the emission lifetimes were measured and the fluorescence decay histograms are presented in Figure 28. The spectra exhibit long-lived emissions for both complexes with the emission lifetime of **44** (*ca.* 1300 ns) exceeding that of **43** (*ca.* 800 ns). The results indicate great stability of the complexes and the residuals suggest that the data in well-fitted.[65]

In conclusion, both complexes **43** and **44** show remarkable luminescence properties in toluene, in which the solubility of **43** was surprisingly good. It is very probable that the strong luminescence is affected by the sensitization of the Eu induced by charge transfer from the $CpPh_n$ (n = 4,5) ligands. The antenna-ligand character is most likely enhanced by the extensive electron conjugation caused by the addition of the Ph substituents. In addition, the intermolecular C–H···C π-interactions cause the shortening of the Eu–Cp (centroid) bonds, which makes the charge transfer more efficient.[65]

7 LUMINESCENT SINGLE-MOLECULE MAGNETS

Lanthanoid complexes have shown great promise in the magnetic and luminescent studies, and a lot of effort goes into combining these two properties. Recently, many optomagnetic materials have been developed with different types of magnetic and optical properties, and this section concentrates specifically on the Ln-SMMs complexes that exhibit luminescent character. These type of complexes can be used in interesting applications, for example optical thermometry, as miniaturizing thermometers could allow much more compact device sizes.[66]

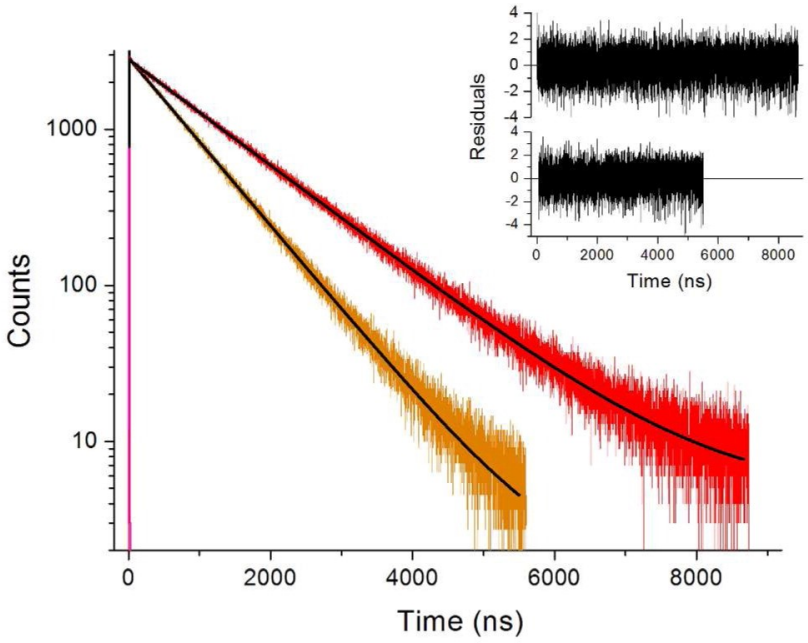

Figure 28. The fluorescence decay histograms of **43** (orange) and **44** (red) in a toluene solution. The fitted decay functions are illustrated with a black line. Reprinted with permission from *Organometallics*, **2015**, *34*, 23, 5624-5636. Copyright 2021 American Chemical Society.

These optical thermometers are not very widely studied with lanthanoids, as only complexes with holmium,[66] ytterbium[67–69] and dysprosium[70] exist. An optomagnetic complex with all three metals will be reviewed in this section. However, it should be noted that none of these optomagnetic lanthanoid-based complexes are lanthanocenes, properties of which have been studied above. Instead, the optomagnetic lanthanoid-based complexes bear ligands that possess donor-atoms, such as oxygen and nitrogen. The SMM properties with the foremen-tioned complexes are inferior to those of the lanthanocenes due to the lack of a strong axial CF.[69]

Designing these multifunctional Ln-based complexes can, however, be very challeng-ing, as the ligand field has a large impact on both magnetic and luminescence properties. The ligands should allow the formation of an axial CF in Ln complexes to enhance the magnetic properties. The trivalent Ln ions are dominant in the study of SMMs, and thus the ligand should also function as an efficient antenna, as the Ln^{3+} ions usually require sensitization of the luminescence.[4]

7.1 HOLMIUM-BASED SINGLE-MOLECULE MAGNET WITH OPTICAL THERMOMETER PROPERTIES

7.1.1 Synthetic and structural details

In 2021, three analogous Ho-based complexes bearing 4-pyridone ligands and hexacyanidomet-allates were synthesized. The general synthetic route was started by preparing a precursor so-lution from $HoCl_3 \cdot 6H_2O$ and 4-pyridone in water (Scheme 16). The heated precursor solution

was poured into an aqueous solution of K[M(III)$(CN)_6$] (M = Co, Rh, Ir) and the obtained mixture was filtered. Yellow crystals of [Ho(4-pyridone)4(H2O)2][M(CN)6]·2H_2O, where M = Co (**45**), Rh (**46**) and Ir (**47**), were obtained from the filtrate.[66]

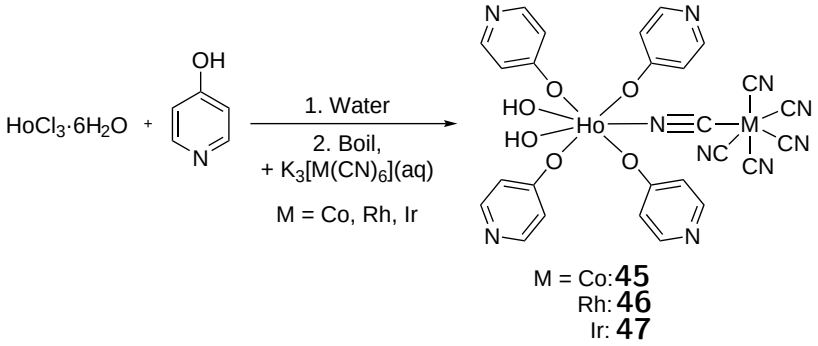

Scheme 16. The general synthesis route for complexes **45**, **46** and **47**.

X-ray crystallographic measurements were done for complexes **45**-**47**, and their crystal structures were obtained. Only the structure of **45** is presented, because all three complexes are isostructural with only slight variation, and they all crystallize in the orthorhombic crystal system in the space group *Cmcm*. The asymmetric unit of **45** consists of only half a molecule, but the whole compound is presented in Figure 29, where free solvent molecules, hydrogens and disorder are omitted for clarity. The structures of **46** and **47** can be found with CSD ID codes NAKRIE and NAKROK, respectively.[66]

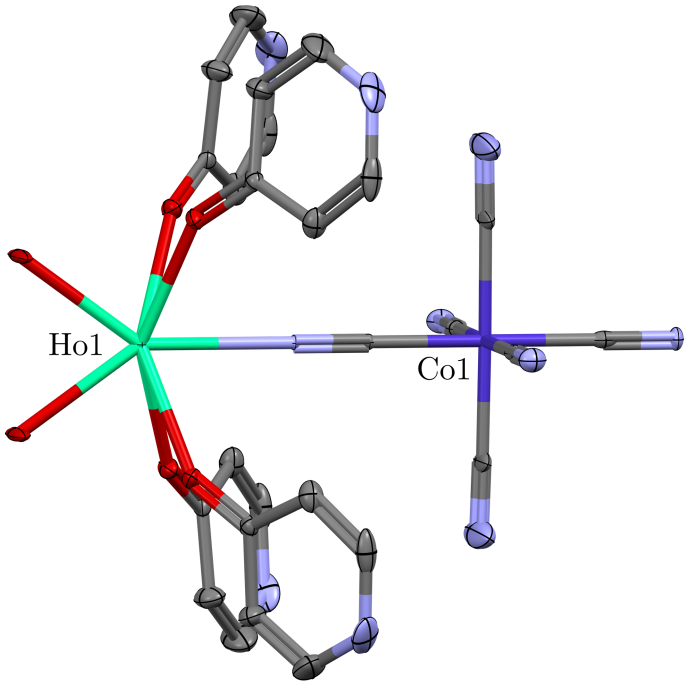

Figure 29. The crystal structure of **45**, where the thermal ellipsoids are drawn at the probability level of 50%. Hydrogens, disorder and free solvent molecules are omitted for clarity. CSD: NAKREA.[66]

The holmium unit and the octahedral [M$(CN)_6$] unit are bridged by a cyano-group,

where the N-atom is coordinated to the Ho-atom. The 4-pyridone ligands are bent towards the [M(CN)$_6$] unit and away from the two coordinated water molecules. When viewing only the coordination sphere of the holmium unit, the coordination geometry acquires a distorted pentagonal bipyramid shape and pseudo-D_{5h} symmetry.[66]

7.1.2 Magnetic properties

Both AC and DC studies were conducted to investigate the magnetic properties of complexes **45**-**47**. The AC measurements were established with a field of 3 Oe to obtain the molar out-of-phase susceptibility χ''_M data. The parameters were plotted as a function of frequency and the results indicated that all three complexes exhibit slow magnetic relaxation at temperatures from 2 K to 17 K in zero DC-field. The plotted data showed almost unchanging peak maxima below 6 K, which indicated strong QTM relaxation for the three complexes. This was most likely due to the magnetic interact ions between the holmium centers.[66]

The AC magnetic measurements were also done using variable DC fields. The experimental data was used to determine the highest energy barriers for an Orbach process by conducting *ab initio* calculations. The barrier heights were 89.8, 86.7 and 78.7 cm^{-1} for **45**-**47**, respectively. The slight differences in the barrier heights can be explained by the slight structural differences seen between the complexes. The *ab initio* calculations also revealed that the relaxation proceeds via Orbach, Raman and QTM processes for compounds **45**-**47**.[66]

Ab initio calculations were also used to investigate the CF effects on the Ho-complexes. The results are visualized in Figure 30, where only the lowest energy states are presented. The $\pm m_J$ states were nearly degenerate despite the non-Kramers nature of Ho^{3+}. The QTM tun-

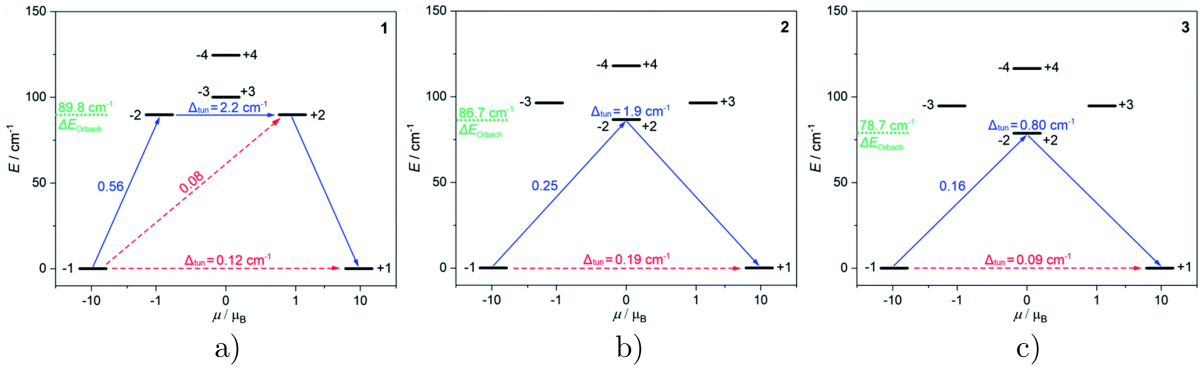

Figure 30. The computational energy splitting of the ground multiplet state $^5I_8$, the Orbach energy barriers (green), the less probable relaxation paths (red) and the most probable relaxation paths (blue) for (a) **45**, (b) **46** and (c) **47**. The QTM tunneling energy gaps are presented with δ_{tun}. Adapted from *Chem. Sci.*, **2021**, *12*, 730-741 with permission from the Royal Society of Chemistry.[66]

neling gap length affect the QTM relaxation rate, which was found the slowest for **47** and the fastest for **46**. It was also determined that the Orbach relaxation proceeds via the first excited state, which could explain the short energy barrier heights that were observed.[66]

7.1.3 Optical properties

The optical properties of complexes **45**, **46** and **47** were incestigated, as all three components Ho^{3+}, 4-pyridone ligands and the $[M(CN)_6]$ units are emissive. UV-vis-NIR absorption spectra were recorded for solid-state complexes **45**-**47**. The spectra showed strong UV-region absorption bands at 270 nm, which were assigned to spin-allowed π-π* transitions of the ligands. In addition, the d-d transitions of the $[M(CN)_6]$ units were also seen at the same region for **45** and **46**, whereas in **47** the UV-region band was dominated by the ligand transitions. The spectra also exhibit weaker bands that cover the vis-region, and they were assigned to the f-f transitions of the Ho^{3+} ions.[66]

Furthermore, emission spectra were recorded for complexes **45**-**47** using several different excitation wavelengths. Using multiple UV-region wavelengths only resulted in weak emission bands assigned to the 4-pyridone ligands ($\lambda_{excitation} = 370$ nm). This was most likely due to strong quenching of luminescence, and more importantly, re-absoption effect in Ho^{3+}. The re-absorption effect was then further investigated, and it showed temperature-dependent character.[66]

The ligand-based emission and the presence of temperature-dependent luminescence re-absorption in **45**-**47** indicates that the complexes could be utilized in the design of optical thermometers. Combining these optical properties with the SMM properties these compounds could be utilized in the applications of SMM-based devices that can self-monitor temperatures.[66]

7.2 YTTERBIUM-BASED SINGLE-MOLECULE MAGNET WITH OPTICAL THERMOMETER PROPERTIES

7.2.1 Synthetic and structural details

In 2020, an Yb-based complex bearing four coordinated hexamethylphosphoramide (hmpa) solvent molecules and two hexacyanocobaltates was synthesized and characterized. First, a precursor $(Bu_3NH)(H_3O)_2[CoIII(CN)_6]$ (**48**) was synthesized by adding HCl and tributylamine into an aqueous solution of $K_3[Co(CN)_6]$ (Scheme 17). Then, solutions of $YbCl_3 \cdot 6H_2O$ and **48** in a 1:1:1 ratio mixture solvent of H_2O/hmpa/MeCN were combined in water to yield crystals of $(H_5O_2^+)_2(H^+)[YbIII(hmpa)_4][CoIII(CN)_6]_2 \cdot 0.2H_2O$ (**49**).[69]

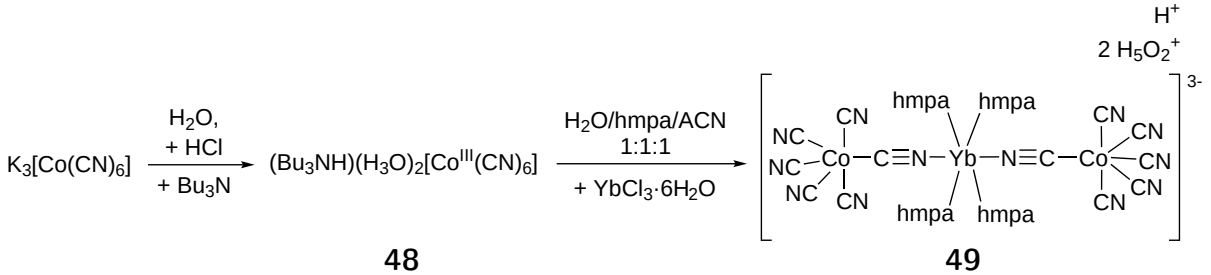

Scheme 17. The general synthesis route for complexes **49**.

X-ray crystallographic measurements were done for **49**, and both the crystal structure and the packing along the crystallographic *c*-axis are presented in Figure 31. The complex crystallizes in the tetragonal crystal system in the space group $I4/mmm$. The structure is very similar to those of **45**-**47** with the [Co(CN)$_6$] units aligning linear to the central Yb and the metals being cyanido-bridged. The packing of **49** along the crystallographic *c*-axis creates a

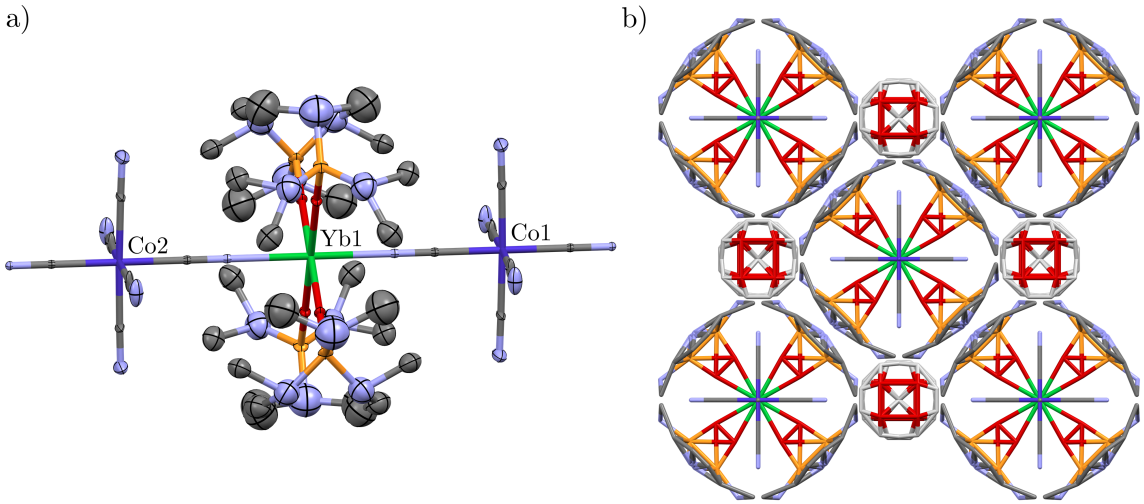

Figure 31. (a) The crystal structure of **49**, where the thermal ellipsoids are drawn at the probability level of 15%. Hydrogens, disorder and both cations are omitted for clarity. (b) The packing of **49**, where hydrogens, disorder and the cations are presented. CSD: GULYUK.[69]

supramolecular network, where the [YbIII(hmpa)$_4$][CoIII(CN)$_6$]$_2^{3-}$ anions bond noncovalently to the $H_5O_2^+$ and H^+ cations. The H^+ cations lie between the terminal cyanide N-atoms of two adjacent molecules, and the $H_5O_2^+$ cations reside between four [Co(CN)$_6$] units of adjacent molecules.[69]

7.2.2 Magnetic properties

In order to investigate the SMM properties of **49**, both AC and DC magnetic measurements were established. The AC measurements were done using an external field of 1000 Oe at temperatures from 2 K to 6 K. The field-dependence of the molar out-of-phase susceptibility χ''_M was studied, and results suggested the presence of slow magnetic relaxation. However, it was absent when the measurements were done using zero external field, possibly due to strong QTM.[69]

The AC and DC magnetic data was used for *ab initio* calculations, which suggested that no Orbach process occurs for **49**. The U_{eff} barrier height that was calculated from the AC data was only 21.7(2) cm^{-1}, while the lowest excited m_J states derived from the DC data were found at 222 cm^{-1}. The energies of the ground state and the three lowest excited m_J states are presented in Figure 32 along with the values derived from the photoluminescence data (see below). The *ab initio* calculations prove the absence of the Orbach type relaxation, and suggest that the dominant relaxation process for **49** is of Raman type.[69]

7.2.3 Optical properties

A photoluminescence spectrum was recorded for **49** to investigate the optical properties of the complex. The spectrum showed a strong peak at 1020 nm, which was assigned to the $^2F_{5/2} \rightarrow {}^2F_{7/2}$ electronic transition of the trivalent Yb. The forementioned emission is due to the sensitization of the Yb-atom emission by metal-to-metal energy transfer from the Co-atoms. This can also be seen in the recorded excitation spectra, where a broad band can be assigned to the $[Co(CN)_6]$ units. The energy transfer to the Yb-atom can be proved by the absence of a red emission assigned to the $[Co(CN)_6]$ units.[69]

A low temperature emission spectrum was also obtained at 6 K, which was used to determine the energies of the ground state, as well as the three lowest lying excited m_J states. The emission spectrum at 6 K showed five distinct bands at 975, 983, 993, 999 and 1019 nm, four latter of which could be assigned to the energy level diagram m_J states. The energy levels that were detemined are presented in Figure 32 in comparison with the energy levels derived from the DC magnetic measurements. The photoluminescence data correlated well with the DC magnetic data, which confirmed the absence of the Orbach type relaxation.[69]

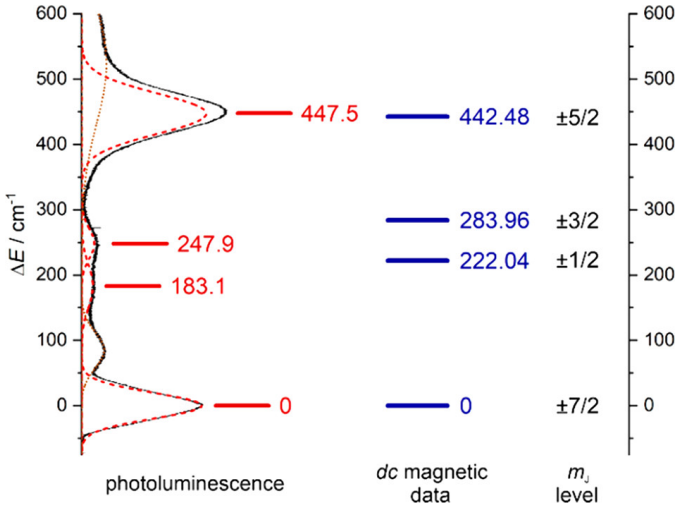

Figure 32. The energy level diagram of the ground state and the three lowest lying excited m_J states of **49**. Reprinted with permission from *J. Am. Chem.*, **2020**, *142*, 8, 3970-3979. Copyright 2021 American Chemical Society.[69]

The highest energy peak at 975 nm, which was not assigned to an m_J state, could be assigned to a temperature-dependent hot transition band. This was confirmed by the increasing emission ($\lambda_{excitation} = 320$ nm) intensity upon heating from 10 K to 300 K (Figure 33). In addition, the strong emission band at 1020 nm showed temperature-dependent character, where the intensity decreased upon heating. This kind of temperature-dependent behaviour is characteristic to optical thermometers. Conclusively, **49** exhibits luminescent thermometer effect, that arises from the optomagnetic properties. However, similar to **45**-**47**, it has a relatively low U_{eff} barrier which causes the lack of the Orbach relaxation.[69]

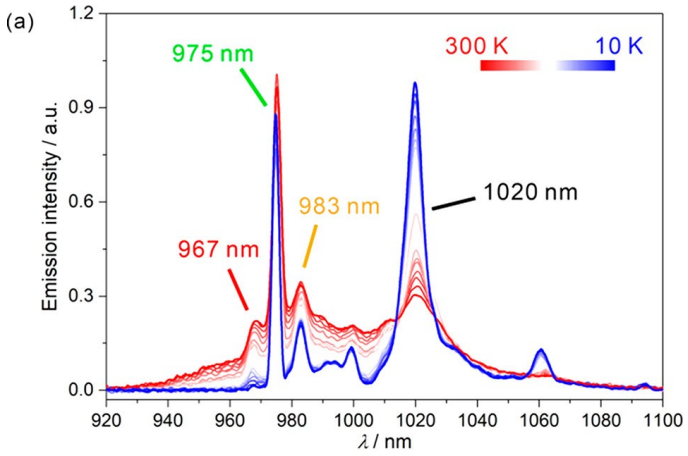

Figure 33. The variable temperature emission spectrum recorded for **49**. Reprinted with permission from *J. Am. Chem.*, **2020**, *142*, 8, 3970-3979. Copyright 2021 American Chemical Society.[69]

7.3 DYSPROSIUM-BASED SINGLE-MOLECULE MAGNET WITH OPTICAL THERMOMETER PROPERTIES

7.3.1 Synthetic and structural details

A dysprosium-based complex exhibiting optomagnetic properties was synthesized in 2019. The dinuclear complex consists of three chelating 1,1,1-trifluoroacetylacetonate ($tfaa^-$) ligands and one bridging 2,2'-bipyrimidine (bpm) ligand. First, ammonia was added into a solution of tfaa in ethanol, as presented in Scheme 18. Into the obtained solution was added bpm in etahnol, after which $DyCl_3 \cdot 6H_2O$ was added. The crude product was slowly evaporated from a DCM solution, and crystals of $[Dy_2(bpm)(tfaa)_6]$ (**50**) were obtained.[70]

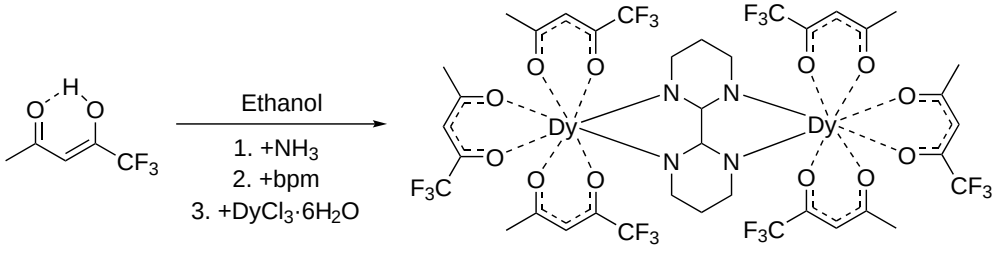

Scheme 18. The general synthesis route for complexes **50**.

X-ray crystalligraphic measurements were established, and the crystal structure of **50** is presented in Figure 34, where the hydrogens and disorder are omitted for clarity. Complex **50** crystallizes in the monoclinic crystal system in the space group $P2_1/n$, and the structure is centrosymmetric. The Dy^{3+} ions are octa-coordinate with six O-atoms coordinating from the bidentate $tfaa^-$ ligands, and two N-atoms coordinating from the bpm ligand bridging between the two Dy-atoms. One $tfaa^-$ ligand on each Dy-atom lies on the same plane with the bridging bpm, while the other two $tfaa^-$ ligands lie on a same plane with each other. According to the *ab*

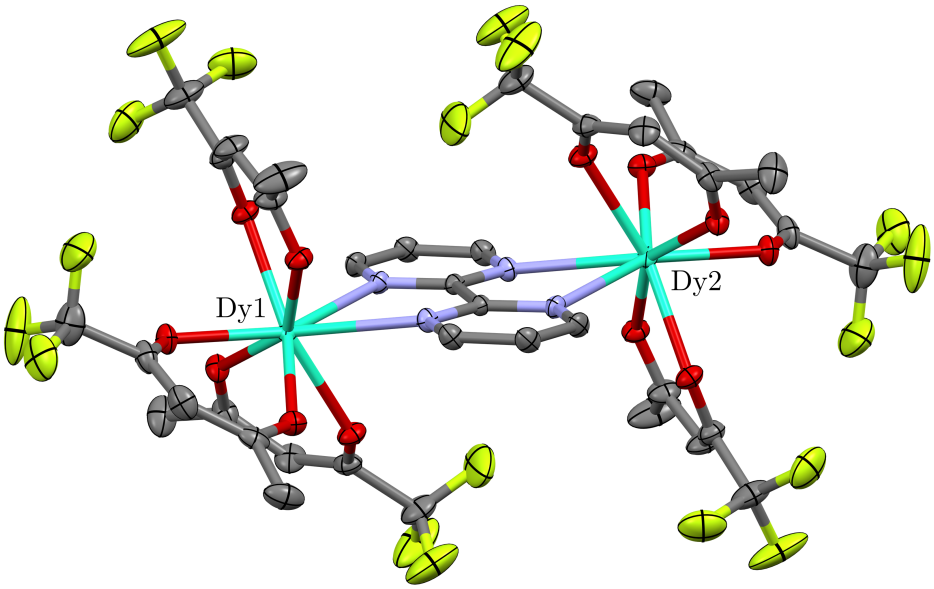

Figure 34. The crystal structure of **49**, where the hydrogens and disorder are omitted for clarity. Thermal ellipsoids are drawn at the probability level of 30%. CSD: XOPLIA.[70]

initio calculations the O-atoms dominate the orientation of the principal magnetic axes, bending them out of the Dy-bpm-Dy plane.[70]

7.3.2 Magnetic properties

The magnetic properties of **50** were investigated by conducting both DC and AC studies. The DC magnetic susceptibility studies were done using an applied field of 1000 Oe at room temperature, and the data was used for *ab initio* calculations. The results revealed that **50** might exhibit SMM properties, and thus the AC magnetic measurements were established.[70]

The AC measurements were done in the frequency range of 0.1-1500 Hz at zero DC field. The data was plotted and frequency-dependent behaviour was observed at temperatures from 6 to 12 K, indicating the presence of slow magnetic relaxation. The relaxation process that was observed below 6 K was of QTM type, which was due to the low symmetry of the coordination sphere of the Dy-atoms.[70]

The magnetic data was used to determine the dominant relaxation process, which was the Raman process. This was also proved by the U_{eff} barrier height of 33 K, which was smaller than the calculated energy of the first excited m_J state. Thus, the slow magnetic relaxation did not proceed via the Orbach process.[70]

7.3.3 Optical properties

Photoluminescence spectra were recorded for **50** to investigate the optical properties of the complex. Emission bands were observed, and they were determined to arise from the sensitising effects of the $tfaa^-$ ligands. Thus, the energy gap S_0-T_1 was measured using a Gd^{3+} analogue of complex **50** to determine the triplet state of the ligand. The energy gap value was 2050 cm^{-1},

which should allow for efficient energy transfer from the ligand to the Dy-atoms. In addition, the back energy transfer from the Dy-atoms to the ligands is very likely limited in the complex. However, the probability of the back energy transfer for **50** is increased upon heating, which indicates that the complex shows temperature-dependent character.[70]

The photoluminescence spectrum recorded at 14 K exhibited components assigned to the $^4F_{9/2} \rightarrow {}^6H_{15/2}$ and $^4F_{9/2} \rightarrow {}^6H_{13/2}$ electronic transitions, as well as the electron population redistribution between the $^4F_{9/2}$ Stark sublevels of Dy^{3+}. These optical properties of **50** indicated that the complex could be utilized in luminescence thermometry. Conclusively, **50** exhibits both magnetic properties and temperature-dependent photoluminescence properties, indicating that it can be exploited in the design of SMM-based devices with optical thermometers.[70]

8 CONCLUSIONS

The design of lanthanoid-based compound that exhibit magnetic and luminescence properties has developed greatly during the recent years. Especially lanthanocenes have shown excellent promise in the fields of single-molecule magnetism and luminescence, as the cyclopentadienyl ligands are very versatile. Cyclopentadienyl rings can be modified in many different ways to tailor the targeted propeties, which is possible because both the magnetic and the luminescence properties are strongly linked to the structural properties of a compound.

SMM behaviour is influenced by the axiality of a crystal field, as well as the equatorially coordinated ligands. In lanthanoids that exhibit oblate shaped electron density (Dy^{3+}, Tb3+), the axial field should be strong, and the equatorial field should be weak, or even absent. The correct choice of the substituents in a Cp ligand can enhance these properties, and alkyl-substituted Cps have shown great promise in the design of lanthanocene SMMs. The best performing SMM up to this day, which can function above liquid nitrogen temperatures (77 K), is a heteroleptic dysprosocene complex with both a methyl-substituted and an *iso*-propyl substituted Cp ligand. This complex is a trivalent lanthanocene, as the trivalent species exhibit better SMM properties than the divalent species. This is due to the electronic structure differences of the Ln^{3+} and Ln^{2+} ions.

In therms of the luminescence properties, there is a great difference between the trivalent and divalent lanthanocene-based complexes. Opposite to what was observed in magnetism, the divalent Ln species are superior the the trivalent species. The Ln^{3+} lanthanocene-based complexes require antenna-ligand to sensitize the Ln emission, which is achievable with the correct choice of ligands. Aryl-substituted Cp ligands have indeed shown great promise as antennas, particularly polyphenyl-substituted Cps.

These polyphenyl-substituted lanthanocene complexes could also be excellent in terms of magnetism, but however, have not yet been studied. The steric bulk of the aryl groups could strengthen the axil CF and prevent the coordination of the equatorial ligands. As Ln^{3+} ions should be used in Ln-SMMs, their luminescence could then be sensitized with the same bulky

ligands. This way the magnetic and the optical properties could be combined.

There are several optomagnetic properties, some of which can be exploited in the design of SMM-based luminescence thermometers. These compounds could allow for the design of miniaturized electromagnetic devices that could have built-in thermal sensing properties. The studies of these types of compounds are only known for three lanthanoids (Ho, Yb, Dy) and they do not include lanthanocene complexes. The existing studies have reported the use of ligands coordinating through N- or O-donor atoms. Thus, the existing complexes do not have an ideal axial crystal field that could allow for an axial principal magnetic axis.

Conclusively, the future studies of the optomagnetic lanthanocenes should be concentrated on the Lns with oblate shaped electron density, specially dysprosium, which has shown excellent promise in the SMM properties. The metals should sandwiched between polyphenyl-substituted Cp ligands that are tailored to sensitize the luminescence and block the equatorial ligands. The study should include both magnetic and luminescence measurements, and possibly temperature-dependent luminescence studies as well.

References

1. Christou, G.; Gatteschi, D.; Hendrickson, D. N. and Sessoli, R., Single-Molecule Magnets. *MRS Bulletin*, **2000**, *25*, 66–71.
2. Sessoli, R.; Gatteschi, D.; Caneschi, A. and Novak, M. A., Magnetic bistability in a metal-ion cluster. *Nature*, **1993**, *365*, 141–143.
3. Aubin, S. M.; Wemple, M. W.; Adams, D. M.; Tsai, H. L.; Christou, G. and Hendrickson, D. N., Distorted Mn(IV)Mn(III)3 cubane complexes as single-molecule magnets. *Journal of the American Chemical Society*, **1996**, *118*, 7746–7754.
4. Jia, J. H.; Li, Q. W.; Chen, Y. C.; Liu, J. L. and Tong, M. L., Luminescent single-molecule magnets based on lanthanides: Design strategies, recent advances and magneto-luminescent studies. *Coordination Chemistry Reviews*, **2019**, *7*, 1–7.
5. Gaita-Ariño, A.; Luis, F.; Hill, S. and Coronado, E., Molecular spins for quantum computation. *Nature Chemistry*, **2019**, *11*, 301–309.
6. Hymas, K. and Soncini, A., Molecular spintronics using single-molecule magnets under irradiation. *Physical Review B*, **2019**, *99*, 179–186.
7. Bunzli, J. C. G.; Comby, S.; Chauvin, A. S. and Vandevyver, C. D. B., New Opportunities for Lanthanide Luminescence. *J. Rare Eearths*, **2007**, *25*, 257–274.
8. Pandya, S.; Yu, J. and Parker, D., Engineering emissive europium and terbium complexes for molecular imaging and sensing. *Dalton Trans.* **2006**, 2757–2766.
9. Slooff, L. H.; Van Blaaderen, A.; Polman, A.; Hebbink, G. A.; Klink, S. I.; Van Veggel, F. C.; Reinhoudt, D. N. and Hofstraat, J. W., Rare-earth doped polymers for planar optical amplifiers. *Journal of Applied Physics*, **2002**, *91*, 3955–3980.
10. Bardonov, D. A.; Komarov, P. D.; Ovchinnikova, V. I.; Puntus, L. N.; Minyaev, M. E.; Nifant'ev, I. E.; Lyssenko, K. A.; Korshunov, V. M.; Taidakov, I. V. and Roitershtein, D. M., Accessing mononuclear triphenylcyclopentadienyl lanthanide complexes by using tridentate nitrogen ligands: Synthesis, structure, luminescence, and catalysis. *Organometallics*, **2021**, *40*, 1235–1243.
11. Goodwin, C. A.; Reta, D.; Ortu, F.; Chilton, N. F. and Mills, D. P., Synthesis and Electronic Structures of Heavy Lanthanide Metallocenium Cations. *Journal of the American Chemical Society*, **2017**, *139*, 18714–18724.
12. Le Roy, J. J.; Jeletic, M.; Gorelsky, S. I.; Korobkov, I.; Ungur, L.; Chibotaru, L. F. and Murugesu, M., An organometallic building block approach to produce a multidecker 4 f single-molecule magnet. *Journal of the American Chemical Society*, **2013**, *135*, 3502–3510.

13. Atanasov, M.; Aravena, D.; Suturina, E.; Bill, E.; Maganas, D. and Neese, F., First principles approach to the electronic structure, magnetic anisotropy and spin relaxation in mononuclear 3d-transition metal single molecule magnets. *Coordination Chemistry Reviews*, **2015**, *289-290*, 177–214.

14. Chiesa, A. et al., Understanding magnetic relaxation in single-ion magnets with high blocking temperature. *Physical Review B*, **2020**, *101*, 1–9.

15. Ding, Y. S.; Chilton, N. F.; Winpenny, R. E. and Zheng, Y. Z., On Approaching the Limit of Molecular Magnetic Anisotropy: A Near-Perfect Pentagonal Bipyramidal Dysprosium(III) Single-Molecule Magnet. *Angewandte Chemie - International Edition*, **2016**, *55*, 16071–16074.

16. Neese, F. and Pantazis, D. A., What is not required to make a single molecule magnet. *Faraday Discussions*, **2011**, *148*, 229–238.

17. Day, B. M.; Guo, F. S. and Layfield, R. A., Cyclopentadienyl Ligands in Lanthanide Single-Molecule Magnets: One Ring to Rule Them All? *Accounts of Chemical Research*, **2018**, *51*, 1880–1889.

18. Newnham, R. E. 1.-2., *Properties of materials : anisotropy, symmetry, structure*, Newnham, R. E. 1.-2., Ed.; Oxford University Press, Oxford ; New York, 2005, pp. 378.

19. Gatteschi, D. and Sessoli, R., Quantum tunneling of magnetization and related phenomena in molecular materials. *Angewandte Chemie - International Edition*, **2003**, *42*, 268–297.

20. Cullity B. D., k., *Introduction to magnetic materials*, 2nd ed. ed., Graham, C. D., Ed., Includes index.; IEEE/Wiley, Hoboken, New Jersey, 2009, pp. 197–205.

21. *Molecular cluster magnets*, Winpenny, R., Ed.; World Scientific series in nanoscience and nanotechnology; World Scientific Pub, Singapore ; Hackensack, N.J., 2012, pp. 299.

22. Hay, M. A.; Sarkar, A.; Marriott, K. E.; Wilson, C.; Rajaraman, G. and Murrie, M., Investigation of the magnetic anisotropy in a series of trigonal bipyramidal Mn(ii) complexes. *Dalton Transactions*, **2019**, *48*, 15480–15486.

23. Gómez-Coca, S.; Aravena, D.; Morales, R. and Ruiz, E., Large magnetic anisotropy in mononuclear metal complexes. *Coordination Chemistry Reviews*, **2015**, *289-290*, 379–392.

24. Krzystek, J.; Telser, J.; Pardi, L. A.; Goldberg, D. P.; Hoffman, B. M. and Brunel, L. C., High-frequency and -field electron paramagnetic resonance of high-spin manganese(III) in porphyrinic complexes. *Inorganic Chemistry*, **1999**, *38*, 6121–6129.

25. Woodruff, D. N.; Winpenny, R. E. P. and Layfield, R. A., Lanthanide Single-Molecule Magnets. *Chemical Reviews*, **2013**, *113*, PMID: 23550940, 5110–5148.

26. Atkins, P. and De Paula, J., *Physical Chemistry*, 9. ed., W. H. Freeman, Company, 2010, pp. 365.

27. Marin, R.; Brunet, G. and Murugesu, M., Shining New Light on Multifunctional Lanthanide Single-Molecule Magnets. *Angewandte Chemie International Edition*, **2019**, *60*, 1728–1746.

28. Long, J.; Guari, Y.; Ferreira, R. A.; Carlos, L. D. and Larionova, J., Recent advances in luminescent lanthanide based Single-Molecule Magnets. *Coordination Chemistry Reviews*, **2018**, *363*, 57–70.

29. Liu, J. L.; Chen, Y. C. and Tong, M. L., Symmetry strategies for high performance lanthanide-based single-molecule magnets. *Chemical Society Reviews*, **2018**, *47*, 2431–2453.

30. Ishikawa, N.; Sugita, M.; Ishikawa, T.; Koshihara, S. Y. and Kaizu, Y., Mononuclear lanthanide complexes with a long magnetization relaxation time at high temperatures: A new category of magnets at the single-molecular level. *Journal of Physical Chemistry B*, **2004**, *108*, 11265–11271.

31. Woodru, D. N.; Winpenny, R. E. P. and Lay, R. A., Lanthanide Single-Molecule Magnets. *Chem. Rev.* **2013**, *113*, 5110–5148.

32. Thomas-Hargreaves, L. R.; Giansiracusa, M. J.; Gregson, M.; Zanda, E.; O'Donnell, F.; Wooles, A. J.; Chilton, N. F. and Liddle, S. T., Correlating axial and equatorial ligand field effects to the single-molecule magnet performances of a family of dysprosium bis-methanediide complexes. *Chemical Science*, **2021**, *12*, 3911–3920.

33. Hiller, M.; Krieg, S.; Ishikawa, N. and Enders, M., Ligand-Field Energy Splitting in Lanthanide-Based Single-Molecule Magnets by NMR Spectroscopy. *Inorganic Chemistry*, **2017**, DOI: 10.1021/acs.inorgchem.7b02704.

34. Bi, Y.; Chen, C.; Zhao, Y. F.; Zhang, Y. Q.; Jiang, S. D.; Wang, B. W.; Han, J. B.; Sun, J. L.; Bian, Z. Q.; Wang, Z. M. and Gao, S., Thermostability and photoluminescence of Dy(III) single-molecule magnets under a magnetic field. *Chemical Science*, **2016**, *7*, 5020–5031.

35. Shao, D. and Wang, X. Y., Development of Single-Molecule Magnets†. *Chinese Journal of Chemistry*, **2020**, *38*, 1005–1018.

36. Cornia, A.; Barra, A. L.; Bulicanu, V.; Clérac, R.; Cortijo, M.; Hillard, E. A.; Galavotti, R.; Lunghi, A.; Nicolini, A.; Rouzières, M.; Sorace, L. and Totti, F., The Origin of Magnetic Anisotropy and Single-Molecule Magnet Behavior in Chromium(II)-Based Extended Metal Atom Chains. *Inorganic Chemistry*, **2020**, *59*, 1763–1777.

37. Evans, W. J., The organometallic Chemistry of the lanthanide elements in low oxidation states. *Polyhedron*, **1987**, *6*, 803–835.

38. De Sousa Filho, P. C.; Lima, J. F. and Serra, O. A., From lighting to photoprotection: Fundamentals and applications of rare earth materials. *Journal of the Brazilian Chemical Society*, **2015**, *26*, 2471–2495.

39. Moore, E. G.; Samuel, A. P. and Raymond, K. N., From antenna to assay: lessons learned in lanthanide luminescence. *Accounts of Chemical Research*, **2009**, *42*, 542–552.

40. Rinehart, J. D. and Long, J. R., Exploiting single-ion anisotropy in the design of f-element single-molecule magnets. *Chemical Science*, **2011**, *2*, 2078–2085.

41. Cheung, T. T. P., *Cyclopentadiene and Dicyclopentadiene*, American Cancer Society, 2001, pp. 219–235.

42. Panda, T. K.; Gamer, M. T. and Roesky, P. W., An improved synthesis of sodium and potassium cyclopentadienide. *Organometallics*, **2003**, *22*, 877–878.

43. SCHUMANN, H.; ALBRECHT, I. and HAHN, E. In *Organometallic Syntheses*, King, R. B. and Eisch, J. J., Eds.; Elsevier: Amsterdam, 1986, pp 9–12.

44. Nifant'ev, I. E.; Vinogradov, A. A.; Minyaev, M. E.; Komarov, P. D.; Lyssenko, K. A.; Birin, K. P.; Dyadchenko, V. P. and Ivchenko, P. V., The structural diversity of heterocycle-fused potassium cyclopentadienides. *RSC Advances*, **2019**, *9*, 29195–29204.

45. Uemura, M.; Yagi, K.; Iwasaki, M.; Nomura, K.; Yorimitsu, H. and Oshima, K., Pentamethylcyclopentadienide in organic synthesis: Nucleophilic addition of lithium pentamethylcyclopentadienide to carbonyl compounds and carbon-carbon bond cleavage of the adducts yielding the parent carbonyl compounds. *Tetrahedron*, **2006**, *62*, 3523–3535.

46. Bordwell, F. G. and Bausch, M. J., Methyl effects on the basicities of cyclopentadienide and indenide ions and on the chemistry of their transition metal complexes. *Journal of the American Chemical Society*, **1983**, *105*, 6188–6189.

47. Guo, F. S.; Day, B. M.; Chen, Y. C.; Tong, M. L.; Mansikkamäki, A. and Layfield, R. A., A Dysprosium Metallocene Single-Molecule Magnet Functioning at the Axial Limit. *Angewandte Chemie - International Edition*, **2017**, *56*, 11445–11449.

48. Field, L. D.; Lindall, C. M.; Masters, A. F. and Clentsmith, G. K., Penta-arylcyclopentadienyl complexes. *Coordination Chemistry Reviews*, **2011**, *255*, 1733–1790.

49. Clark, D. L.; Gordon, J. C.; Scott, B. L. and Watkin, J. G., Synthesis and characterization of a mixed-ring bis-cyclopentadienyl derivative of neodymium. X-ray crystal structures of (η-C5Me5)NdI2(py)3 and (η-C5Me5)(η-C5H4SiMe 3)NdI(py). *Polyhedron*, **1999**, *18*, 1389–1396.

50. Goodwin, C. A.; Ortu, F.; Reta, D.; Chilton, N. F. and Mills, D. P., Molecular magnetic hysteresis at 60 kelvin in dysprosocenium. *Nature*, **2017**, *548*, 439–442.

51. Guo, F. S.; Day, B. M.; Chen, Y. C.; Tong, M. L.; Mansikkamäki, A. and Layfield, R. A., Magnetic hysteresis up to 80 kelvin in a dysprosium metallocene single-molecule magnet. *Science*, **2018**, *362*, 1400–1403.

52. Goodwin, C. A.; Reta, D.; Ortu, F.; Liu, J.; Chilton, N. F. and Mills, D. P., Terbocenium: Completing a heavy lanthanide metallocenium cation family with an alternative anion abstraction strategy. *Chemical Communications*, **2018**, *54*, 9182–9185.

53. Randall McClain, K.; Gould, C. A.; Chakarawet, K.; Teat, S. J.; Groshens, T. J.; Long, J. R. and Harvey, B. G., High-temperature magnetic blocking and magneto-structural correlations in a series of dysprosium(iii) metallocenium single-molecule magnets. *Chemical Science*, **2018**, *9*, 8492–8503.

54. Evans, P.; Reta, D.; Whitehead, G. F.; Chilton, N. F. and Mills, D. P., Bis-monophospholyl dysprosium cation showing magnetic hysteresis at 48 K. *Journal of the American Chemical Society*, **2019**, *141*, 19935–19940.

55. Nief, F., Complexes containing bonds between group 3, lanthanide or actinide metals and non-first-row main group elements (excluding halogens). *Coordination Chemistry Reviews*, **1998**, *178-180*, 13–81.

56. Nief, F.; Ricard, L. and Mathey, F., Phospholyl (phosphacyclopentadienyl) and arsolyl (arsacyclopentadienyl) complexes of ytterbium(II) and samarium(II). Synthetic, structural and multinuclear (31P and 171Yb) NMR studies. *Polyhedron*, **1993**, *12*, 19–26.

57. Gould, C. A.; McClain, K. R.; Yu, J. M.; Groshens, T. J.; Furche, F.; Harvey, B. G. and Long, J. R., Synthesis and Magnetism of Neutral, Linear Metallocene Complexes of Terbium(II) and Dysprosium(II). *Journal of the American Chemical Society*, **2019**, *141*, 12967–12973.

58. Moutet, J.; Schleinitz, J.; La Droitte, L.; Tricoire, M.; Pointillart, F.; Gendron, F.; Simler, T.; Clavaguéra, C.; Le Guennic, B.; Cador, O. and Nocton, G., Bis-Cyclooctatetraenyl Thulium(II): Highly Reducing Lanthanide Sandwich Single-Molecule Magnets. *Angewandte Chemie - International Edition*, **2021**, *60*, 6042–6046.

59. Harder, S.; Naglav, D.; Ruspic, C.; Wickleder, C.; Adlung, M.; Hermes, W.; Eul, M.; Pöttgen, R.; Rego, D. B.; Poineau, F.; Czerwinski, K. R.; Herber, R. H. and Nowik, I., Physical properties of superbulky lanthanide metallocenes: Synthesis and extraordinary luminescence of [EuII(CpBIG)2] (CpBIG=(4-nBu-C6H4)5- cyclopentadienyl). *Chemistry - A European Journal*, **2013**, *19*, 12272–12280.

60. Roitershtein, D. M.; Puntus, L. N.; Vinogradov, A. A.; Lyssenko, K. A.; Minyaev, M. E.; Dobrokhodov, M. D.; Taidakov, I. V.; Varaksina, E. A.; Churakov, A. V. and Nifant'Ev, I. E., Polyphenylcyclopentadienyl Ligands as an Effective Light-Harvesting μ-Bonded Antenna for Lanthanide +3 Ions. *Inorganic Chemistry*, **2018**, *57*, 10199–10213.

61. Zwaschka, M. Z.; Becker, D.; Berben, D.; Fiedler, T.; Jermann, F. and F., Phosphors for solid state lighting. *Light-Emitting Diodes: Research, Manufacturing, and Applications XII*, **2008**, *6910*, 181–188.

62. Eliseeva, S. V. and Bünzli, J. C. G., Lanthanide luminescence for functional materials and bio-sciences. *Chemical Society Reviews*, **2010**, *39*, 189–227.

63. Latva, M.; Takalob, H.; Mukkala, V. M.; Matachescu, C.; Rodríguez-Ubis, J. C. and Kankare, J., Correlation between the lowest triplet state energy level of the ligand and lanthanide(III) luminescence quantum yield. *Journal of Luminescence*, **1997**, *75*, 149–169.

64. Arumugam, S.; Reddy, P. G.; Francis, M.; Kulkarni, A.; Roy, S. and Mondal, K. C., Highly fluorescent aryl-cyclopentadienyl ligands and their tetra-nuclear mixed metallic potassium-dysprosium clusters. *RSC Advances*, **2020**, *10*, 39366–39372.

65. Kelly, R. P.; Bell, T. D.; Cox, R. P.; Daniels, D. P.; Deacon, G. B.; Jaroschik, F.; Junk, P. C.; Le Goff, X. F.; Lemercier, G.; Martinez, A.; Wang, J. and Werner, D., Divalent Tetra- and Penta-phenylcyclopentadienyl Europium and Samarium Sandwich and Half-Sandwich Complexes: Synthesis, Characterization, and Remarkable Luminescence Properties. *Organometallics*, **2015**, *34*, 5624–5636.

66. Wang, J.; Zakrzewski, J. J.; Zychowicz, M.; Vieru, V.; Chibotaru, L. F.; Nakabayashi, K.; Chorazy, S. and Ohkoshi, S. I., Holmium(iii) molecular nanomagnets for optical thermometry exploring the luminescence re-absorption effect. *Chemical Science*, **2021**, *12*, 730–741.

67. Brunet, G.; Marin, R.; Monk, M. J.; Resch-Genger, U.; Gálico, D. A.; Sigoli, F. A.; Suturina, E. A.; Hemmer, E. and Murugesu, M., Exploring the dual functionality of an ytterbium complex for luminescence thermometry and slow magnetic relaxation. *Chemical Science*, **2019**, *10*, 6799–6808.

68. Fondo, M.; Corredoira-Vázquez, J.; García-Deibe, A. M.; Sanmartín-Matalobos, J.; Amoza, M.; Botas, A. M.; Ferreira, R. A.; Carlos, L. D. and Colacio, E., Field-induced slow magnetic relaxation and luminescence thermometry in a mononuclear ytterbium complex. *Inorganic Chemistry Frontiers*, **2020**, *7*, 3019–3029.

69. Wang, J.; Zakrzewski, J. J.; Heczko, M.; Zychowicz, M.; Nakagawa, K.; Nakabayashi, K.; Sieklucka, B.; Chorazy, S. and Ohkoshi, S. I., Proton Conductive Luminescent Thermometer Based on Near-Infrared Emissive {YbCo2} Molecular Nanomagnets. *Journal of the American Chemical Society*, **2020**, *142*, 3970–3979.

70. Errulat, D.; Marin, R.; Gálico, D. A.; Harriman, K. L.; Pialat, A.; Gabidullin, B.; Iikawa, F.; Couto, O. D.; Moilanen, J. O.; Hemmer, E.; Sigoli, F. A. and Murugesu, M., A Luminescent Thermometer Exhibiting Slow Relaxation of the Magnetization: Toward Self-Monitored Building Blocks for Next-Generation Optomagnetic Devices. *ACS Central Science*, **2019**, *5*, 1187–1198.